

Computer Techniques for Electromagnetic Interaction Modelling

by

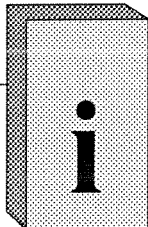
Joe LoVetri

A thesis submitted to
the School of Graduate Studies and Research
in partial fulfillment of the requirements
for the degree of
Doctor of Philosophy

Ottawa-Carleton Institute for Electrical Engineering
Department of Electrical Engineering
Faculty of Engineering
University of Ottawa
Ottawa, Ontario, Canada
K1N 6N5

August 1990

© 1990, *J. LoVetri*



Abstract

Computer techniques for the modelling of complex electromagnetic interactions are explored. The main thesis is that these techniques, or methods, can be divided into two types: *non-algorithmic* and *algorithmic techniques*. Approximate algorithmic methods for the modelling of electromagnetic interactions have undergone great advances in the past twenty years but they are still only feasible for relatively small problems (i.e. where the space-time discretization produces and requires only a relatively small number of unknowns). The computer implementation of non-algorithmic methods have recently become a reality with the maturing of *expert system technology* and *knowledge based engineering*.

In Part I of this thesis, a knowledge-based approach for the modelling of electromagnetic (EM) interactions in a system is described. The purpose is to determine any unwanted EM effects which could jeopardize the safety and operation of the system. Modelling the interactions in a system requires the examination of the compounded and propagated effects of the electromagnetic fields. A useful EM modelling approach is one which is incremental and constraint-based. The approach taken here subdivides the modelling task into two parts:

- a) the definition of the related physical topology, and
- b) the propagation of the electromagnetic constraints.

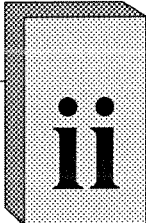
Abstract

A prototype of some of the EM constraints has been implemented in Quintus Prolog under NeWS on a Sun workstation. User interaction is through a *topology drawing tool* and a stack-based attribute interface similar to the HyperCard™ interface of the Apple Macintosh computer.

In Part II, numerical methods which discretize the space-time region of interest and provide a solution to the electromagnetics problem, given appropriate initial and boundary conditions, are investigated. Specifically, time-domain finite difference methods as applied to Maxwell's equations are analyzed, compared and implemented. As the basis of this analysis, Maxwell's equations are expressed as a system of hyperbolic conservation laws. Analytical properties of these systems, based on the method of characteristics, are used to study the numerical solution of Maxwell's equations.

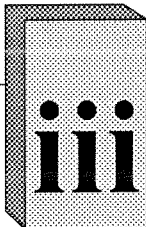
Practical issues, such as computational efficiency and memory requirements, are discussed for the implementation of the finite difference schemes. Advanced programming techniques are used to implement all the finite difference schemes discussed. The schemes are used to solve the problem of the penetration of electromagnetic energy through a shield with a thick gap.

A two-dimensional time-domain finite element method, implemented as the software package PDE/PROTRAN, is also applied to shielding problems. The software package is first validated for simple hyperbolic problems and is then applied to perfectly conducting shields with apertures.



Contributions

The specific contributions made in this thesis are in the general area of electromagnetic interaction modelling. It is shown how the methods used by engineers to investigate electromagnetic interaction problems can be divided into algorithmic and non-algorithmic techniques. Specifically, for the non-algorithmic techniques, the first *expert system* for the analysis of electromagnetic interaction phenomena is formulated and implemented on a computer. This consists of structuring the domain knowledge in an amenable form for computer implementation. For the algorithmic techniques, an analysis is made of finite difference time domain methods for the solution of Maxwell's equations. New methods based on computational fluid dynamics are analyzed and implemented. Advanced programming techniques are used to implement the difference schemes.



Acknowledgments

The work done in this thesis has taken two years to complete. During this time, I have had the pleasure of working with *many* people on the ideas and principles which are involved. Specifically, I would like to thank Suhayya Abu-Hakima for her time in the many technical discussions which we had on knowledge-based systems, as well as for her moral support throughout the structuring of the ideas of Part I. I would also like to thank Darin P. W. Graham for his help in the implementation of HardSys, and Tim Taylor for his implementation of HardDraw. I am also indebted to Marek Wartek for the many discussions we had about hyperbolic conservation laws. The help I received from Gordon Squires and Peter Tzivanopoulos in the plotting of fields is also greatly appreciated. I also thank Gilbert Soulodre for his reading of the entire thesis and for his useful comments.

The guidance of my thesis supervisor and friend, George Costache, has been very fruitful and I wish to thank him for this and his moral support. For the freedom allotted to me by my work supervisor, Andrew S. Podgorski, I am greatly indebted. I could not have completed this project without his belief in the subject.

Finally, and most importantly, I would like to thank *Karen, Natalie, Peter, Silvana*, and little *Carmela* for their support when I was falling, for their love and encouragement always, for the sacrifices they have had to endure because of this thesis, and for their patience, patience, patience.

I dedicate this thesis to them.



Table of Contents

<i>i Abstract</i>	1
<i>ii Contributions</i>	3
<i>iii Acknowledgments</i>	4
<i>iv Table of Contents</i>	5
<i>v List of Figures</i>	9

Part 1 Non-Algorithmic Techniques

Chapter 1 Introduction to Electromagnetic Interactions	15
Chapter 2 Electromagnetic Interaction Modelling	17
2.1 Problem Definition ...	17
2.2 Traditional Approach ...	18
2.3 Computer Aided Electromagnetic Modelling ...	19
Chapter 3 Electromagnetic Topology of Systems	21
3.1 Topological Decompositions ...	22
3.2 Some Graph Theory Definitions and Techniques ...	24
3.3 Equivalent Graph of Volume/Surface Topology ...	32
3.4 Summary of Topological Decomposition ...	35
Chapter 4 Electromagnetic Component and Interaction Path Attributes	37
4.1 Frequency Domain Representation ...	38
4.2 Electromagnetic Disturbance Representation ...	44

Table of Contents

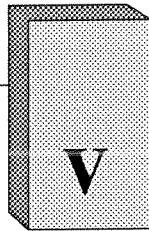
4.2.1 Electromagnetic Disturbance Simplifications ...	46
4.2.2 Examples of Ambient Field Attributes ...	51
4.2.3 Parallel Addition and Frequency Normalization ...	54
4.3 Component Susceptibility Representation and Approximation ...	56
4.4 Interaction Path Shielding Effectiveness Representation ...	60
4.4.1 Examples of Path SE Attributes ...	63
4.4.1.1 Field-Field Path Nodes ...	63
4.4.1.2 Circuit-Circuit Path Nodes ...	68
4.4.1.3 Field-Circuit Path Nodes ...	68
4.4.1.4 Circuit-Field Path Nodes ...	69
4.4.2 Physical Example with All Interaction Types ...	70
Chapter 5 Using Constraints to Characterize EMI	73
5.1 Topology Definition Constraints ...	73
5.2 Global Frequency Range Constraint ...	74
5.3 Volume/Surface Attribute Definition Constraints ...	75
5.4 Worst Case Shielding Path ...	78
5.5 Propagation of Electromagnetic Disturbance ...	80
5.5.1 Justification for Ambient Field Propagation ...	82
5.6 Likelihood of Failure Determination ...	83
5.6.1 Justification of Failure Index Determination ...	86
5.7 Grouping of Electromagnetic Volume Nodes ...	87
Chapter 6 Implementation	90
6.1 HardDraw: Smart Topology Drawing Tool ...	90
6.1.1 GoodNeWS ...	91
6.1.2 HyperNeWS ...	91
6.1.3 HardDraw as a Stack ...	91
6.2 HardSys: Electromagnetic Interaction Expert System ...	93
6.2.1 Electromagnetic Volume Nodes as Objects ...	93

Table of Contents

6.2.2 Surface Nodes as Objects ...	95
6.2.3 Spanning Tree Calculations ...	96
6.3 Future Implementation Issues ...	97
Chapter 7 An Application: Helicopter EMI	98
7.1 NEMP Hardening of Typical Helicopter ...	98
7.1.1 Specific Electromagnetic Topology Used ...	98
7.1.2 Electromagnetic Disturbance ...	100
7.1.3 System Susceptibility ...	101
7.1.4 Shielding Effectiveness of Surfaces ...	103
7.1.5 Results and Software Performance ...	105
Chapter 8 Conclusions and Future Plans for the EMI Advisor	106
<hr/>	
Part 2 Algorithmic Techniques	
<hr/>	
Chapter 9 Introduction to Numerical Methods	109
Chapter 10 Maxwell's Equations	112
Chapter 11 Hyperbolic Systems of Conservation Laws	115
11.1 Hyperbolic Conservation Laws ...	115
11.2 Formulation of Maxwell's Equations in Conservation Law Form ...	116
11.3 Systems in One Space Dimension and Time ...	118
11.4 Maxwell's Equations in One Space Dimension and Time ...	121
11.4.1 Wave equation in a non-dissipative medium ($\sigma = 0$) ...	122
11.4.2 Wave equation in a dissipative medium ($\sigma \neq 0$) ...	130
Chapter 12 Finite Difference Methods	133
12.1 Some Finite Difference Terminology ...	134

Table of Contents

12.2 Classical Finite Difference Schemes ...	137
12.3 Schemes Based on Upwinding and Flux-Splitting Techniques ...	140
12.4 Numerical Flux Determination ...	144
12.5 Comparison of Schemes for 1-D Electromagnetics ...	148
Chapter 13 Finite Differences in Higher Dimensions	156
13.1 Leap-frog: Yee Algorithm ...	157
13.2 Lax-Wendroff: Two Step Method ...	160
13.3 Upwind Schemes ...	163
13.4 Numerical Fluxes for Maxwell's Equations ...	167
Chapter 14 Finite Difference Practical Implementation and Results	170
14.1 Memory Requirements ...	170
14.2 Practical Implementation: Dynamic Memory Allocation ...	172
14.3 Results for Two-Dimensional TM Fields ...	175
14.4 Three Dimensional Schemes ...	186
Chapter 15 Finite Elements for 2-D Shield Problems	187
15.1 Formulation of 2-D Shielding Problems ...	187
15.2 Program Validation and Numerical Results ...	189
Chapter 16 Conclusions and Future Work for Numerical Techniques	195
Bibliography	197
Index	207



List of Figures

Part 1 Non-Algorithmic Techniques

Figure 1	Office automation scenario as an EM interaction problem.	16
Figure 2	Summary of terminology	18
Figure 3	Example of a specific volume/surface topology	23
Figure 4	Example of a general graph	24
Figure 5	Example of a bipartite graph	25
Figure 6	Dijkstra's algorithm with shortest path determination	28
Figure 7	Example application of shortest path algorithm	29
Figure 8	Cut vertex and cut edge examples	30
Figure 9	Grouped vertex example	31
Figure 10	Equivalent graph (interaction sequence diagram) of volume/surface topology	32
Figure 11	Bipartite Graph of Example Topology	33
Figure 12	Digraph representation	34
Figure 13	Bipartite digraph representation	35
Figure 14	Single electromagnetic interaction path	37
Figure 15	Example frequency range description	41

List of Figures

Figure 16 Fourier transform from the FFT of a pure sinusoid	43
Figure 17 Field type power density disturbance definitions	48
Figure 18 Circuit type power disturbance definitions	49
Figure 19 Ambient field attributes for a typical volume node.	51
Figure 20 Lightning emission	52
Figure 21 Example ambient field representation	53
Figure 22 Frequency normalization algorithm	55
Figure 23 Parallel addition algorithm	56
Figure 24 System susceptibility definitions	58
Figure 25 Example system susceptibility representation	59
Figure 26 System susceptibility attributes for a typical volume node	60
Figure 27 Interaction path representations	61
Figure 28 Shielding effectiveness definitions	62
Figure 29 Interaction path types	63
Figure 30 Typical shield imperfections	64
Figure 31 Shielding effectiveness of apertures	66
Figure 32 Two topological representations of the same shielding imperfection	67
Figure 33 Emission from current loop above ground	70
Figure 34 Examples of system characterization via topology and equivalent graph representation involving all four types of nodes	71
Figure 35 Definition of SE variable	79
Figure 36 Example worst case shielding path for a specific frequency	80
Figure 37 Ambient field discrete levels	81

List of Figures

Figure 38 Ambient field propagation through SE	81
Figure 39 High ambient field approximation propagated through good SE	82
Figure 40 Discrete system susceptibility values	83
Figure 41 Likelihood of failure discrete levels	84
Figure 42 Likelihood of Failure Chart	85
Figure 43 Overlap of PAF ranges with SS ranges to determine FI	86
Figure 44 Example of grouping a subgraph in a cut-node	88
Figure 45 Example HardDraw session	92
Figure 46 Two heuristics to stop the MST search	96
Figure 47 Simplified helicopter electromagnetic topology	99
Figure 48 Equivalent bipartite graph for helicopter topology	99
Figure 49 Approximation of the electromagnetic threats used	100
Figure 50 System susceptibility for electronics node	102
Figure 51 Approximations for cable shielding	104
Figure 52 Tabular output of likelihood of failure information	105

Part 2 Algorithmic Techniques

Figure 53 Numerical methods issues	110
Figure 54 Characteristic lines for wave equation	124
Figure 55 Region with abrupt boundary	126
Figure 56 Characteristic theory for boundary problem	127
Figure 57 Exact numerical procedure for layered medium	129

List of Figures

Figure 58 Table of linear finite difference operators	133
Figure 59 Computational molecule for leap-frog scheme	139
Figure 60 Interlaced mesh for leap-frog	140
Figure 61 Domain of dependence of physical and numerical problem	141
Figure 62 1-D electromagnetic solutions for a perfectly conducting boundary	149
Figure 63 1-D electromagnetic solutions for dielectric boundary	150
Figure 64 1-D electromagnetic solutions for dielectric conducting boundary	152
Figure 65 1-D electromagnetic solutions for conducting medium	153
Figure 66 1-D electromagnetic solutions for conducting medium	154
Figure 67 Separate plots for square initial D in conducting medium	155
Figure 68 Location of components for leap-frog scheme	159
Figure 69 Computational molecules for 2-D Richtmyer schemes	162
Figure 70 Courant numbers for Richtmyer schemes	163
Figure 71 Example of solution vector and material constants data structures	173
Figure 72 Time domain Gaussian pulse	176
Figure 73 Leap-frog solution (D_z) for a Gaussian D line source	177
Figure 74 Lax-Wendroff solution (D_z) for a Gaussian D line source	179
Figure 75 Shankar-Osher solution (D_z) for a Gaussian D line source	180
Figure 76 Test case 2: perfectly conducting thick shield with gap	181
Figure 77 Leap-frog solution (D_z) for TM shielding of Gaussian pulse	182
Figure 78 Perfect conducting boundary condition for Lax-Wendroff	183
Figure 79 Lax-Wendroff solution (D_z) for TM shielding of Gaussian pulse	184

List of Figures

Figure 80 Shankar-Osher solution (D_z) for TM shielding of Gaussian pulse	185
Figure 81 Initial Triangulation of 2-D Shielding Problem	188
Figure 82 One-dimensional test problem for PDE/PROTRAN (E field)	192
Figure 83 One-dimensional test problem for PDE/PROTRAN (H field)	193
Figure 84 Two-dimensional shield problem (B field)	194



Non-Algorithmic Techniques

The use of non-algorithmic techniques to solve electromagnetic interaction problems is investigated in Part 1. These techniques and procedures are used daily by engineers to solve electromagnetic interference problems in electrical systems. The purpose here is to establish an appropriate symbolic description or knowledge representation of the fundamental components in an electromagnetic interaction problem as well as the strategies or heuristics used to reason about these components. These strategies are derived from well known engineering principles and can be viewed as constraints on the electromagnetic interaction problem.

Chapter 1

Introduction to Electromagnetic Interactions

The effects of electromagnetic interactions in electrical systems are of concern because of the increased pollution of the environment with electromagnetic emissions and because of the increasing susceptibility of system components. The term electrical system is used herein in the general sense to include more than just networks consisting of electronic components. Systems containing biological and/or mechanical components of varying complexity are also included when reference to the term electrical systems is made. Electromagnetic emissions from components within the electrical system, and also disturbances originating external to it, can be classified as deriving from intentional as well as non-intentional sources. The interaction effects on the susceptible components within these systems range from minor to catastrophic; they cannot always be predicted nor are they always understood. Study and control of this problem is very desirable and has involved the efforts of many persons from varying fields. Thus many viewpoints can be (and have been) adopted when confronting this problem.

From a theoretical standpoint, understanding the phenomena of electromagnetic interactions between electrical systems requires no more complicated theory than that explicated by Maxwell in his *Treatise on Electricity and Magnetism*. Of course, the elaboration of this theory over the years has given insight into *mechanisms* of

Part 1

electromagnetic interaction. Mechanisms of interaction, associated with an electrical system, manifest a complex called the *electromagnetic system*.

From a practical point of view, it is not at all obvious how the electromagnetic integrity of systems can be *assured* even for relatively small interaction problems (or what at first may seem to be a small problem). Identification of the group or set of electromagnetic interaction mechanisms in an electromagnetic system does not define the problem uniquely. What is also required is the *topology* of the set which gives the relationship between components in an electromagnetic system. Thus, understanding electromagnetic interaction problems consists of understanding the basic mechanisms involved as well as the higher level topology describing the electromagnetic system.

An example of a common electromagnetic interaction problem may help to clarify the above discussion. Consider the electrical system depicted below in Figure 1. This system is typical of an office automation scenario of today.

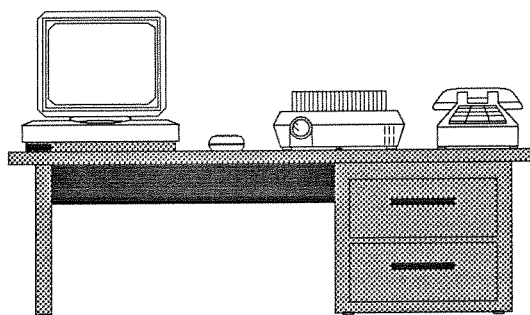


Figure 1 Office automation scenario as an EM interaction problem.

Each of the components depicted in Figure 1 are both emitters and susceptors of electromagnetic energy. Electromagnetic interactions between the components can be characterized via well understood mechanisms. For example, the electromagnetic fields emitted by the printer can couple to the telephone lines, VDT emissions may cause harm to the human operator, and external fields (e.g. lightning emissions) can couple to the power and telephone lines. All of these interactions may cause malfunction or harm to the system.

Chapter 2

Electromagnetic Interaction Modelling

2.1 Problem Definition

Electromagnetic interaction modelling is one of those all-encompassing terms which subsumes the areas of electromagnetic interference and compatibility, electromagnetic pulse (EMP) interactions, and biological effects of electromagnetics. This subsumption is high level and does not concern itself with domain specific details. As is described later, domain-specific details can manifest themselves as user-specific constraints. A summary of the terminology used herein is given in Figure 2. Note that only the terms *EMI*, for *electromagnetic interaction*, and *electromagnetic hardening* (defined below) are used. Other terms which have often been used to describe electromagnetic effects on systems, for example *RFI* (radio frequency interference), *EMI* (electromagnetic interference), *EMP* interactions, and *EMC* (electromagnetic compatibility), are superfluous in the present context.

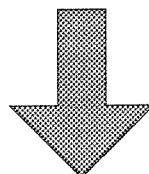
The problem is to model the electromagnetic interactions which take place between electrical components in a complex system. External disturbances are considered as deriving from an *external component* in the system. The process of rendering these systems acceptably immune to the interactions is called *electromagnetic hardening* and, once achieved, the system is said to be *electromagnetically hardened*.

Part 1

2.2 Traditional Approach

Traditionally, the formal approach to the control of electromagnetic effects has been through the use of official standards (see [Keiser 87],[White 73]) such as *FCC Rules and Regulations, Parts 15 and 18* and *Mil-Std-461C, Electromagnetic Emissions and Susceptibility Requirements for the Control of Electromagnetic Interference*. These standards are written by government and industry officials with the purpose of rendering susceptible systems electromagnetically safe and compatible in their environments. Thus, a typical standard will impose: a) limits on the electromagnetic emissions from electronic equipment; and b) maximum acceptable susceptibility levels for manufactured systems. Producers of equipment must then ensure the compliance of their product to the applicable standards.

- Radio Frequency Interference (RFI).
- Electromagnetic Interference (EMI).
- Electromagnetic Pulse (EMP).
- Electromagnetic Compatibility (EMC).



- Electromagnetic Interaction (EMI).
- Electromagnetic Hardening.

Figure 2 Summary of terminology

Part 1

Inherent in this approach is the *politics* of meeting standards. That is, when the producer's effort goes into meeting the standard only *after* the equipment has been designed, the real purpose of the standard, that of producing safe and compatible systems, may be lost. Often, little forethought to possible EM problems is put into the design of the equipment. When EM problems are found, it is not uncommon for an equipment manufacturer to spend more time writing *waivers* than trying to solve the problems.

The question arises as to whether or not this is the *best* approach. Certainly, from an enforcement point of view, *standards are necessary*; whether these standards are the only criteria a producer should use to verify a system is questionable. Of course this is up to the scrutiny of the producer and is dependent on prudent discrimination.

2.3 Computer Aided Electromagnetic Modelling

The purpose here is *not* to derive a foolproof method of enforcing certain standards but to give equipment producers (and other interested parties) a useful tool in the form of a constraint-based advisor, in order to make systems:

- 1) electromagnetically safe and compatible while *at the same time*;
- 2) compliant with appropriate standards.

Most importantly, the advisor could eventually be used at the planning stages in the design of a system in order to make the system electromagnetically reliable.

Modelling of electromagnetic interactions between physical systems requires the examination of the compounded and propagated effects of the associated electromagnetics. This is why a useful approach is one which is *incremental* and *constraint based*. To model it as such, it is essential to subdivide the modelling task into several processes which operate in a distributed manner. The knowledge required in modelling the electromagnetic interactions of systems includes the *electromagnetic topology* of the system and the

Part I

electromagnetic attributes of each node in the topology. The representation of this knowledge in a form amenable to computer implementation is discussed in Chapters 3 to 5.

A prototype of some of the constraints used to model electromagnetic interactions has been implemented in Quintus Prolog™ on a Sun™ workstation [LoVetri 89, 90b, 90c]. The advisor, *HardSys*, determines the emitter, susceptor, shielding effectiveness and the likelihood of failure of an electromagnetically affected system. *HardSys*, is interfaced to a unique topology input drawing tool, *HardDraw*, which runs under an NRC interface implemented in the NeWS™ windowing environment. The implementation of *HardSys* and *HardDraw* is described in Chapter 6.

The application of these tools to the NEMP hardening (Nuclear Electromagnetic Pulse) of a typical helicopter is described in Chapter 7. Part 1 is concluded in Chapter 8 with some of the planned future work for the advisor and drawing tool.

Chapter 3

Electromagnetic Topology of Systems

In order to model the EM interaction of a system, it is first necessary to understand and represent the *relevant physical* attributes of the system. An example of a procedure for accomplishing this has been described by Baum [Baum 80, 85], Messier [Messier 85, 86] and Tesche [Tesche 78]. In this procedure, an electromagnetic system is decomposed into an *electromagnetic shielding topology* and its dual graph or *interaction sequence diagram*.

The electromagnetic topology consists of a description of the electromagnetically distinct volumes and their associated surfaces. The distinct volumes are used to define the *electromagnetic components* involved in the interaction. The interaction sequence diagram keeps track of the *interaction paths* throughout the system. The two procedures are not independent of each other since the interaction sequence diagram can usually be derived from a given electromagnetic shielding topology and the associated electromagnetic attributes of each item in the topology. Variations on the labelling of these graphs and topology have been investigated by Noss [Noss 86]. Many labelling schemes are possible, each having its own advantages and disadvantages. Labelling will turn out to be unimportant as considered herein since each volume and surface node will be labelled with a physically meaningful name in the software implementation. In the following sections the terminology and labelling scheme used by Baum [Baum 85] is followed.

Part 1

3.1 Topological Decompositions

The topological description of a system divides its Euclidean space \Re^3 into a set of volumes denoted $\{V_\delta\}$. The superscript $+$ will be used for the closure of a set and the superscript $-$ for the removal of closure from a set. Thus the complete \Re^3 space can be represented as a union over the set of volumes $\{V_\delta\}$ of a specific volume decomposition of \Re^3 as

$$\Re^3 = \bigcup_{\delta} V_{\delta}^{+} \quad (3.1)$$

where the volumes are defined such that

$$V_{\delta} \cap V_{\delta'} = \begin{cases} V_{\delta}; (\delta \equiv \delta') \\ \emptyset; (\delta \neq \delta') \end{cases} \quad (3.2)$$

and $\bigcup_{\delta} V_{\delta}$ denotes union over all subscripts, \cap denotes intersection, and \emptyset is the empty set. Each element of the volume decomposition set $\{V_\delta\}$ has an associated set of boundary surfaces denoted $\{S_{\delta;\delta'}\}$. The closure of $S_{\delta;\delta'}$ is given by

$$S_{\delta;\delta'}^{+} \equiv V_{\delta}^{+} \cap V_{\delta'}^{+} \equiv S_{\delta';\delta}^{+} \text{ for } \delta \neq \delta'. \quad (3.3)$$

Boundary and contour operators can now be defined as

$$S(V_{\delta}) \equiv V_{\delta}^{+} - V_{\delta} \equiv S(V_{\delta}^{+}) \quad (3.4)$$

and

$$C(S_{\delta;\delta'}) \equiv S_{\delta;\delta'}^{+} - S_{\delta;\delta'} \equiv C(V_{\delta;\delta'}^{+}) \quad (3.5)$$

respectively. An example is given in Figure 3.

Part 1

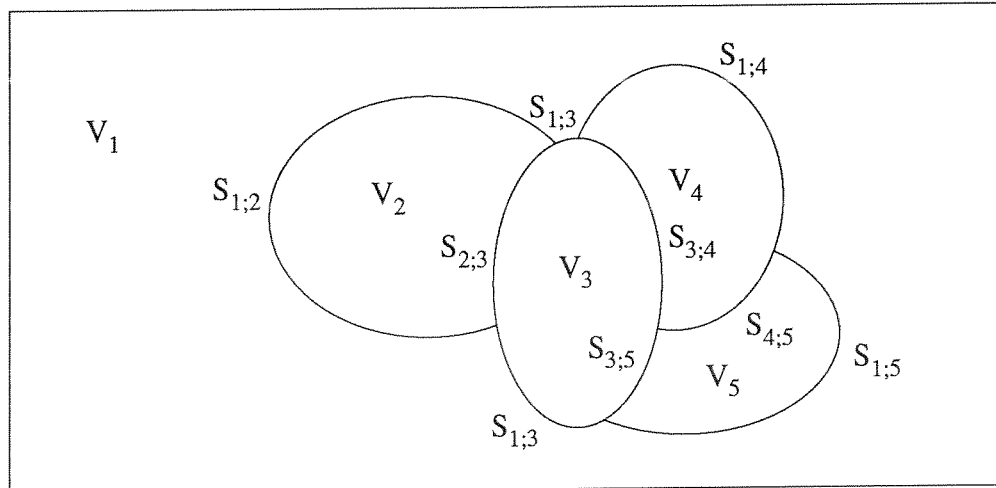


Figure 3 Example of a specific volume/surface topology

As can be seen in Figure 3, the surfaces can be disjoint. For example, surface $S_{1;3}$ is made up of two disjoint pieces. The outer volume, V_1 has a boundary surface given by

$$S(V_1) = S(V_1^+) = \bigcup_{\delta \neq 1} S_{1;\delta}^+ \quad (3.6)$$

which, in this specific case, can be written out as $S(V_1) = S_{1;2} + S_{1;3} + S_{1;4} + S_{1;5}$. In fact the total surface surrounding any volume can be written as the union over the individual surfaces between the volume and all other volumes as

$$S(V_\delta) = S(V_\delta^+) = \bigcup_{\delta' \neq \delta} S_{\delta';\delta}^+ , \quad (3.7)$$

where this total surface contains no boundary curve (i.e. $C(S(V_\delta))=0$). Also, curves themselves have no end points since the boundary of a surface $S_{\delta;\delta'}$ is in general a closed curve with no beginning or end.

Part 1

3.2 Some Graph Theory Definitions and Techniques

In this section some terminology taken from graph theory (see Bondy [Bondy 76]) will be defined. This terminology will be used throughout the subsequent discussions. Some techniques developed for weighted graphs will also be explored.

A graph G can be described in an ordered triple $(V(G), E(G), \psi_G)$; where $V(G)$ is a nonempty set of vertices, $E(G)$ is a set of edges disjoint or independent of V , and ψ_G is an *incidence function* which associates a (not necessarily distinct) unordered pair of vertices of G to each edge of G . Thus, a graph defined by $(V(G), E(G), \psi_G)$ where

$$V(G) = \{v_1, v_2, v_3, v_4\},$$

$$E(G) = \{e_1, e_2, e_3, e_4, e_5, e_6\},$$

and the incidence function is given as

$$\begin{aligned}\psi_G(e_1) &= v_1v_2, \psi_G(e_2) = v_2v_3, \psi_G(e_3) = v_3v_3, \psi_G(e_4) = v_3v_4, \psi_G(e_5) = v_4v_1, \text{ and} \\ \psi_G(e_6) &= v_1v_2,\end{aligned}$$

is depicted below in Figure 4.

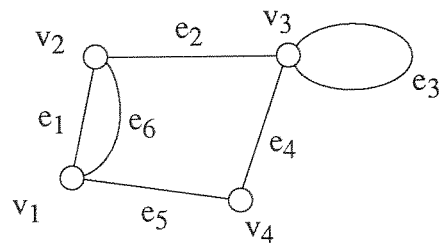


Figure 4 Example of a general graph

If a graph contains no loops (edge e_3 in the above figure is a loop) and no two edges join the same pair of vertices (as do e_1 and e_6 above) then it is called a *simple graph*.

Part 1

A *bipartite graph* is a graph in which the vertex set, say $V(G)$, can be partitioned into two subsets, say X and Y , such that each edge of the graph has one end in X and the other end in Y . The partition (X, Y) is called the bipartition of the graph. The graph shown below in Figure 5 is obviously bipartite where the vertices corresponding to the two sets of the bipartition are depicted differently (i.e. solid and hollow).

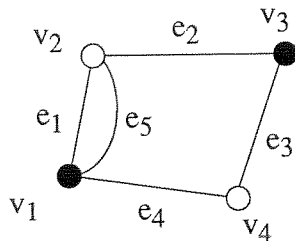


Figure 5 Example of a bipartite graph

Given two graphs G and H , H is said to be a *subgraph* of G , denoted $H \subseteq G$, if $V(H) \subseteq V(G)$, $E(H) \subseteq E(G)$, and ψ_H is the restriction or imposition of ψ_G to $E(H)$. If $H \subseteq G$ but $H \neq G$ then H is said to be a proper subgraph of G , denoted $H \subset G$. Also, G is said to be a *supergraph* of H . A *spanning subgraph* of G is a subgraph H with $V(H) = V(G)$. If H_1 and H_2 are subgraphs of G then H_1 and H_2 are said to be *disjoint* if they have no vertex in common and *edge-disjoint* if they have no edge in common.

The *union* of two graphs H_1 and H_2 , denoted $H_1 \cup H_2$, is a subgraph with vertex set $V(H_1) \cup V(H_2)$ and edge set $E(H_1) \cup E(H_2)$. If H_1 and H_2 are disjoint then their union is denoted $H_1 + H_2$. The *intersection* of H_1 and H_2 , denoted $H_1 \cap H_2$, is a subgraph with vertex set $V(H_1) \cap V(H_2) \neq \emptyset$ and edge set $E(H_1) \cap E(H_2)$.

The *vertex degree* $d_G(v)$ of a vertex v in G is the number of edges of G incident with vertex v , where a loop (i.e. an edge with incidence function being an ordered pair of the same vertex) counts as two edges. The *minimum degree* of vertices of G is denoted $\delta(G)$ while the *maximum degree* is denoted $\Delta(G)$. Thus the vertex degree of the surface vertices

Part 1

(i.e. the Y partition vertices) in a topological decomposition is exactly two. Therefore the minimum degree is less than or equal to two. It can be shown (see Bondy [Bondy 76]) that in any graph the number of vertices of odd degree is even. Therefore, since the surface vertices have even degree, the number of volume vertices with odd degree must be even.

A *walk* in a graph G is a finite non-null sequence $W = v_0e_1v_1e_2v_2 \dots e_kv_k$ whose terms are alternately vertices and edges such that for $1 \leq i \leq k$ the ends of e_i are the vertices v_{i-1} and v_i . The walk W may be denoted as $W = (v_0, v_k)$ and W is said to be a walk from vertex v_0 to vertex v_k . Also, v_0 is said to be the *origin* of the walk and v_k the *terminus*. The vertices v_1 to v_{k-1} are called *internal vertices* while k is the *length* ($\varepsilon(W)$) of the walk. A *section* of walk from v_i to v_j is a subsequence of W denoted as a (v_i, v_j) section of W. Walks can be *concatenated* if the terminus of one walk, say W, is the origin of another, say W' , and the resulting walk is denoted by WW' . Walks can also be *inverted*, denoted W^{-1} , where the sequence is taken backwards from terminus to origin. If the edges of a walk W are distinct then W is called a *trail*; if the vertices are *also* distinct then W is called a *path*.

Two vertices of a graph G, u and v say, are said to be *connected* if there is a (u, v) path in G. A graph G can be partitioned into *components* $G[V_1], G[V_2], \dots, G[V_\omega]$ of G, generated by partitioning V into nonempty subsets $V_1, V_2, \dots, V_\omega$ such that two vertices of V are connected if and only if they belong to the same subset V_i . The graph G is said to be *connected* if all its vertices are connected, otherwise it is called a *disconnected* graph.

A *closed walk* is one in which the origin and terminus are the same. A *cycle* is a closed trail wherein the origin and the internal vertices are distinct. A *k-cycle* is a cycle of length k while a *3-cycle* is also called a triangle. Thus it can be shown that a graph is bipartite if and only if it contains no odd cycles. An *acyclic* graph is one which contains no cycles. An acyclic graph which is also connected is called a *tree*. In a tree, any two vertices are connected by a unique path.

Part 1

A graph G is called a *weighted graph* if for every edge $e \in E(G)$ there exists a weight $w(e) \in \mathbb{R}$ (real number). If H is a subgraph of G then the weight of H is given as the sum of the individual edge weights in H

$$w(H) = \sum_{e \in E(H)} w(e) \quad (3.8)$$

and the weight of a path in G is called the *length* of the path. The minimum weight of a (u, v) path is called the *distance* $d(u, v)$. If two vertices, u and v , are not connected by an edge, that is if $uv \notin E$, then the weight of uv is assumed infinite (i.e. $w(uv) = \infty$).

A graph algorithm for finding the shortest path from a root vertex u_0 to all other vertices in the graph is *Dijkstra's algorithm* named after its founder (see [Dijkstra 59], and [Bondy 76] pp 19 - 20). This algorithm will be of use later when the worst case electromagnetic shielding paths will need to be found. Actually, in Dijkstra's 1959 article he gives two algorithms. The first finds the tree of minimum weight which spans a connected graph G , called the *minimum spanning tree* of the graph. The second finds the path of minimum distance between a root vertex u_0 and the rest of the vertices of G , called the *minimal spanning tree single source problem*. It is this second algorithm which is required for later discussions of electromagnetic modelling.

The algorithm uses the fact that if S is a proper subset of V , where the root vertex is chosen so that it is an element of S , then

$$d(u_0, \bar{S}) = \min \{ d(u_0, u) + w(uv) \} \Big|_{u \in S, v \in \bar{S}} \quad (3.9)$$

where \bar{S} is $V - S$. An increasing sequence of subsets S_0, S_1, \dots, S_v of V is constructed (with $S_0 = \{u_0\}$) so that once the i^{th} subset is constructed the shortest paths from the root vertex u_0 to all the vertices in S_i will be known. These shortest paths will be denoted $P(u_0v)$ where $v \in S_i$. The algorithm is shown in Figure 6.

Part 1

Dijkstra's Algorithm

$S = \{u_0\}; \bar{S} = V - S; L(u_0) = 0;$

Loop 1: $\forall v \in \bar{S};$

$L(v) = \infty; P(u_0 v) = \{u_0\};$

end Loop 1;

$i = 0;$

Loop 2: *while* $\bar{S} \neq \emptyset;$

min_label = $\infty;$

Loop 3: $\forall v \in \bar{S};$

if $L(u_i) + w(u_i v) < L(v)$ *then*

$L(v) = L(u_i) + w(u_i v);$

$P(u_0 v) = P(u_0 u_i) \cup v;$

endif

if $L(v) < \text{min_label}$ *then*

$\text{min_v} = v; \text{min_label} = L(v);$

endif

end Loop 3;

$u_{i+1} = \text{min_v}; S = S \cup u_{i+1}; \bar{S} = \bar{S} - u_{i+1}; i = i + 1;$

end Loop 2;

Figure 6 Dijkstra's algorithm with shortest path determination

Part 1

When the algorithm terminates, the labels at each vertex $L(v)$, $v \in V$, will contain the distance from the root vertex u_0 and the path variable $P(u_0 v)$ will contain the minimum path specification as a list of vertices from the root vertex to v . Note that a list of vertices is sufficient to represent a path in a simple graph. An example of the use of this algorithm is given below in Figure 5 where the labels and paths after each step are shown next to the graph. The edge weights and the root vertex are identified in the first drawing.

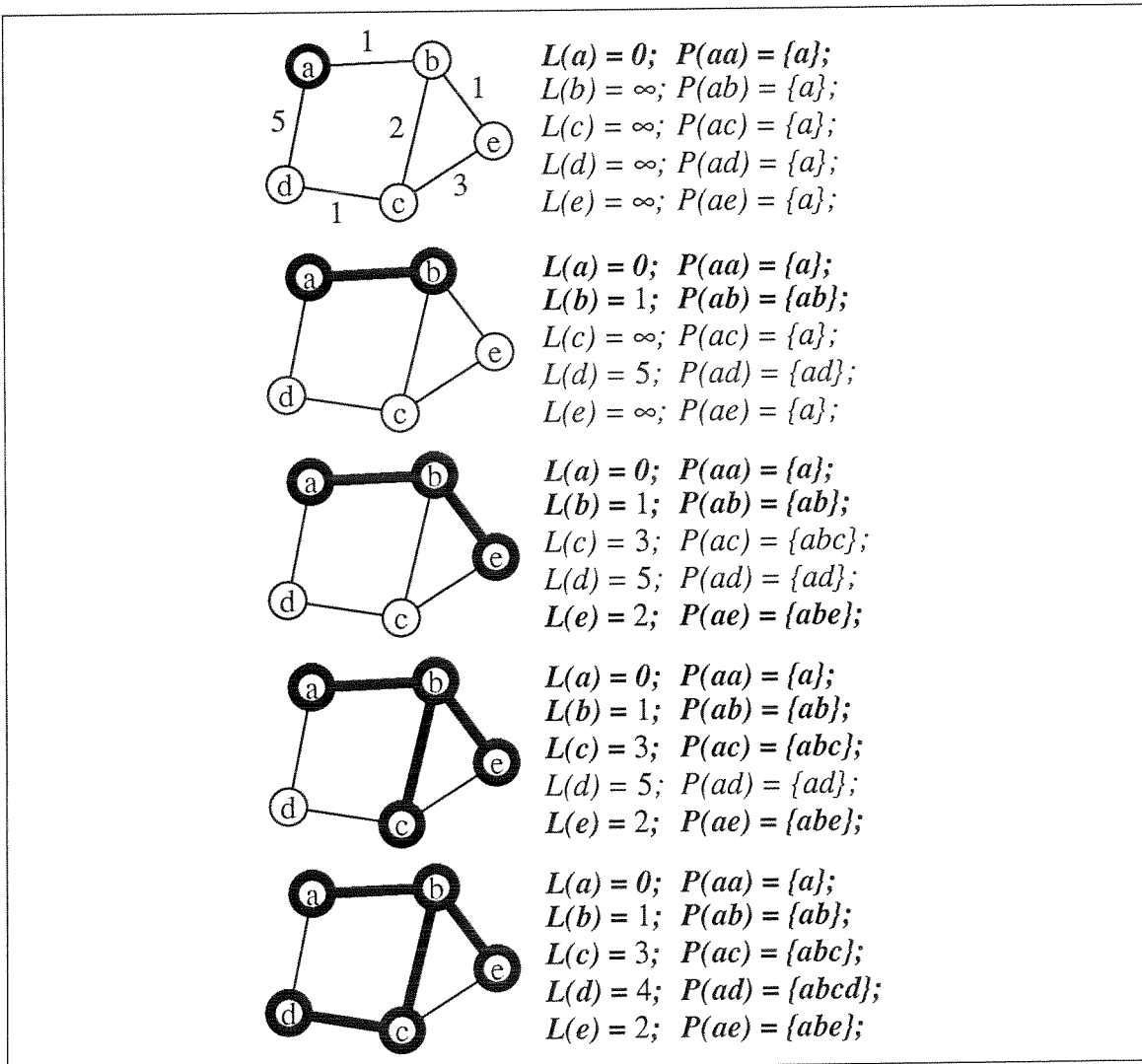


Figure 7 Example application of shortest path algorithm

Part 1

In Figure 5 the bold vertices represent the elements of each subset S after each step in the algorithm. The final paths are shown in the bottom diagram of the figure with the distances given by the labels. Of course, if the distance to only one vertex from the root vertex is required, the algorithm is terminated when that vertex is reached. This algorithm, albeit a *good* algorithm (i.e. it is of order v^2 where v is the number of vertices), will still end up taking an enormous amount of computer time for some practical situations where $v \approx 100$ is reasonable (as will be discussed later).

In order to reduce the computer time required to determine minimum paths through a graph the concepts of a *cut vertex*, a *cut edge*, and *grouping* will be introduced here for later use.

Given a graph $G = \{V, E, \psi_G\}$, if E can be partitioned into two nonempty subsets, say E_1 , and E_2 , such that the subgraphs generated from these subsets, that is $G[E_1]$ and $G[E_2]$, have just a vertex v in common, then v is called a cut vertex. If G is a tree then v is a cut vertex if and only if $d(v) > 1$. If G is nontrivial (i.e. it has more than one vertex) and contains no loops, then a vertex v is a cut vertex of G if and only if $\omega(G-v) > \omega(G)$ where the number $\omega(G)$ denotes the number of components of G . Thus, if removing a vertex v increases the number of components of G , then v is a cut vertex. A cut edge is an edge e of G such that if the edge is removed from G , the number of components will increase, that is $\omega(G - e) > \omega(G)$. An edge e is a cut edge if and only if it is not contained in any cycles of G . Examples of a cut edge (in bold) and a cut vertex (in bold) are given below in Figure 8.

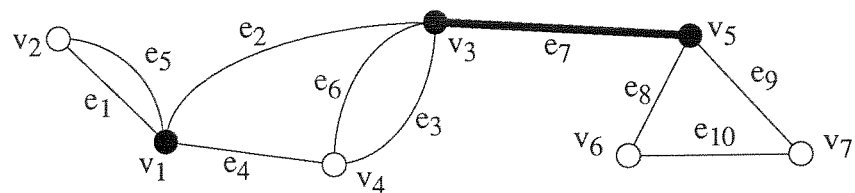


Figure 8 Cut vertex and cut edge examples

Part 1

Thus, in Figure 8, vertices v_1 , v_3 , and v_5 are cut vertices while edge e_7 is the only cut edge. A set of vertices forms a valid grouping if it is equal to a vertex set of one of the subgraph partitions generated by a cut vertex. The valid grouping includes the cut vertex and the group can be represented in the graph by a *grouped vertex* in place of the cut vertex. For example, in Figure 9 below, vertices v_5 , v_7 , v_6 , and cut vertex v_3 of Figure 8 form a valid grouping and are represented by grouped vertex v_3 .

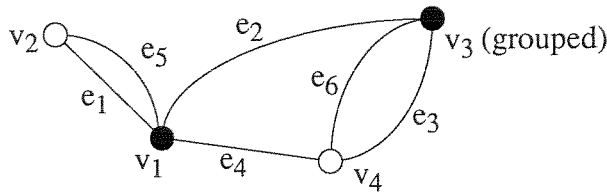


Figure 9 Grouped vertex example

Similarly vertices v_1 , v_2 , and v_4 , could also have been grouped into vertex v_3 . Thus, there are usually many options for grouping in a graph. The process of grouping will be required to reduce the search space when minimum path algorithms are used. For example, if in Figure 8 the minimum paths from root vertex v_2 to all other vertices in the graph have been found and there is a change in the graph which affects the minimum path to v_3 , then this change will also affect the minimum paths from the root vertex to the grouped vertices.

The subgraph containing vertices which are not expected to change may be grouped as a valid grouping. This results in the removal of the grouped vertices from the search space of the minimum path algorithm. That is, once the minimal path tree from the grouped vertex to the rest of the vertices in the group has been determined, changes in other parts of the graph will not affect *this* minimal path tree.

Part 1

3.3 Equivalent Graph of Volume/Surface Topology

The interaction sequence diagram can be obtained as a *graph* with *nodes* or *vertices* representing volumes, and *edges* representing surfaces. For example, the equivalent graph G of Figure 3 can be described by the set of vertices and edges

$$V(G) = \{V_1, V_2, V_3, V_4, V_5\}, \quad (3.10)$$

$$E(G) = \{e_1, e_2, e_3, e_4, e_5, e_6, e_7, e_8\}, \quad (3.11)$$

with incidence function defined as

$$\psi_G = \psi_G(e_i = S_{\delta; \delta'}) = V_\delta V_{\delta'}, \quad (3.12)$$

where $e_1 = S_{1;2}$, $e_2 = S_{1;4}$, $e_3 = S_{2;3}$, $e_4 = S_{3;4}$, $e_5 = S_{1;3}$, $e_6 = S_{3;5}$, $e_7 = S_{4;5}$, $e_8 = S_{1;5}$. This graph is shown below in Figure 10.

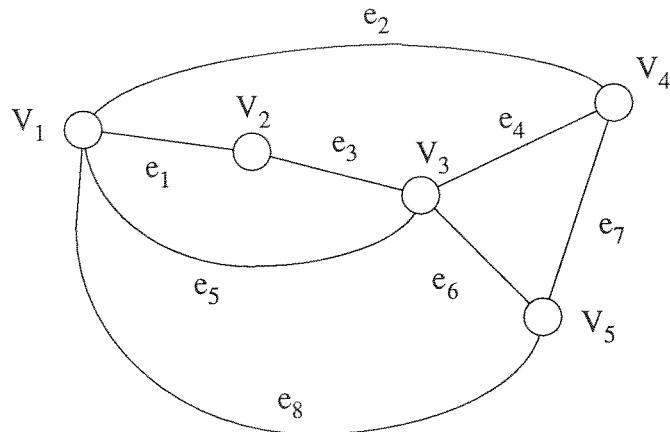


Figure 10 Equivalent graph (interaction sequence diagram) of volume/surface topology

The representation of the surfaces can be made more explicit by using the bipartite graph (see Baum, p.9 [Baum 85]). The bipartite graph corresponding to the topology of Figure 3 is shown in Figure 11.

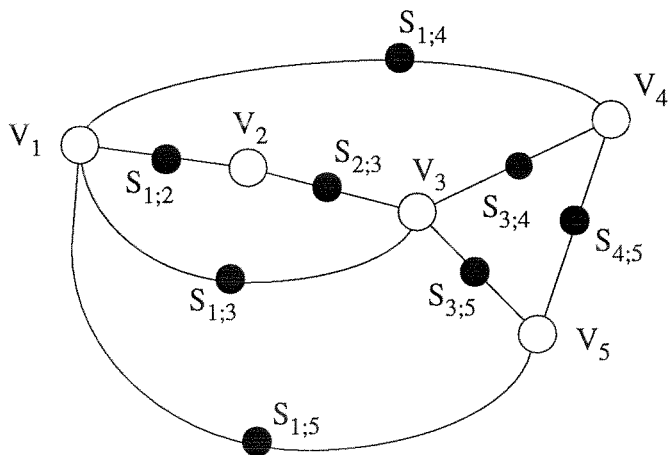
Part 1

Figure 11 Bipartite Graph of Example Topology

For the above example the bipartition is given as

$$(X, Y) = (\{V_1, V_2, V_3, V_4, V_5\}, \{S_{1;2}, S_{1;3}, S_{1;4}, S_{2;3}, S_{3;4}, S_{3;5}, S_{4;5}\}) \quad (3.13)$$

where now the surfaces themselves are represented as the set Y of surface nodes. It should be noticed that although the bipartite graph definition does *not* require it, all bipartite graph representations of volume/surface topologies will be such that the surface nodes connect to *exactly* two edges. Thus, the way in which it is used herein, the surface nodes are really edge labels. It is useful to maintain the notation of separate surface nodes since specific attributes will be stored in each of the surface nodes and it is reasonable to have them explicitly depicted in the graph diagrams.

As will become apparent later in the use of this representation, the attributes associated with surface nodes may be *directed attributes*. This can easily be handled by the use of a *directed graph* or *digraph*. A digraph D can be described the same way as a normal graph except that the edges are now called *arcs* and the incidence function ψ_D associates with each arc of D an *ordered* pair of (not necessarily distinct) vertices or nodes of D. Usually, the arcs are depicted with arrows as shown in Figure 12. In this figure the arc labels

Part 1

are given explicitly on the graph so that the incidence function ψ_D is equivalent to ψ_G of equation (3.12).

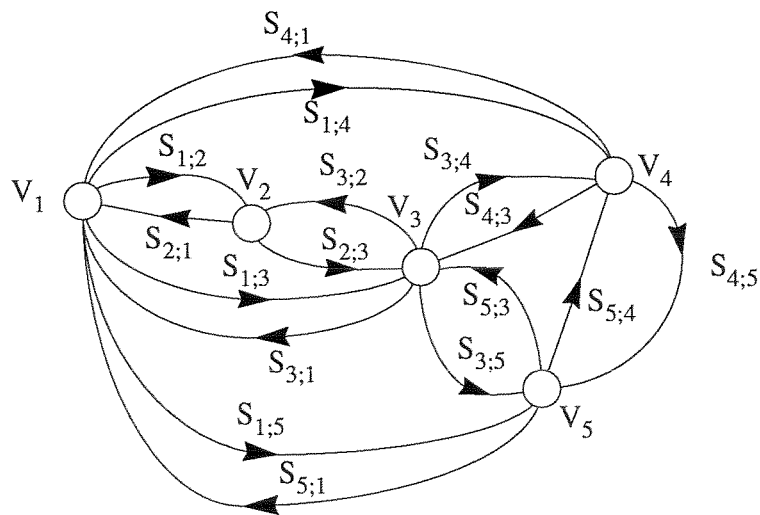


Figure 12 Digraph representation

The digraph of Figure 12 can be directly transformed to the more explicit bipartite type representation by labelling each arc with a *directed surface node* as in Figure 13. The directed attributes will be stored in the appropriate surface nodes of the bipartite digraph and each topological surface may be represented by up to two directed surface nodes.

It will be apparent from the context of the discussion when the directional aspects of the path through a surface is being referred to. Thus, in order to simplify the diagrams of the following discussions, both directed surface nodes will not be drawn in the graph representations. Also, the arrows will be omitted since the direction of the arc will be implied by the name of the directed surface node. Hence, the bipartite digraph of Figure 13 may be drawn simply as that of Figure 11 (which does not depict the specific directed nodes) when it is unambiguous to do so.

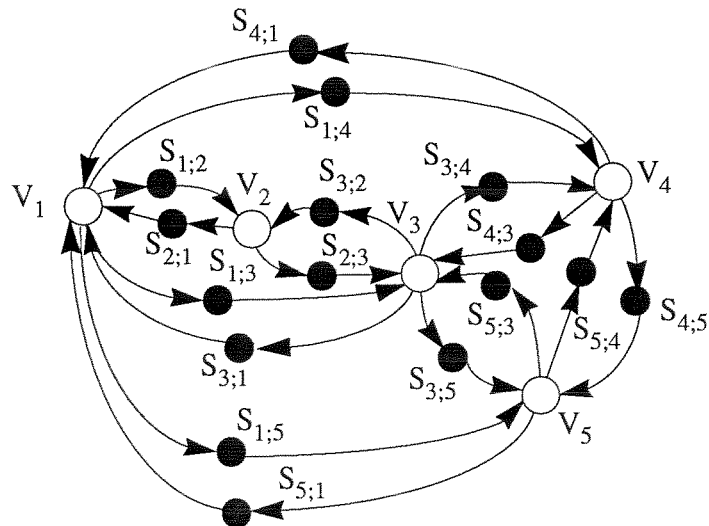


Figure 13 Bipartite digraph representation

3.4 Summary of Topological Decomposition

A physical system can be *mapped* into an electromagnetic topology, or equivalently into a bipartite digraph which characterizes the interaction paths between electromagnetic components. This mapping of the physical system into an electromagnetic topology is not unique; many different mappings can be found to partially describe the interactions which will take place in the system. The specific topology used will depend on the type of interactions of interest, as well as the level of detail required in the model. Examples of this will be given in the next chapter where typical electromagnetic components are topologically decomposed.

A summary of the equivalent terms used in the different representations, including implementation terminology to be described later, is summarized in Table 3.1.

Part 1

Table 3.1
Summary of Terminology

Physical System	Electromagnetic Component	Interaction Path or Mechanism
Electromagnetic Topology	Volume	Surface
Bipartite Digraph	Vertex or Node	Directed Vertex or Node
Prolog Implementation	Object	Object

The characterization of a real system using this method requires a detailed understanding of electromagnetic interactions through shielding nodes. Each volume contains its own emitters of electromagnetic energy and susceptors to electromagnetic energy. The emissions propagate throughout the graph to reach other susceptors located at other nodes. Evaluating the exact electromagnetic interaction for even the simple graph shown in Figure 11 is numerically difficult, if not impossible.

Chapter 4

Electromagnetic Component and Interaction Path Attributes

The first step in modelling a complex system is to approximate the propagation of electromagnetic energy from one volume node to another. This is accomplished by defining the electromagnetic attributes of each electromagnetic component in the topology as well as attributes for the interaction paths between the components. These attributes *constrain* the propagation of the electromagnetic disturbances throughout the topology. The implementation of these attributes as a *constraint network* representing the complete electromagnetic topology will be described in the next chapter.

Presently, the definition of the relevant electromagnetic attributes of the individual nodes of the bipartite graph representation of a topology will be discussed. It is sufficient to consider just one electromagnetic interaction path as shown in Figure 14.

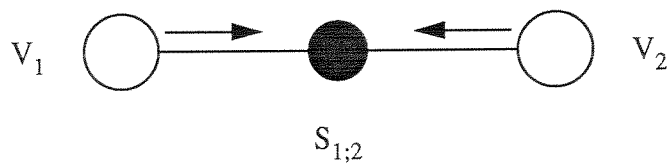


Figure 14 Single electromagnetic interaction path

Part 1

The attributes are used to represent the electromagnetic knowledge which is known about a system. It must be realized that many representations of this knowledge are possible but that the acceptable scheme is the one which achieves an acceptable trade off between approximation and usefulness. The characteristics given in Table 4.1 below are desirable in an electromagnetic representation.

Table 4.1
Desirable Qualities of an Electromagnetic Approximation Scheme

1. Must be easily derivable from available experimental/numerical data.
2. Must be an amenable qualitative form (symbolic manipulation).
3. Useful quantitative results and recommendations can be derived.
4. Has the capability to handle exceptions.
5. Has variable levels of approximation (coarse to fine).

These desirable qualities of an electromagnetic approximation scheme are used as a guide in defining an appropriate heuristic approach to the understanding of electromagnetic interactions.

4.1 Frequency Domain Representation

Most electromagnetic interaction phenomena are calculated, measured, and reported as quantified data in the frequency domain. The reason for this is that most useful engineering information about fields, susceptibilities, and paths of interaction can be characterized *only* in the frequency domain.

For example, the concept of frequency domain filtering can be used to characterize almost all *linear* paths of interaction. It is well known that an aperture in a shield acts as a high-pass filter in the path of the electromagnetic fields (see [Schulz 88]). Emissions from equipment are often measured using receivers with specific bandwidths of reception over

Part 1

large ranges of frequency (see [Mil-Std-462] and [Mil-Std-461C]). Furthermore, susceptibilities of electronic components such as microelectronic circuitry are also calculated in the frequency domain.

The advantages of frequency domain representations are obvious for linear systems; almost any waveform can be transformed into the frequency domain via the Fourier coefficients or transform. The following definition of the Fourier coefficients and transform (from [Körner 88]) may help in the understanding of representing time domain data in the frequency domain.

If the function $f: T \rightarrow \mathfrak{I}$ (where $T = \mathfrak{R}/2\pi \mathfrak{N}$ is the unit circle, and \mathfrak{R} , \mathfrak{N} and \mathfrak{I} are the set of real, integers and complex numbers respectively) and the function $g: \mathfrak{R} \rightarrow \mathfrak{I}$. Then the Fourier coefficients of f are defined over $r \in \mathfrak{N}$ as:

$$\hat{f}(r) = \frac{1}{2\pi} \int_T f(t) e^{-irt} dt; \quad [r \in \mathfrak{N}]; \quad (4.1)$$

and the Fourier transform of g is defined over $\zeta \in \mathfrak{R}$ as:

$$\hat{g}(\zeta) = \int_{\mathfrak{R}} g(t) e^{-i\zeta t} dt; \quad [\zeta \in \mathfrak{R}]. \quad (4.2)$$

The Fourier coefficients and transform are in general complex numbers (i.e. may be represented with an *amplitude* and a *phase*). This should be considered when the above are used in approximations. Notice that if instead of being defined on the *unit* circle a function of time $f(t)$ is periodic with period a then equation (4.1) is transformed to:

$$\hat{f}(r) = \frac{1}{2\pi} \int_T f\left(\frac{ta}{2\pi}\right) e^{-irt} dt = \frac{1}{a} \int_{T \times \frac{a}{2\pi}} f(\tau) e^{-i2\pi r \frac{\tau}{a}} d\tau; \quad [r \in \mathfrak{N}]; \quad (4.3)$$

or re-writing the coefficients in terms of $f_0 = 1/a$ and $f_r = rf_0$ equation (4.3) becomes

Part 1

$$\hat{f}(f_r) = \frac{1}{a} \int_{T \times \frac{a}{2\pi}} f(t) e^{-i2\pi r f_0 t} dt; [r \in \mathbb{N}] ; \quad (4.4)$$

which is the usual form for writing the Fourier series coefficients.

In practice, the *Discrete Fourier Transform* (DFT) is used to calculate the Fourier coefficients of a discretized or sampled time domain signal and an algorithm known as the *Fast Fourier Transform* (FFT) is used to implement the DFT efficiently (see Brigham [Brigham 74] and Roden, pp 50-53 [Roden 79]).

If a time domain signal $g(t)$ is sampled with a sampling period of Δt for N samples and if it is assumed that this signal is a time limited function (i.e. zero outside the interval $0 < t < N\Delta t$) then the Fourier transform can be written as:

$$\hat{g}(\zeta) = \int_0^{N\Delta t} g(t) e^{-i\zeta t} dt ; [\zeta \in \mathfrak{R}] ; \quad (4.5)$$

which for the sampled waveform $g(r\Delta t)$ can be approximated by the summation:

$$\hat{g}(\zeta) = \sum_0^{r-1} g(r\Delta t) e^{-i\zeta r \Delta t} \Delta t ; [r \in \mathbb{N}] . \quad (4.6)$$

Now the DFT is calculated at the discrete frequencies $\zeta_s = 2\pi f_s = 2\pi s f_0 = 2\pi s/a$ as:

$$\hat{g}(f_s) = \left(\frac{1}{N} \right) \sum_0^{r-1} g(r\Delta t) e^{-isr2\pi f_0 \Delta t} ; [r, s \in \mathbb{N}] . \quad (4.7)$$

Therefore, comparing equation (4.6) and equation (4.7) it is seen that after the calculation of the DFT using a FFT algorithm has been performed, the result should be multiplied by $a = N\Delta t$ in order that an approximation to the Fourier transform can be obtained. In actual

Part 1

fact then, the DFT/FFT procedure is an approximation to the Fourier series coefficients and as such produces an approximation to the *periodic continuation* (with period a) of the time limited function $g(t)$.

Explicit use of these formulae to obtain data will be rare since, as has already been noted, experimental and theoretical results are already reported in the frequency domain. Thus, in order to satisfy *desirable quality* one and three of table 4.1, all electromagnetic component and path attributes are represented in the frequency domain via the Fourier transform. All attributes presented in the following sections are specified over quantized frequency ranges. For example, the frequency ranges may be defined as shown below.

Example Frequency Ranges

$f < 100 \text{ Hz}$
$100 < f < 1 \text{ KHz}$
$1\text{KHz} < f < 10 \text{ MHz}$
$10 \text{ MHz} < f < 100 \text{ MHz}$
$100 \text{ MHz} < f < 1 \text{ GHz}$
$1 \text{ GHz} < f$

Figure 15 Example frequency range description

Each attribute does not need to be specified over the same frequency ranges. A normalization procedure is used to combine attributes specified over different frequency ranges.

Now when multiple sets of time domain data are converted to the frequency domain one must be careful that the same transform technique is used for all the sets of data. This point can be made clearer by a careful study of the units which the transformed data takes on.

Part 1

For example, assume that two sets of time domain waveforms are sampled, each having the units appropriate to electric field strength (i.e. [V/m]). Applying a Fourier transform to these waveforms would produce the units [Vs/m] as can easily be seen from equation (4.2). Now due to the linearity property of the Fourier transform operator the two sets of data can be summed in the frequency domain (i.e. summation of complex numbers) and transformed back to time producing the sum of the time domain waveforms.

If the Fourier coefficients are derived from the time domain data (assuming periodicity of period a) then the [V/m] units remain the same for the coefficients. This is not at all obvious from the form of equation (4.1) but can be seen more clearly from equation (4.4). Thus it would *not* be correct to compare a Fourier coefficient with the corresponding amplitude of the Fourier transform at the same frequency ($\zeta_s = 2\pi sf_0$).

This point can be further demonstrated by actually performing the Fourier transform of a simple time domain waveform. For the electric field intensity given by the time domain function $E(t) = 50 \sin(2\pi t/a)$ [kV/m], where a is the period of the sinusoid. This represents a continuous wave (cw) signal with a 50 kV/m amplitude. It can easily be shown that the Fourier coefficients $\hat{f}(f_r)$ of this function are given by

$$\hat{f}(f_1) = -i25 \frac{kV}{m}, \quad f_1 = \frac{2\pi}{a}, \quad (4.8)$$

$$\hat{f}(f_{-1}) = i25 \frac{kV}{m}, \quad f_{-1} = \frac{-2\pi}{a}, \quad (4.9)$$

and zero for all other values r . The Fourier transform of $E(t)$ can be determined with the use of *generalized functions*:

$$\hat{g}(\zeta) = i50\pi [\delta(\zeta + \zeta_0) - \delta(\zeta - \zeta_0)] \left[\frac{kVs}{m} \right]; \quad (4.10)$$

Part 1

where $\zeta_0 = 2\pi f_0 = 2\pi/a$. Now in a practical situation, where the signal $E(t)$ is to be compared to either another signal or to a level produced via the Fourier transform with the same units, it is difficult to know how to compare the generalized function $\delta(\zeta)$ to a level on a graph. In general, whenever the time domain functions are periodic the Fourier transform consists of delta functions of varying amplitude along the frequency axis. The amplitude of these delta functions is proportional to the Fourier series coefficients.

One way to compare the Fourier transform of a pure sinusoid to other levels on a graph is by taking the FFT of the sinusoid and then approximating the Fourier transform by multiplying the FFT by a (i.e. the period over which the FFT was taken). This is shown below in Figure 16 where 65536 points were used to perform the FFT of a pure sinusoid over 50 periods.

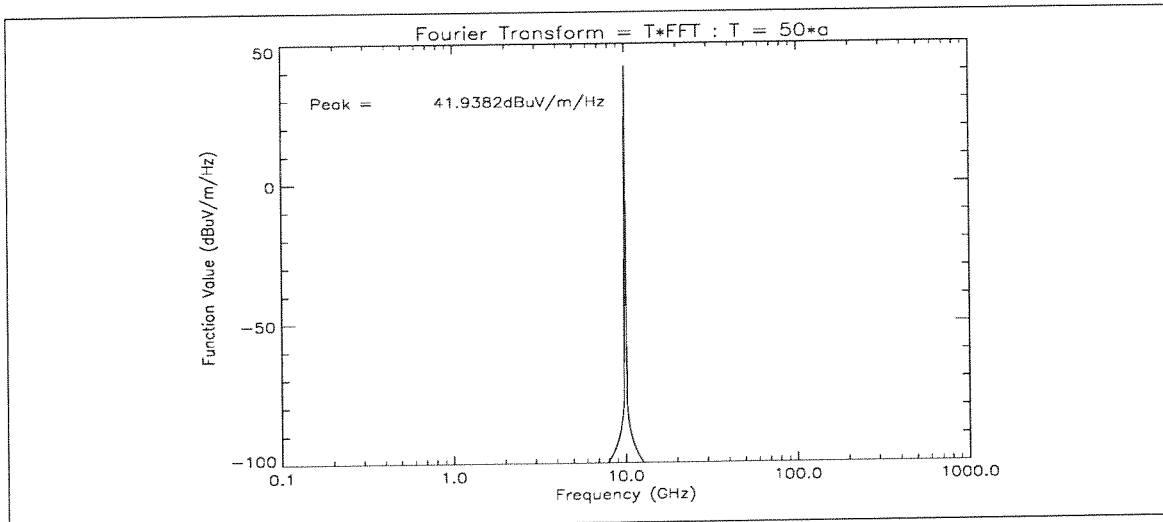


Figure 16 Fourier transform from the FFT of a pure sinusoid

As can be seen in the figure the peak amplitude in the Fourier transform domain of the pure sinusoid is 41.9382 dB μ V/m/Hz which is equivalent to 125.0 μ V/m. Since the FFT was performed over 50 periods or a total time $a = 5$ ns, the graph can be divided through by 5 ns to give the correct Fourier coefficient of 25.0 kV. The FFT assumes the periodic

Part 1

continuation of the time domain function, thus care must be taken to ensure that the time domain function starts and ends at zero (if it is not truly periodic) or that it is applied for an integer number of periods (if it is periodic). If more than 50 periods of the sinusoid would have been used then in the Fourier transform domain the peak amplitude would have become larger. In the limit as $T \rightarrow \infty$, the delta function $\delta(\zeta)$ would be obtained for the Fourier transform, but the Fourier series coefficient would remain the same at 25.0 kV.

Thus it can be seen that the level to be used in the Fourier transform domain is dependent on the time during which the time domain signal lasts. This can also be understood by studying the transform of $\sin(2\pi t/T) \{ u(t+t_0) - u(t-t_0)\}$ where $u(t)$ is the unit step function. The transform of this is equal to:

$$\frac{1}{2\pi i} \left(\frac{\sin(2\pi t_0(f - f_0))}{(f - f_0)} - \frac{\sin(2\pi t_0(f + f_0))}{(f + f_0)} \right) \quad (4.11)$$

a pair of shifted $\text{sinc}(\cdot)$ functions. This function has a height equal to $2t_0$ and the main peak becomes narrower. Thus as $t_0 \rightarrow \infty$, the delta function may be obtained intuitively.

4.2 Electromagnetic Disturbance Representation

It is possible for each component node in an electromagnetic topology to have an electromagnetic disturbance associated with it. The first question which arises is as to what types of electromagnetic disturbances are possible. The usual case is to define the disturbance in terms of either field quantities or circuit quantities. Thus an appropriate classification is to define either:

- 1) electric field E with units of [V/m or dBV/m];
- 2) magnetic field H with units of [A/m or dBA/m];
- 3) and power density P_d with units of [W/m² or dBW/m²];

for **field nodes**, or:

Part 1

- 1) voltage V with units of [V or dBV];
- 2) current I with units of [A or dBA];
- 3) and power P with units of [W or dBW];

for *circuit nodes*. The electromagnetic component node can thus be classified as being either a field node or a circuit node. Examples of the representation of real components will be given later.

The above quantities are not independent of each other and can be related to each other via the wave impedance \bar{Z} (since E and H are generally vectors, \bar{Z} is a tensor of rank two or dyadic) for field nodes as:

$$P_d = (E \times H) \quad (4.12)$$

$$E = \bar{Z}H \quad (4.13)$$

or through a circuit impedance Z for circuit nodes as:

$$P = IV \quad (4.14)$$

$$V = ZI \quad (4.15)$$

where now Z is a scalar quantity.

An understanding of the wave impedance Z is attained through an examination of the nature of the field quantities at different distances away from a source. If the maximum dimension of a radiating component (i.e. current carrying component or aperture) is given as D then a boundary distance between the *far field* and *near field* region can be defined as:

$$r = \frac{\lambda}{2\pi}, \text{ for } D \ll \lambda \quad (4.16)$$

$$r = \frac{D^2}{2\lambda}, \text{ for } D \geq \frac{\lambda}{2} \quad (4.17)$$

Part 1

where λ is the wavelength of the emission (see [Duff 88] pp 2.10-2.21).

In the far field, or *radiation field*, the electric and magnetic field vectors can be shown to propagate perpendicular to each other with an impedance of $\approx 377 \Omega$ (see [Harrington 61]) and both fall off or attenuate in proportion to $1/r$. In the near field, or *induction field*, the impedance between the perpendicular components of the electric and magnetic field vectors is $>> 377 \Omega$ for *electric or high-impedance fields* and $<< 377 \Omega$ for *magnetic or low-impedance fields*. Also, in the near field region all the directional components of the E , H and P_d , vectors may exist, whereas in the far field the E and H vectors are orthogonal to each other and lie in the plane perpendicular to P_d which is directed radially away from the source.

The scalar impedance Z for circuit nodes is the usual concept of circuit analysis. This quantity can range greatly (theoretically from 0 to ∞) in value depending on the application of the circuit. Thus with an understanding of these concepts, a representation of an electromagnetic disturbance can be approximated for an electromagnetic component.

4.2.1 Electromagnetic Disturbance Simplifications

It is now necessary that a *simplified* representation be formulated for the electromagnetic disturbance. In deriving this, the desirable qualities given in Table 4.1 must be kept in mind.

For field nodes the electromagnetic disturbance represents either the actual measured electromagnetic field emitted by the component node or an approximation to this field based on numerical and/or experimental fields of similar components. The first simplification which will be made is to ignore the directional properties of the magnetic and electric fields (i.e. they are treated as scalars). Thus E becomes E , H becomes H , and P_d becomes P . In a sense, this assumes the worst case field orientation properties and does not account for the possibility of poor coupling of fields from emitter to susceptor due to

Part 1

physical orientation in space [McDonnel 78]. This approximation, however, makes the attributes much more amenable to computer implementation. In many practical situations, the exact orientation of the field vectors will not be exactly known, therefore it is reasonable to assume a worst case orientation in the representation.

Implementing this approximation equations (4.3) and (4.4) become

$$P = EH = \frac{E^2}{Z} = H^2 Z \quad [\text{W/m}^2], \quad (4.18)$$

and

$$E = ZH \quad [\text{V/m}], \quad (4.19)$$

which are now in a form isomorphic to the scalar circuit quantities.

Next, a representation of the values of the respective impedances must be determined. Instead of giving the impedance Z a continuous range of values, it is adequate to quantize the domain of Z into three values. These quantized values are chosen to be one of the following:

- 1) electric ($Z > 377 \Omega$);
- 2) magnetic ($Z < 377 \Omega$); or
- 3) plane wave ($Z \approx 377 \Omega$);

for field nodes, or:

- 1) high ($Z \gg 1 \text{ k}\Omega$);
- 2) low ($Z \ll 10 \Omega$); or
- 3) medium ($10 \ll Z \ll 1 \text{ k}\Omega$);

for circuit nodes. The value 377Ω is natural for the field node since this is the impedance of free space. The circuit node impedance values are chosen heuristically since they provide

Part 1

a good characterization of many electrical components. For example, most power line circuits run high currents over *low* impedance lines. Many communication/antenna circuits implement impedances of about 50 to 100 Ω , and many logic circuits have *high* input impedances (circuit boards have medium impedance).

Knowledge of the impedance attribute is used to determine the way in which the electromagnetic disturbance propagates through an interaction path. Details of this will be discussed later.

The next approximation to be considered is the quantization of the disturbance strength. Since the impedance description is now a part of the attribute, the quantity used to represent the disturbance strength is optional. That is, one of voltage, current, or power for circuit nodes and one of electric field, magnetic field, or power density for field nodes. The *decibel* scale is usually used for such representations due to the large range of emission levels possible from the wide range of emitters of electromagnetic radiation. Thus, the appropriate form for the representation of an electromagnetic disturbance is in a *quantized* form.

<i>extreme</i>	if PD is $> 84 \text{ dBm/m}^2/\text{Hz}$ ($> 10 \text{ kV/m/Hz}$)
<i>high</i>	if PD is $44 - 84 \text{ dBm/m}^2/\text{Hz}$ ($.1 - 10 \text{ kV/m/Hz}$)
<i>medium</i>	if PD is $4 - 44 \text{ dBm/m}^2/\text{Hz}$ ($1 - 100 \text{ V/m/Hz}$)
<i>low</i>	if PD is $-36 - 4 \text{ dBm/m}^2/\text{Hz}$ ($10 \text{ mV/m} - 1 \text{ V/m/Hz}$)
<i>very low</i>	if PD is $< -36 \text{ dBm/m}^2/\text{Hz}$ ($< 10 \text{ mV/m/Hz}$)
<i>nil</i>	--> no disturbance
<i>unknown</i>	(propagate as unknown throughout)

Figure 17 Field type power density disturbance definitions

Part 1

The field type disturbances are denoted by PD and are defined in terms of *power density* P_d . These are shown in Figure 17 where the bracketed values represent the equivalent electric field for free space far fields. The units $\text{dBm}/\text{m}^2/\text{Hz}$ signify decibels above 1 milliwatt of power density per Hz. Note that the above units are /Hz since they are frequency domain representations.

The circuit type disturbances are denoted by P and are defined in terms of *power* in units of dBm/Hz . These are shown in Figure 18 below, where the bracketed values represent the voltage equivalent in a 50Ω circuit.

<i>extreme</i>	if $P > 84 \text{ dBm/Hz} (> 3.5 \text{ kV/Hz})$
<i>high</i>	if $P > 44-84 \text{ dBm/Hz} (35 \text{ V/Hz} - 3.5 \text{ kV/Hz})$
<i>medium</i>	if $P > 4-44 \text{ dBm/Hz} (350 \text{ mV/Hz} - 35 \text{ V/Hz})$
<i>low</i>	if $P > -36-4 \text{ dBm/Hz} (3.5 \text{ mV/Hz} - 350 \text{ mV/Hz})$
<i>very low</i>	if $P < -36 \text{ dBm/Hz} (< 3.5 \text{ mV/Hz})$
<i>nil</i>	--> no disturbance
<i>unknown</i>	(propagate as unknown throughout)

Figure 18 Circuit type power disturbance definitions

The specific values shown above for both field nodes and circuit nodes are chosen heuristically based on experience of electromagnetic disturbance levels and on the requirement for a useful number of ranges. The values assigned to each quantized range are quite arbitrary, but once these values are chosen, the creation of a useful database of disturbances requires that these values remain constant.

Part 1

These disturbances or emissions, whether they are from circuit nodes or field nodes, can be classified as *narrowband* or *broadband* relative to the receiving bandwidth of the susceptor. This information is implicit in the amplitude characterization given for an emission along with the characterization of the susceptibility of the receiving component.

Now it is clear from the theory of the Fourier transform (see [Körner 88]) that the frequency representation of a *unique* time domain waveform requires not only the amplitude information but the phase information as well. The phase information can mean the difference between a *coherent wideband* emission and an *incoherent wideband* emission (see [Mil-Std-462] and [Duff 88]). A coherent broadband emission will produce a disturbance at the receiver which is proportional to the receiver bandwidth, while an incoherent broadband emission will produce a disturbance at the receiver which is proportional to the *square root* of the receiver bandwidth. Thus the importance of classifying an emission as coherent or incoherent relates to how the emission interacts with its path and, ultimately, with the susceptor. For example, if a receiver or susceptor is sensitive to peak voltage disturbances, then an emission which is coherent in the bandwidth of the susceptor will produce twice the peak voltage as that of an incoherent emission in the same bandwidth. Thus the representation of a disturbance will also contain a *slot*, or location, for the specification of pertinent phase information. This information may also vary over specific frequency ranges.

Each component node in a topology, whether it is a circuit type node or a field type node, may contain many disturbance representations derived from all the sources present in that volume. The individual disturbance attributes for all the sources associated with a volume node (say V_1) can be *frequency range normalized* and *added in parallel* to determine the *total disturbance* emitted from that node.

Since the normalization procedure and parallel addition procedures are independent of the type of node (circuit or field), the disturbance for the node will be denoted as *ambient field* (AF) to simplify discussion. Thus, in the following discussions,

Part 1

whenever the term AF is used the disturbance in terms of either P or PD. Before these procedures are described, an example is given in the next section of some ambient fields which can be stored in a volume node.

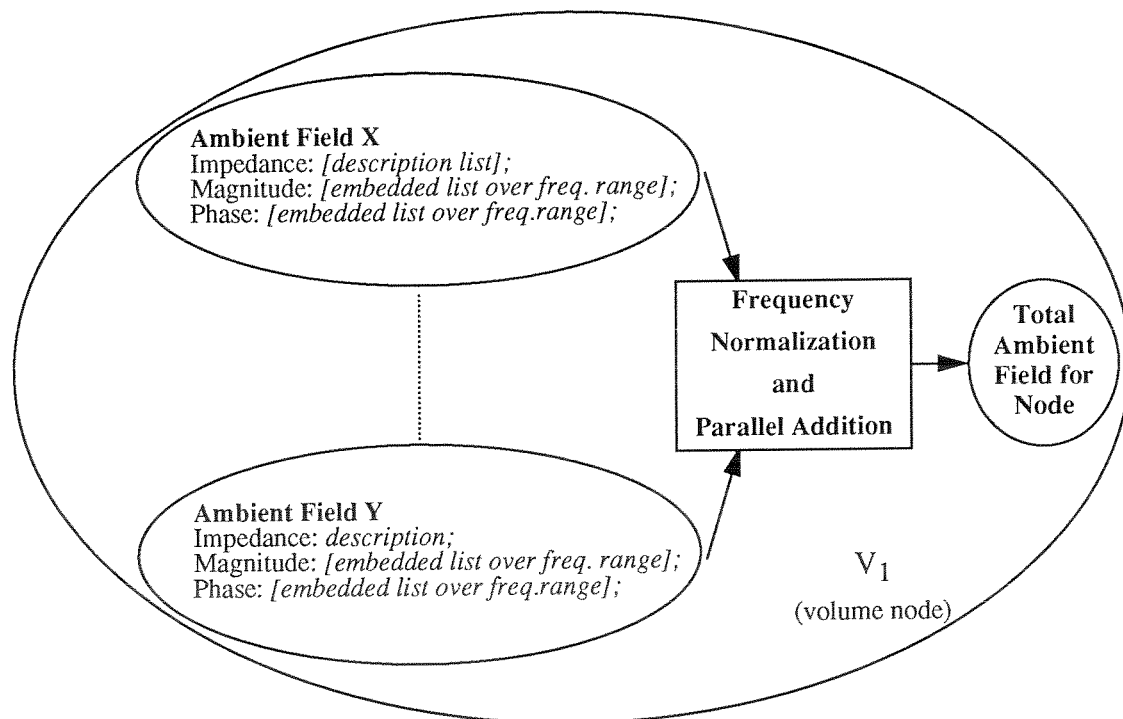


Figure 19 Ambient field attributes for a typical volume node.

4.2.2 Examples of Ambient Field Attributes

The fields emitted by a lightning strike can be simulated by the fields produced by a current pulse with pulse width $\tau \approx 50 \mu\text{s}$ and a 10 to 90 percent rise time $\tau_r \approx 500 \text{ ns}$ (see [Duff 88]). The average strike has a current amplitude of 30 kA. At a distance of 0.1 km the electric field may be approximated by a double exponential waveform of peak amplitude equal to 50 kV/m. Plots of the time domain representation and Fourier transform of this waveform are shown in Figure 20.

Part 1

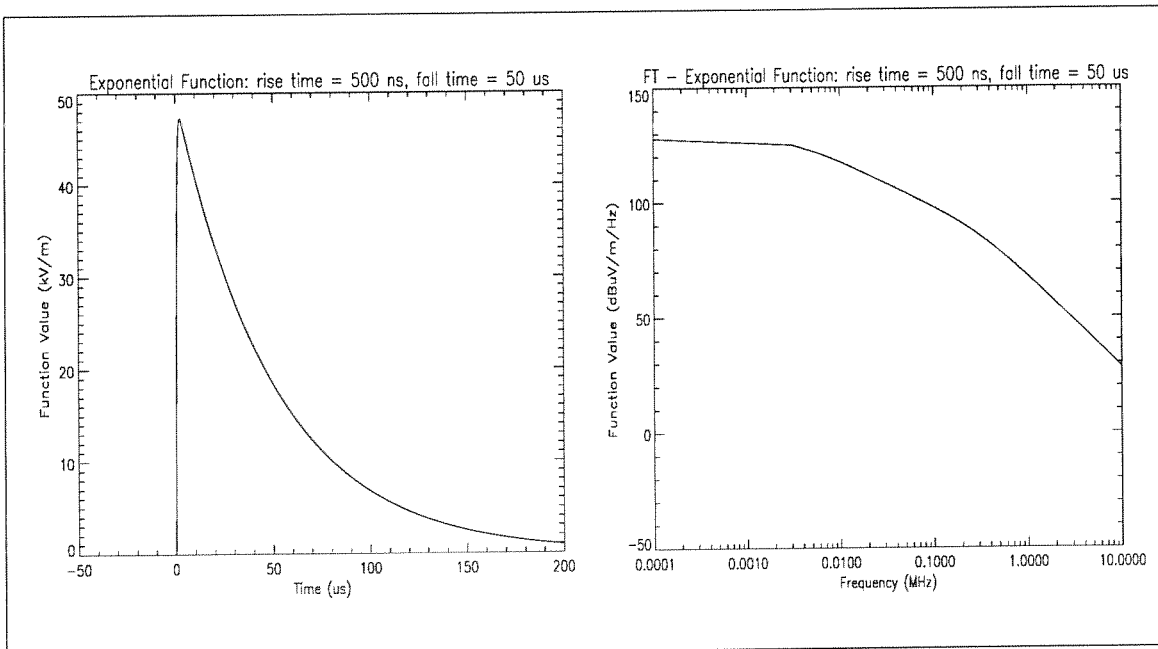


Figure 20 Lightning emission

The time domain waveform is calculated from:

$$E(t) = E_o \left(e^{-\frac{t}{\tau_f}} - e^{-\frac{t}{\tau_r}} \right) \quad (4.20)$$

with the peak value of the waveform given by:

$$E_o \left[1 + \left(\frac{\tau_r}{\tau_f} \right) \left(\ln \left(\frac{\tau_r}{\tau_f} \right) - 1 \right) \right] \quad (4.21)$$

and the 10% - 90% rise time given by $2.2 \tau_r$ and the duration of the pulse (from start of disturbance to time when pulse has decayed to 10% of the peak value) given by $2.3 \tau_f$ (see [Lee 86]).

Part 1

The Fourier transform of this pulse is given by

$$\hat{E}(\omega) = \frac{\tau_f - \tau_r}{1 - \tau_r \tau_f \omega^2 + j\omega (\tau_f + \tau_r)} \quad (4.22)$$

where: $\omega = 2\pi f$ is the angular frequency;

j is the imaginary number $\sqrt{-1}$;

$\tau_r = 500$ ns;

$\tau_f = 50$ us,

and $E_0 = 50$ kV is the waveform magnitude.

The above disturbance would then be represented in the database according to the previously defined levels as:

Ambient field strength: Lightning Emission (0.1 km)

Impedance: [Plane Wave]

Magnitude: $f < 10$ kHz \rightarrow medium

$100 < f < 400$ kHz \rightarrow low

400 kHz $< f < 1$ GHz \rightarrow very-low

1 GHz $< f \rightarrow$ nil

Phase: [Coherent]

Figure 21 Example ambient field representation

Part 1

4.2.3 Parallel Addition and Frequency Normalization

The total ambient field produced at a node (say V_1) due to the individual ambient fields imposed in that node volume needs to be determined in an appropriate manner so that *one* consistent representation can be propagated throughout a system topology. It is assumed for the moment that the total nodal ambient field AF_T is required over a specific frequency range set F_g (*global* frequency range set) given by N frequency ranges:

$$F_g = ((f_{g0}, f_{g1}), (f_{g1}, f_{g2}), \dots (f_{gj-1}, f_{gj}), \dots (f_{gN-1}, f_{gN})). \quad (4.23)$$

If a specific ambient field AF_x is stored over a specific frequency range set F_x given by the M frequency ranges:

$$F_x = ((f_{x0}, f_{x1}), (f_{x1}, f_{x2}), \dots (f_{xj-1}, f_{xj}), \dots (f_{xM-1}, f_{xM})), \quad (4.24)$$

then AF_x can be represented by the set of M ambient field amplitudes:

$$AF_x = ((af_{x1}), (af_{x2}), \dots (af_{xj}), \dots (af_{xM-1}), (af_{xM})), \quad (4.25)$$

for a certain impedance attribute AFZ_x . Each of the af_{xj} 's is one of the quantized amplitude levels described previously. Now before AF_x can be summed into the total ambient field AF_T it must be normalized to the global frequency range F_g and can be written as AF_{xn} where

$$AF_{xn} = ((af_{xn1}), (af_{xn2}), \dots (af_{xnj}), \dots (af_{xnN-1}), (af_{xnN})), \quad (4.26)$$

This is performed by the algorithm shown in Figure 22.

Part 1***Frequency Normalization Algorithm***

Loop 1: over the F_g ranges (f_{gj-1}, f_{gj}), $j=1, \dots, N$;

set af_{xnj} to ***unknown***;

Loop 2: over the F_x ranges (f_{xi-1}, f_{xi}), $i=1, \dots, M$;

If $f_{xi} \leq f_{gj-1}$ then end loop 2;

If $f_{xi-1} \geq f_{gj}$ then end loop 2;

set af_{xnj} to ***worseAF***(af_{xnj}, af_{xi});

continue *Loop 2*;

continue *Loop 1*;

Figure 22 Frequency normalization algorithm

The function ***worseAF***(af_1, af_2) returns the higher value ambient field, but returns ***unknown*** if and only if both af_1 and af_2 are ***unknown***. For example:

- ***worseAF(unknown, very low)*** returns ***very low***;
- ***worseAF(unknown, unknown)*** returns ***unknown***;
- and ***worseAF(high, low)*** returns ***high***.

Thus the effect of frequency normalization is to take, for the new normalized ambient field value corresponding to a global frequency range, the worst case ambient field value from the set of specific ambient field values whose corresponding frequency ranges overlap the global frequency range for all global frequency ranges. Obviously the choice of global frequency ranges will have an effect on the ambient field value which is ultimately propagated throughout the system topology.

Part 1

Now when more than one specific ambient field is specified for a volume node a procedure called ***Parallel Addition*** is performed. Given k ambient field representations in a node, say $AF_1, AF_2, \dots, AF_j, \dots, AF_{k-1}, AF_k$, the first step is to frequency normalize these as $AF_{1n}, AF_{2n}, \dots, AF_{jn}, \dots, AF_{(k-1)n}, AF_{kn}$. At this point, each of the k ambient fields consists of a set of N ambient field values. The total ambient field AF_T can now be determined as the worst case ambient field value for each global frequency range. Specifically, the algorithm shown below can be applied.

Parallel Addition Algorithm:

Loop 1: over the AF_j ambient field sets, $j = 1, \dots, k$;

frequency normalize AF_j ;

continue Loop 1;

Loop 2: over the F_g ranges (f_{gi-1}, f_{gi}), $i = 1, \dots, N$;

set af_{Ti} to *unknown*;

Loop 3: over the AF_j ambient field sets, $j = 1, \dots, k$;

if $af_{ji} = \text{unknown}$ then set *unknown flag*;

set af_{Ti} to *worseAF*(af_{Ti}, af_{ji});

continue Loop 3;

continue Loop 2.

Figure 23 Parallel addition algorithm

4.3 Component Susceptibility Representation and Approximation

Each component node in an electromagnetic topology may also have a *system susceptibility* (SS) associated with it. This system susceptibility value represents either the

Part 1

actual measured susceptibility of the component node or an approximation to this value based on numerical predictions of component models and/or experimental measurements made on similar components.

The system susceptibility is inversely related to the level of disturbance which will cause either:

- 1) *upset*; or
- 2) *permanent damage*;

of the susceptible component. That is, the lower the disturbance level which will cause upset or damage to a component the higher the defined susceptibility of that component.

There are many ways to define the specific susceptibility of an electromagnetic component. For instance, many logic circuits will be upset by peak voltage disturbances at their input terminals (see [Ott 88]). These disturbances must fall within the bandwidth of the logic device in order for an effect to be seen. Communication type systems are characterized as having a less definite upset susceptibility. This is because the analogue circuits involved in this type of system are sensitive to very low disturbance levels in the sense that the noise is noticed by an operator but the operator is still capable of deriving the correct operation of the system. Thus, in the case of analogue circuits, definition of a definite disturbance level where upset occurs is not as simple as for logic type circuits. For these type of circuits, damage level may be easier to define.

Damage and upset levels of many integrated circuit technologies (both logic and analogue circuits) have been tabulated in the McDonnel Douglas report *Integrated Circuit Electromagnetic Susceptibility Handbook* (see [McDonnel 78]). These tables were obtained from experiments as well as from numerical data based on circuit models of the integrated circuits. Sinusoidal and pulsed sinusoidal disturbances of varying frequencies (from 100 MHz to 40 GHz) were presented to the inputs of the integrated circuits and the minimum power levels causing interference were noted. The interference levels were

Part 1

defined according to some criterion depending on the circuit being tested. Damage levels were obtained for pulsed power interference; the *pulse power* and *pulse widths* sufficient to cause damage were reported.

It is obvious from the above discussion that the system susceptibility representation of an electromagnetic component should relate to the type of disturbance. The susceptibility can only have meaning when defined in the context of the disturbing source. Therefore in order to achieve compatibility with the ambient field representation the system susceptibility is also represented in the frequency domain. This allows a direct comparison to the ambient field quantity.

The representation of the component susceptibilities is also in a *quantized* form (40 dB steps), similar to that of the ambient field. These are defined in terms of either received *power* or *power density* and are shown in the Figure 24 below where the type of units are dictated by the type of node being characterized.

<i>very low</i>	if SS is $> 84 \text{ dBm/m}^2/\text{Hz}$ <i>or</i> dBm/Hz
<i>low</i>	if SS is $44 - 84 \text{ dBm/m}^2/\text{Hz}$ <i>or</i> dBm/Hz
<i>medium</i>	if SS is $4 - 44 \text{ dBm/m}^2/\text{Hz}$ <i>or</i> dBm/Hz
<i>high</i>	if SS is $-36 - 4 \text{ dBm/m}^2/\text{Hz}$ <i>or</i> dBm/Hz
<i>extreme</i>	if SS is $< -36 \text{ dBm/m}^2/\text{Hz}$ <i>or</i> dBm/Hz
<i>nil</i>	--> not susceptible
<i>unknown</i>	propagate as unknown throughout

Figure 24 System susceptibility definitions

Part 1

Along with this *level representation*, information about the type of sensitivity and the effect of failure (i.e. upset or damage) can be given for each frequency range. Thus for example, the SS for CMOS integrated circuits may be specified as shown below (see [McDonnel 78]).

System Susceptibility: CMOS Integrated Circuit

Level:	$f < 200\text{MHz} \rightarrow$ high
	$200\text{ MHz} < f < 10\text{ GHz} \rightarrow$ medium
	$10\text{ GHz} < f \rightarrow$ nil
Type:	[peak sensitive]
Effect:	[upset]

Figure 25 Example system susceptibility representation

Each component node in the topology may contain many system susceptibility characterizations. For example, the component node representing a circuit board may be characterized by specifying susceptibilities for CMOS, TTL, and line driver integrated circuits. These specific SS values are stored in a database and can be retrieved by the user to characterize each node in a topology.

Once the specific system susceptibilities of a component node have been defined, the frequency normalization and parallel addition routines, similar to those used in the ambient field case, can be used. The difference will be that the function *worseAF(af₁, af₂)* will be replaced by the function *worseSS(ss₁, ss₂)*. This function will return the worse system susceptibility of the two component susceptibilities ss₁, and ss₂. A pictorial

Part 1

description of how each system susceptibility is used to create a total system susceptibility for the component node is given in Figure 26.

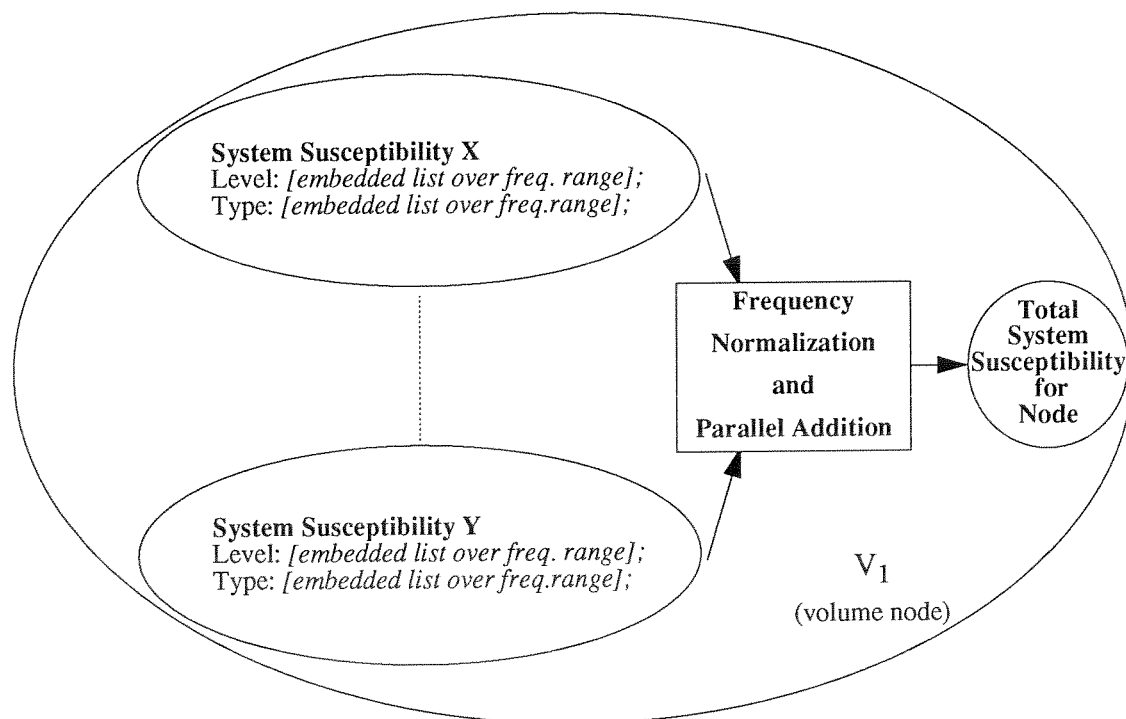


Figure 26 System susceptibility attributes for a typical volume node

4.4 Interaction Path Shielding Effectiveness Representation

The shielding effectiveness (SE) is a representation of the path characteristics between two volume nodes and is used to determine the amount of attenuation the ambient field will encounter before the field energy reaches the susceptor. Recall that in the graphical representation the interaction path nodes correspond to surfaces between volumes of the topological representation. Each interaction path may be made up of a number of different parallel paths between electromagnetic component nodes. Each of these parallel paths will be given an SE characterization and these characterizations will again be frequency normalized and added in parallel via algorithms similar to the ambient

Part 1

field and system susceptibility algorithms. The topological and graphical representations of these interaction paths can be summarized as shown in Figure 27. Note that the total interaction path is made up of the individual parallel paths.

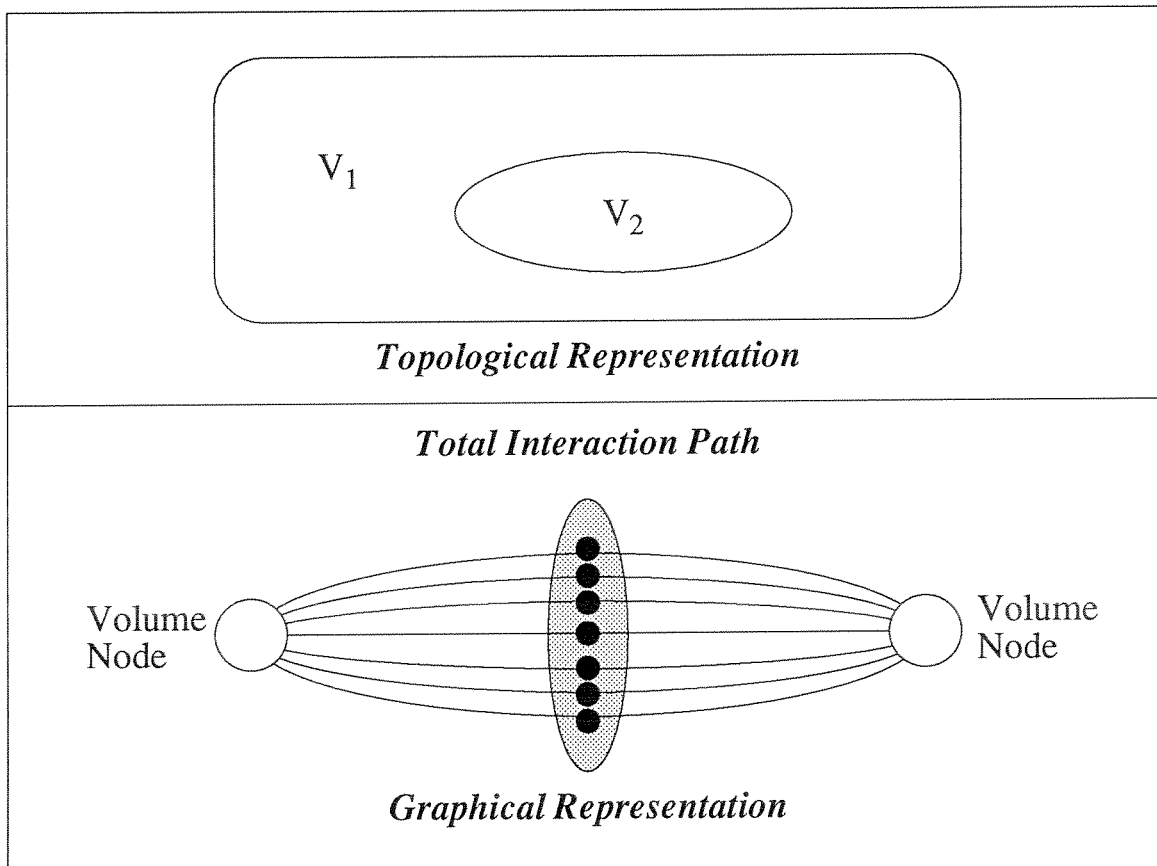


Figure 27 Interaction path representations

The SE is also given over discrete frequency ranges in order that its representation be compatible with that of the ambient field and the system susceptibility. The question of units for this quantity depends on the two volume nodes which it connects. For example, the SE between a circuit node and a field node will require units appropriate to the task of converting the ambient field from one node to the units of the other. As in the ambient field and system susceptibility representations, the SE is defined with discrete *qualitative* levels.

Part 1

These are given in Figure 28 where the specified units are for paths between nodes of similar type.

<i>excellent</i>	if $SE > 100$ dB
<i>good</i>	if $80 < SE < 100$ dB
<i>fair</i>	if $60 < SE < 80$ dB
<i>not good</i>	if $40 < SE < 60$ dB
<i>poor</i>	if $SE < 40$ dB
<i>nil</i>	--> no shielding
<i>unknown</i>	propagate as unknown throughout

Figure 28 Shielding effectiveness definitions

These levels are quantized in 20 dB ranges since these are typical ranges for real paths. *Non-linear* paths which depend on the AF crossing can be implemented by having the specific path representation be dependent on the ambient fields. This will be discussed in the next chapter on constraint propagation.

Since the susceptibility of EM components is usually given in terms of the actual received power (see the report [McDonnel 78]), a coupling coefficient *may* be represented in this SE in order to convert the ambient field data to the units of *power* or *power density* required. Thus the SE nodes in the bipartite representation must deal with the conversion from field node to circuit node and vice versa (note that this implies the importance of directionality in the graph).

Part 1

4.4.1 Examples of Path SE Attributes

Paths between field nodes, which will be denoted *ff-paths*, take field quantities and attenuate them producing field quantities on the other side. Paths between circuit nodes, *cc-paths*, attenuate circuit disturbances. The other two possible combinations are *fc-paths* and *cf-paths* with corresponding meanings. These are summarized in the figure below.

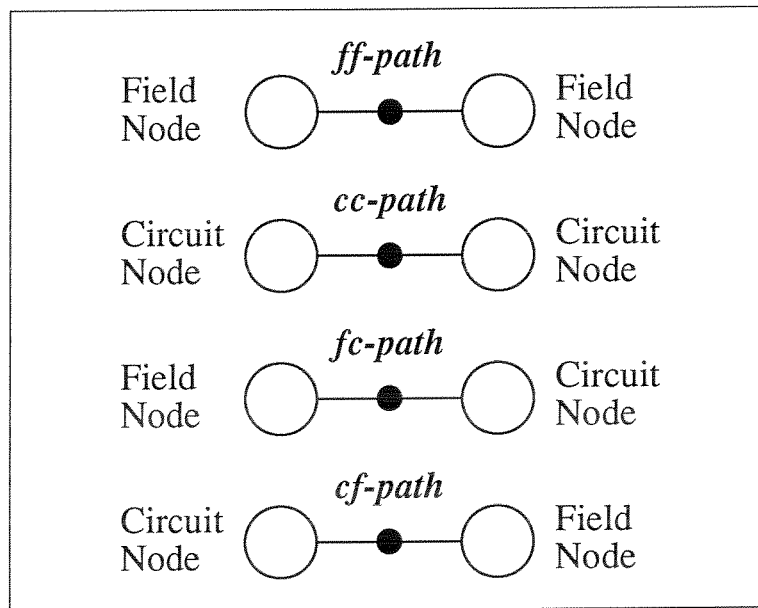


Figure 29 Interaction path types

Examples of specific instances for each of these cases will be given in the following subsections. Each type of path node has conceptual characteristics of its own, but as will be discussed later, the stored SE characteristics are handled in the same manner for all four types of interaction.

4.4.1.1 Field-Field Path Nodes

An example of a ff-node is a conducting shield separating two volumes. This is recognized in the electromagnetic topology representation as a surface between two volumes. Now a practical shield is far from perfect in that it contains many imperfections

Part 1

which will allow fields to propagate between the two separate volumes. An excellent review of *shielding theory* is given by Schulz (see [Schulz 88]). Some typical imperfections which may exist in a conducting shield are depicted in Figure 30.

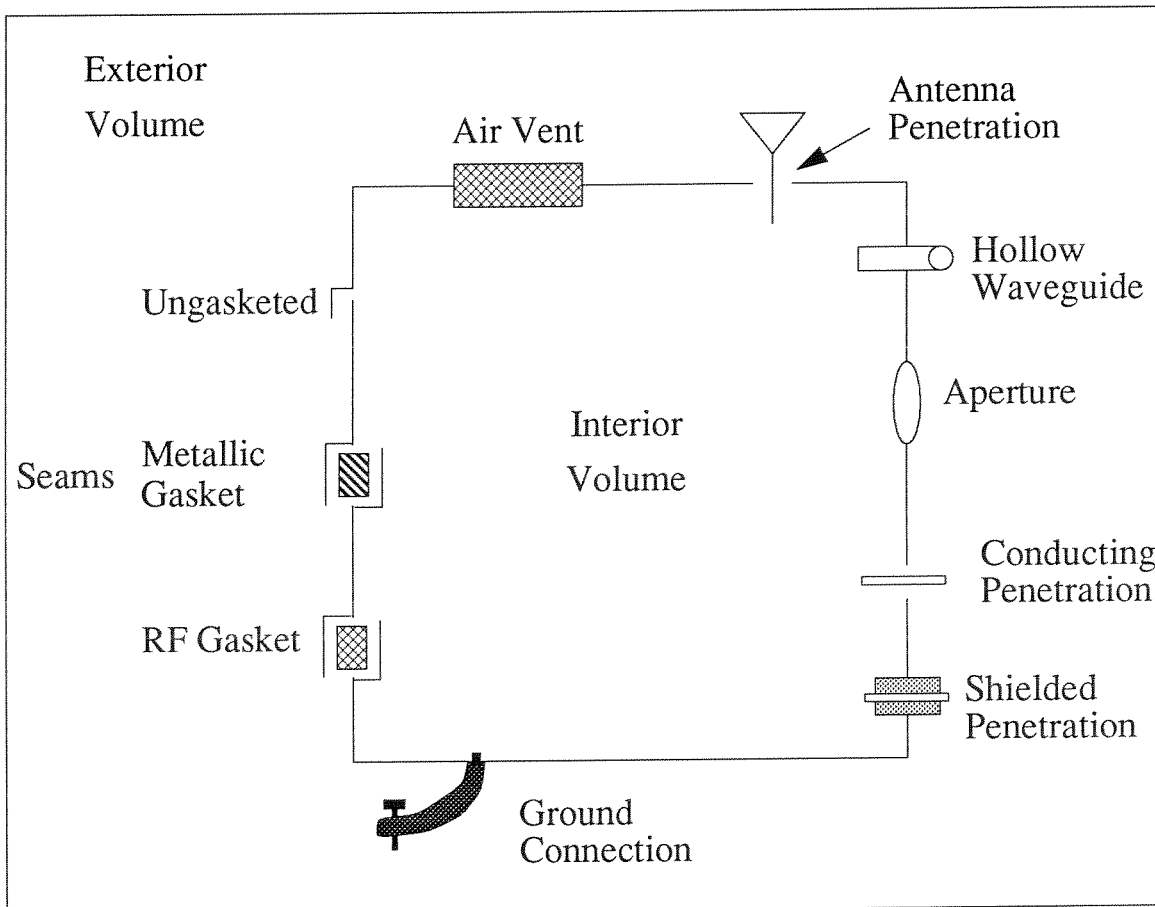


Figure 30 Typical shield imperfections

The imperfections shown above are very typical interaction paths between two volume nodes. These are found in real world entities such as shielded rooms or buildings, electronic equipment enclosures, or even the skin of an aircraft body. Each of these imperfections will have an SE characterization derived from either experimental or theoretical models.

Part 1

For example, shielding effectiveness of apertures in thin conducting shields has been investigated by many authors. A heuristic rule for the determination of the shielding effectiveness of apertures to plane waves has been given by Ott (see [Ott 88]) as

$$SE_{dB} = 20\log\left(\frac{\lambda}{2L}\right) \text{ for } \lambda > 2L, \quad (4.27)$$

and

$$SE_{dB} = 0 \text{ for } \lambda < 2L, \quad (4.28)$$

where: λ is the wavelength of the wave [meters], and

L is the longest dimension of the aperture [meters].

A more recent rule based on measurements made in a specially designed TEM cell has been given by Vitek (see [Vitek 89]) as

$$SE_{dB} = 20\log\left(\frac{75r}{d(9 + 5.5r)^{\log\left(\frac{f}{2}\right)}}\right) \text{ for } \lambda > 2L, \quad (4.29)$$

and

$$SE_{dB} = 0 \text{ for } \lambda < 2L, \quad (4.30)$$

where: f is the frequency of the wave [MHz], and

r is the length to width ratio of the aperture [dimensionless].

The shielding effectiveness derived from both of these models for apertures having lengths of 0.5 and 0.1 meters and widths of 0.1 and 0.01 meters respectively are shown in Figure 31. The solid line was calculated from the Ott equation (4.27) while the broken line was calculated from the Vitek model (equation (4.29)). It is apparent from the figures and

Part 1

from the coarseness of the required approximations that either of these models can be used to derive SE values to characterize the interaction path due to apertures. Thus the simpler model should be used as a first approximation. If the aperture happens to be on a critical path (to be described later) a more accurate model should be used.

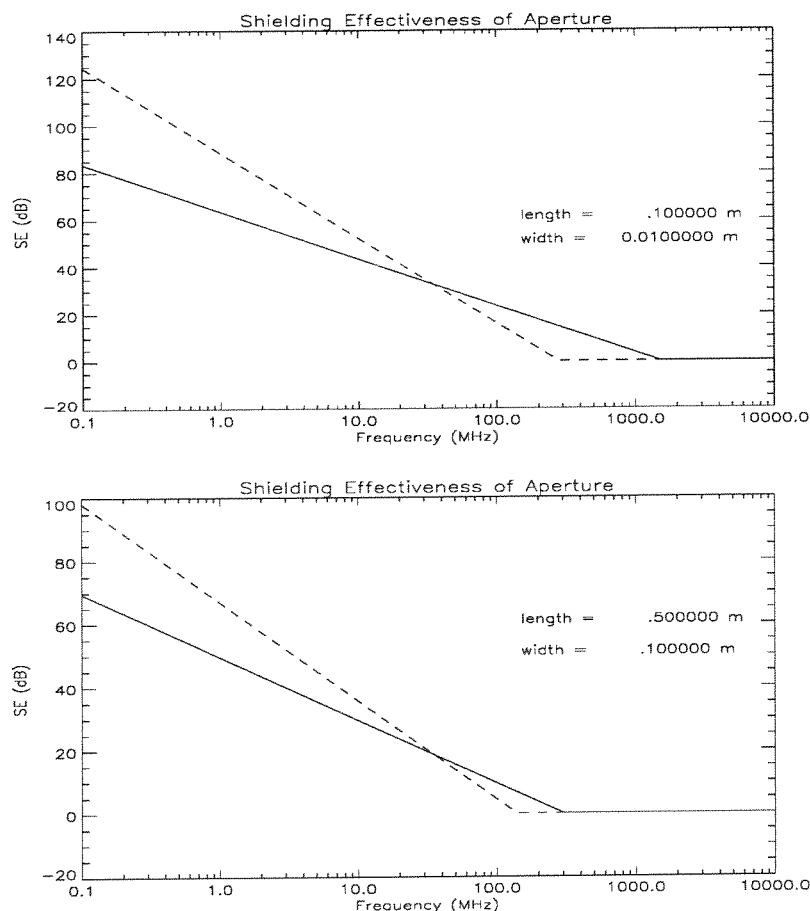


Figure 31 Shielding effectiveness of apertures

Similarly, simple models for each type of possible imperfection for a conducting shield are available in the literature and in manufacturer specifications for these components. It is not the intent here to accumulate the required models which would exist

Part 1

in the database of the advisor but to show the types of models which are appropriate and available.

As a final example, and in order to demonstrate an important point concerning the decomposition of complex systems into their respective topologies, conducting penetrations will now be examined. A conducting penetration can render to nil the shielding effectiveness of an enclosure in certain bandwidths. This is because field energy can couple onto the conductor penetrating the shield and then be radiated again on the other side. This becomes more clear if the topology of this path is modelled more closely. In the figure below a more detailed topology model of this type of shield imperfection is shown along with the simpler topological model.

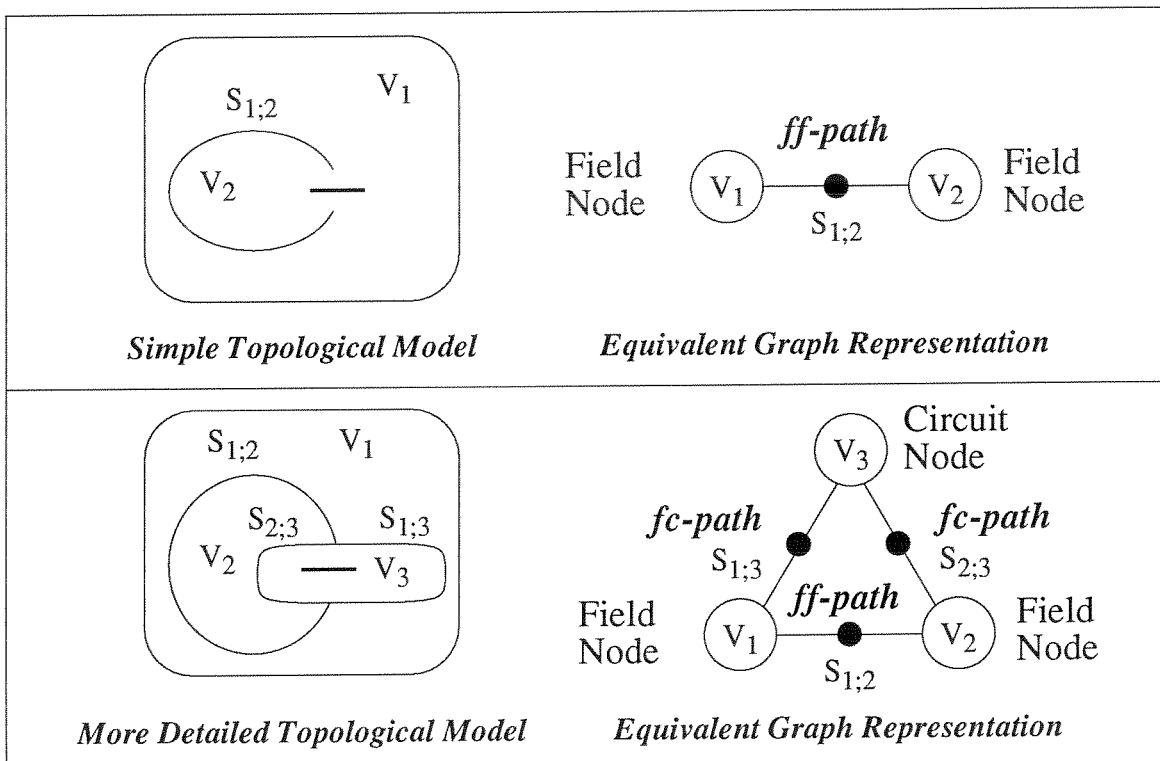


Figure 32 Two topological representations of the same shielding imperfection

Part 1

Thus a more detailed topological model may help to understand an interaction path phenomenon. Once the detailed model is instantiated, that is, once those path attributes which give an acceptable model have been determined, then it can be collapsed into the simpler representation with new composite attributes. This is discussed in the next chapter.

4.4.1.2 Circuit-Circuit Path Nodes

Circuit-circuit path nodes are used to model any interaction between circuit nodes. For example, most power-line entries into an equipment enclosure are electrically filtered, ribbon cable connectors on a circuit board may also be handled as cc-nodes and finally, data transmission cables between circuits may also be modelled in this way. In effect, any electrical circuit connection can be modelled by a cc-node. The level of modelling detail required for the system will dictate the definition and introduction of cc-nodes into the topology.

4.4.1.3 Field-Circuit Path Nodes

Field-circuit nodes are used to define the coupling of field quantities to circuit nodes. For example, the coupling of far fields to *printed wiring boards* (PWB's) may be approximated by a half-wave dipole where the received power P is calculated from the incident power density P_d as:

$$P = A_{\text{em}} P_d [\text{W}]; \quad (4.31)$$

where A_{em} is the *maximum effective aperture* for a half-wave dipole:

$$A_{\text{em}} = 0.13 \lambda^2 [\text{m}^2]; \quad (4.32)$$

and λ is the wavelength (in meters) of the incident radiation. This has been found to be a good approximation for frequencies ranging from 100 MHz to 10 GHz [McDonnel 78]. For lower frequencies a maximum effective aperture of $A_{\text{em}} = 1$ is an appropriate worst case approximation.

Part 1**4.4.1.4 Circuit-Field Path Nodes**

The circuit-field nodes are used to represent the emission of fields from circuit nodes. From Maxwell's equations it is known that fields are produced by currents and charges (sources). Thus, for example, currents existing on a printed wiring board will radiate energy in terms of electric and magnetic fields. Some example estimations for the level of these emissions are derived from approximating the sources as loop and dipole radiators. The worst case far field power density emitted from a loop above a ground plane can be approximated by (see [Ott 88]):

$$P_d = 40\log(f) + 20\log\left(\frac{AI}{r}\right) - 267 \text{ dBm/m}^2/\text{Hz} \quad (4.33)$$

where: f is the frequency of the emission [Hz];

A is the loop area [m^2];

r is the distance from the loop [m]; and

I is the current magnitude carried by the loop [A].

The emission from a current loop with $A = 25 \text{ cm}^2$, $I = 25 \text{ mA}$, and a distance $r = 3 \text{ m}$ is plotted in Figure 33 for the frequency range of 0.1 MHz - 10 GHz using the above approximation. Note that the above formula is not valid for near fields and thus the portion of the plot below 10 MHz is not accurate.

Of course more accurate models are obtainable for emissions from circuit boards (see for instance [Raut 86]) but considering the use of the results in the topology model, a coarse worst case model may be sufficient as a first approximation. Also, experimental data may be used for specific circuit boards which have been tested. Thus a complete data base of emission level data for the set of circuit boards of interest may be kept. The database would then be fine tuned as better models or experimental data become available.

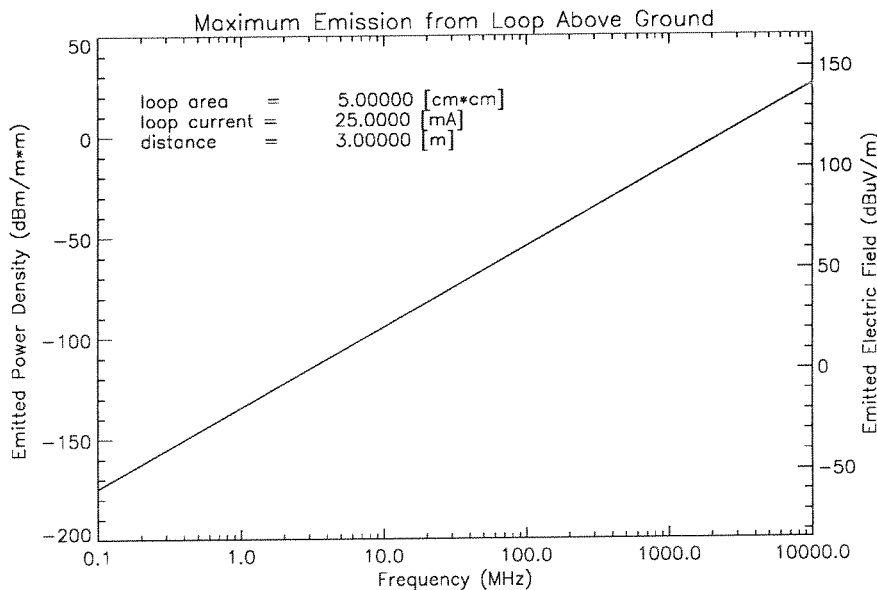
Part 1

Figure 33 Emission from current loop above ground

4.4.2 Physical Example with All Interaction Types

In order to better visualize the four types of interaction paths between the two types of nodes, an example of the topological decomposition of a real physical system will now be given. Considered here is the electromagnetic interactions within a small computer system surrounded by the external ambient. This physical system is depicted in Figure 34 along with the topological decomposition and the equivalent bipartite graph.

As can be seen from the figure, the ambient volume may contain natural disturbances such as lightning emissions, and man made disturbances such as radar antenna emissions or radio station broadcasts. From the topological decomposition and the graph, it can be seen that these disturbances have three paths of entry into the computer system. These are depicted as the surfaces between the ambient field volume and: 1) the power cable; 2) the EMI filter enclosure; and 3) the computer enclosure. The computer system itself is decomposed into the electronic circuitry, the internal power distribution circuitry, the EMI filter

Part 1

enclosure, and the EMI filter circuitry. The node types for each of these components are depicted as cross-hatched nodes representing circuit nodes, hollow nodes representing field nodes, and the small solid nodes representing interaction paths or surfaces.

Thus, for example, there exists a fc-node (interaction path) from the computer enclosure field node to the internal power distribution circuit node which models the fields coupling onto the power distribution circuits. This same interaction path node may contain the representation for a cf-node which models the emissions from the internal power distribution circuit.

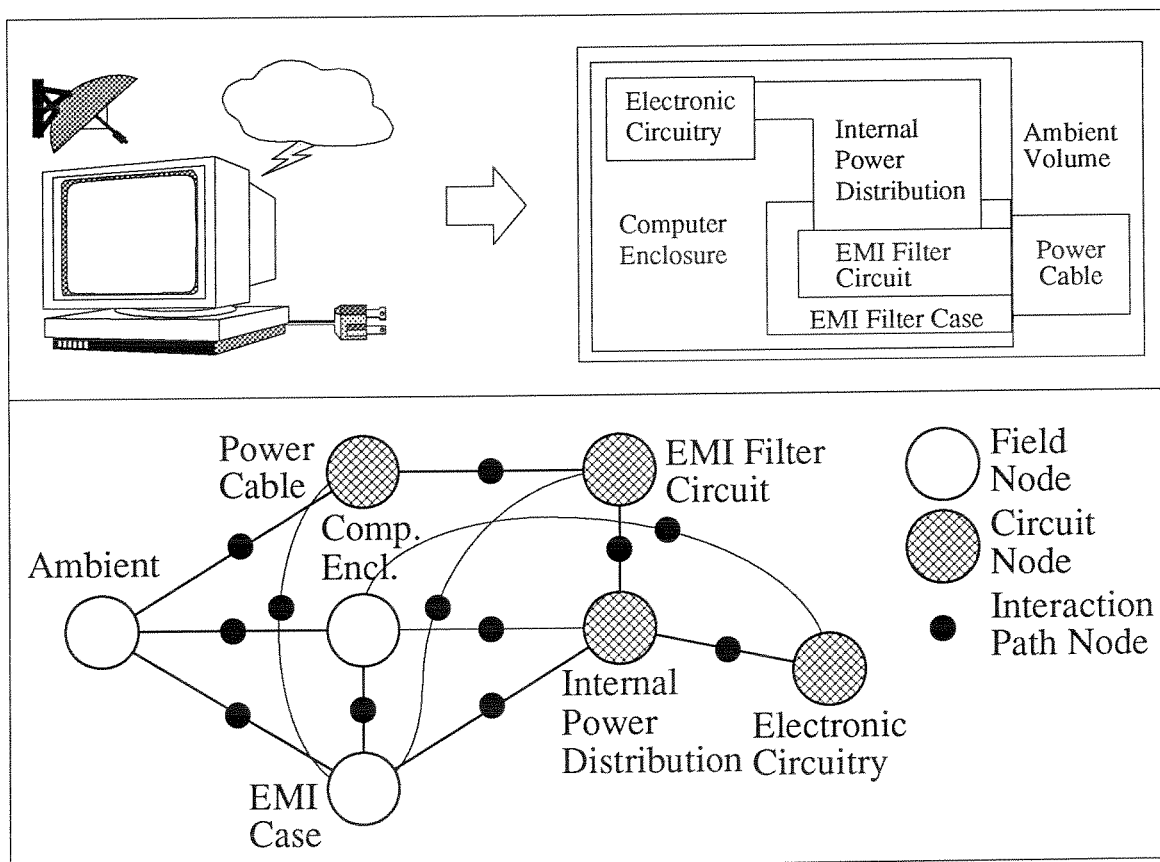


Figure 34 Examples of system characterization via topology and equivalent graph representation involving all four types of nodes

Part 1

Of course this is not the only possible topological decomposition of this physical system. Many other decompositions are possible and some may in fact be more appropriate depending on which component and via which interaction path the greatest risk of failure manifests itself. These considerations cannot be known *a priori* unless previous experience with similar electromagnetic components and topologies is available.

For example, in the computer system depicted in Figure 34, data cables and I/O ports have not been included in the topological decomposition. This may prove to be an error if in fact these components end up causing failures in the system. On the other hand, they may have been intentionally ignored since previous experience may have shown that there is little disturbance through the paths associated with the data I/O circuitry. Thus the topology may have been reduced in size by not including these electromagnetic components.

Chapter 5

Using Constraints to Characterize EMI

The language of *Constraints* was described by Sussman and Steele in [Sussman 80] as a method of deriving useful consequences by propagating conditions through a constraint network. A formal overview of constraint networks as applied to picture processing has been presented by Montanari [Montanari 74]. Presently, a constraint type language is defined in order to characterize an electromagnetic interaction problem. The constraints are used to define an electromagnetic topology. They are also used to define emission and susceptibility attributes of component nodes and shielding attributes of interaction paths in the topology. The *likelihood* of a component node *failing* is also derived via the propagation of imposed conditions in the topology through appropriate constraints. The details of this procedure will now be explained.

5.1 Topology Definition Constraints

The first step in the solution of an electromagnetic interaction problem is to define the electromagnetic topology of the system to be studied. This is accomplished by defining the discrete electromagnetic volumes (i.e. each node) with a suitable name. In essence this is just a declaration of the existence of each node. For example, the statements:

node(external_vol).

node(computer).

node(cpu).

node(power distribution).

node(power cord).

node(power supply).

Part 1

would declare the existence of six nodes in the current topology. Once the nodes are declared the common surfaces between nodes must be represented. This is achieved by declaring surfaces between electromagnetic volumes. Continuing with the above example, the surfaces may be defined as:

surface(external_vol, computer).	surface(external_vol, power cord).
surface(external_vol, power supply).	surface(computer, cpu).
surface(computer, power distribution).	surface(computer, power supply).
surface(cpu, power distribution).	surface(power distribution, power supply).
surface(power supply, power cord).	

where nine surfaces have been identified. Thus, with these 15 statements, a small electromagnetic topology has been defined. A surface declaration is said to *constrain* two volumes into sharing a surface. Although the above statements *look like* Prolog code, they are meant to be independent of implementation and any resemblance is coincidental with the fact that Prolog is declarative in nature. It should also be noticed that the above declarations define a graph G with vertices given by the node statements and the edges defined by the surface statements.

5.2 Global Frequency Range Constraint

As was described in the previous chapter, all electromagnetic attributes associated with the volume nodes and the surfaces between nodes are characterized in the frequency domain over a set of discrete frequency ranges. In order to compare attributes they are all normalized to a global frequency range. The specific discrete frequency ranges to be used for the global frequency ranges are chosen by the user and can be set as coarsely or as finely as is desired. This is accomplished by constraining the global frequency variable to a specific frequency range found in the knowledge base. For example, the statement:

global_frequency(frequency_range_x).

Part 1

will constrain the global frequency variable to the frequency ranges defined in *frequency_range_x* which would appear in the knowledge base as a list of discrete frequency ranges.

It should be noted that the number of discrete frequency ranges defined will affect the speed of computation for the 1) frequency normalization, 2) parallel addition, 3) worst case shielding path determination, and 4) risk of failure operations. Therefore, it is best to start with a coarsely defined frequency range and then refine it in regions of high likelihood of failure.

5.3 Volume/Surface Attribute Definition Constraints

Once the electromagnetic topology has been defined the specific electromagnetic attributes unique to each electromagnetic volume as well as each surface can be determined. Thus the statement:

disturbance(node(*external_vol*), [[standard, NEMP], [standard, LEMP], [cw, HF]]).

will constrain the *external_vol* node to have disturbances associated with a *standard Nuclear Electromagnetic Pulse*, a *standard Lightning Electromagnetic Pulse*, and a disturbance defined as a *continuous wave - High Frequency* type disturbance. All three of these disturbances would exist in the knowledge base in the form described in the previous chapter. Entering these constraints would trigger the *frequency normalization* and *parallel addition* algorithms described previously in order to produce a total disturbance for this node. Nodes which are not instantiated with specific attributes are taken to be *unknown* over all frequency ranges of the global frequency range. Certain specific disturbances may also contain an *unknown* level in a specific frequency range (as defined in the data base).

A classification is made of the different disturbance data available in order to organize the knowledge base. The disturbance data in the knowledge base is divided into specific types and sub-types. Currently this classification consists of the types:

Part 1

- 1) standard;
- 2) transient;
- 3) continuous wave; and
- 4) user specific disturbance (user defined then stored for later use).

The type *standard* refers to disturbances defined by official documents with sub-types defined from standards such as the NEMP NATO standard, Mil-Std-461C susceptibility standards (see [Mil-Std-461C]), and LEMP threat standards. The type *transient* generally defines disturbances produced by coherent or incoherent transient sources such as spark discharges, power line surges, and switching devices. The type *continuous wave* is used for sub-types such as radio/TV transmitters, 60 Hz power equipment, VDT's, and other continuous wave equipment.

As well, provision is made for user defined types and sub-types which do not fit in the other categories of the classification. These can be defined at any time by the user, being derived possibly from experimental measurements or numerical models.

In a similar fashion, the susceptibility of an electromagnetic volume node can be constrained to one or many of previously defined susceptibility attributes stored in the knowledge base. As an example, the statements

```
susceptibility( node( cpu), [[digital, TTL], [digital, CMOS], [analogue, line_driver]]).
susceptibility( node( power supply), [[analogue, volt_regulator], [digital, comparator]]).
```

would constrain the two specified nodes to have total susceptibilities derived from the susceptibilities of the listed components.

The knowledge base classification of susceptibility data currently being used is:

- 1) digital technology components (e.g. TTL, CMOS devices);
- 2) analogue technology components (e.g. OP AMPS);

Part 1

- 3) power technology devices (e.g. voltage regulators); and
- 4) user specific susceptibilities (defined then stored for later use).

These were compiled from the multitude of literature available on the electromagnetic susceptibility of devices (see for example [Duff 88], [Keiser 87], [McDonnel 78], [Ott 88], and [White 73]).

Finally, the shielding effectiveness attribute can be used to constrain any of the surfaces in the topology. It should be noted that, although the path or interface between two volume nodes is being referred to as a surface, in general a path may bear no resemblance to a surface at all (for example the path between two circuit nodes). The term surface is being used for convenience. Thus the following statements:

```

shielding( surface( external_vol, computer), [[shield, aperture, length, depth],
                                              [shield, wire-mesh-gasket],
                                              [shield, honey-comb-cooling-vent]]).

shielding( surface( external_vol, power cord), [[coupling, short-cable]]).

shielding( surface( external_vol, power supply), [[shield, wire-mesh-gasket]]).

shielding( surface( computer, cpu), [[coupling, pcb, 30cmX30cm]]).

shielding( surface( computer, power distribution), [[coupling, short-ribbon-cable]]).

shielding( surface( computer, power supply), [[shield, aluminum]]).

shielding( surface( cpu, power distribution), [[filter, nil]]).

shielding( surface( power distribution, power supply), [[filter, feed-thru caps]]).

shielding( surface( power supply, power cord), [[filter, EMI-461]]).

```

constrain the shielding effectiveness of particular interaction paths in the previously defined electromagnetic topology.

The classification of the shielding effectiveness data for use in the knowledge base is more difficult than for the disturbance and susceptibility attribute data. This is due to the fact that four types of paths exist (i.e. ff-paths, cc-paths, fc-paths, and cf-paths).

Part 1

The first level of classification distinguishes between the different path types:

- 1) shield (ff-paths);
- 2) filter (cc-paths);
- 3) coupling (fc-paths); and
- 4) radiation (cf-paths).

Categories or sub-types of *shield imperfections* can be classified as:

- 1) conductive penetrations;
- 2) filtered conductive penetrations;
- 3) non-conductive apertures (openings);
- 4) gasketed apertures;
- 5) special viewing apertures; and
- 6) special venting or cooling apertures.

Typical *filter* sub-types are feed-thru capacitors, emi-filters, and *nil* representing a direct circuit connection. Sub-types for the *coupling* type path are such mechanisms as printed circuit board coupling, and cable coupling. The *radiation* type is the dual of coupling but the specific values are not necessarily related to the coupling path (hence the importance of the directed interaction sequence diagram).

5.4 Worst Case Shielding Path

Thus far the shielding attribute has been used to constrain the shielding effectiveness between two electromagnetic volume nodes which share a common surface. This knowledge represents heuristic information about the interaction path between two neighboring nodes. Implicit in this knowledge, along with the knowledge of the electromagnetic topology, is information regarding the heuristic interaction between any

Part 1

two nodes in the topology. This information can be explicitly derived by determining the worst case shielding path between all susceptible nodes and all emitting nodes.

In order to accomplish this a search must be conducted, using each susceptible node as the root node, in order to find the worst case shielding path to all other emitting nodes. Technically the search is performed using Dijkstra's algorithm for this *single-source shortest path problem* (see Figure 6). The discrete heuristic shielding effectiveness levels given in Figure 28 are converted to numbers as shown in Figure 35.

<i>excellent</i>	SE = 3.0
<i>good</i>	SE = 2.0
<i>fair</i>	SE = 1.5
<i>not good</i>	SE = 1.0
<i>poor</i>	SE = 0.5
<i>nil</i>	SE = 0.0 --> no shielding, and
<i>unknown</i>	propagate as unknown throughout

Figure 35 Definition of SE variable

Using the above values as *distances* in an interaction sequence graph, the worst case shielding effectiveness is found. For example, in Figure 36, where only one susceptible node exists, the worst case shielding path to the two emitting nodes is shown in bold. Thus for this particular case the total shielding for the two interaction paths would be represented as

```
total_shielding( path( v1, v4), [ ... [not-good] ... ]).
total_shielding( path( v1, v5), [ ... [good] ... ]).
```

Part 1

where the second argument of *total_shield* is an imbedded list of the shielding effectiveness for each frequency range. Notice that although the total SE variable for path(v1, v5) adds up to 2.5 (corresponding to slightly *above* the good level) the value of *good* is displayed for the total shielding. Internally though the value of 2.5 is maintained for the total SE variable.

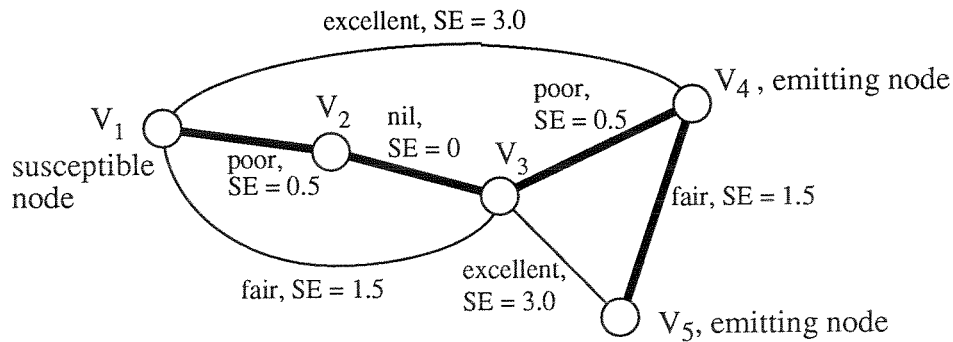


Figure 36 Example worst case shielding path for a specific frequency

During the worst case path search the individual surfaces are sorted from those with poorest total shielding to the best total shielding. In this way the user can tell which specific surface is the determining factor in the total shielding for the path. In effect, the determination of a total shielding between two nodes which are not neighbors is the same as imposing a shielding effectiveness constraint between these two nodes. This is similar to the concept of *slices* in Sussman and Steele's constraint language [Sussman 80].

5.5 Propagation of Electromagnetic Disturbance

Before the likelihood of failure can be determined at the susceptible nodes, a heuristic method of *propagating* the electromagnetic disturbance from an emitting node to a susceptible node must be determined. Both circuit and field disturbances will be handled similarly and thus either disturbance will be denoted as the AF (ambient field). The ranges defined in Figure 17 and Figure 18 are assigned a discrete numerical value as shown in Figure 37.

Part 1

<i>extreme</i>	AF = 5;
<i>high</i>	AF = 4;
<i>medium</i>	AF = 3;
<i>low</i>	AF = 2;
<i>very low</i>	AF = 1;
<i>nil</i>	AF = -2 --> no disturbance;
<i>unknown</i>	(propagate as unknown throughout);

Figure 37 Ambient field discrete levels

The propagated ambient field is then determined by subtracting the total shielding effectiveness of the path traversed (i.e. the SE value) from the AF value. Now, since non integer values of SE exist (for example a shielding effectiveness of fair \leftrightarrow SE = 1.5), it is *not* always the case that after passing through a shielded path the ambient field drops a level. This is shown visually in Figure 38 below where the ambient field is reported as the darkest shade in a column but held internally as a non integer value.



Figure 38 Ambient field propagation through SE

5.5.1 Justification for Ambient Field Propagation

Setting an ambient field or disturbance attribute to a certain level over a specific frequency range implies that there is an equal probability for the disturbance amplitude taking on any value in the range of amplitudes covered by the level. For example, if in the frequency range (1 MHz - 10 MHz) a disturbance level of *high* is specified then this approximates the disturbance with equal probability over a 40 dB ambient field range as shown below.

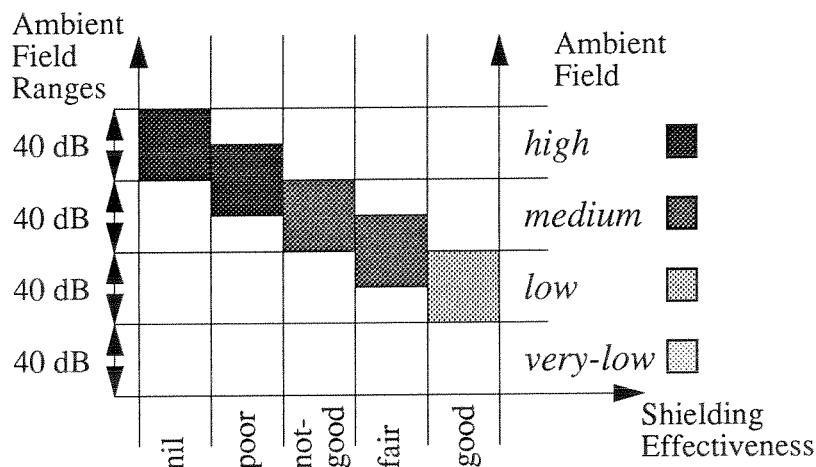


Figure 39 High ambient field approximation propagated through good SE

If this ambient field is propagated across a *poor* shield (i.e. $SE < 40$ dB) the resulting AF probability distribution would lie somewhere between the *high* level and the *medium* AF level as shown above. Taking a worst case scenario this would be reported as still being *high*. Following this logic, a *good* shielding effectiveness (i.e. $80 < SE < 100$ dB) would bring the *high* AF down by at least 80 dB which means the propagated AF would be reduced to the *low* level.

The above logic is efficiently modelled using the AF and SE numerical values described previously (and summarized in Figure 35 and Figure 37) and calculating the

Part 1

propagated AF (denoted PAF) as $PAF = TAF - TSE$ where TAF is the total ambient field emitted by a node and TSE is the total shielding effectiveness of a path.

5.6 Likelihood of Failure Determination

Once the propagated ambient field to a node from all other emitting nodes in the topology has been determined, it is necessary to determine the *likelihood of failure* of any susceptible component. The propagated ambient fields from all the nodes are then added in parallel using the parallel addition algorithm of Figure 23. In doing this, a trace of the highest PAF (propagated AF) to lowest PAF is kept for each frequency range in the global frequency range (recall that each PAF has already been frequency normalized when the self ambient field of each emitting node was created).

Once this has been done, the total propagated AF can be compared to the total susceptibility of the receiving node in order to determine if an interaction problem causing failure of the susceptible component exists. This is performed by assigning numbers to each of the possible system susceptibility levels defined in Figure 24 as shown in Figure 40.

<i>nil</i>	SS = 8	--> not susceptible
<i>very low</i>	SS = 5	
<i>low</i>	SS = 4	
<i>medium</i>	SS = 3	
<i>high</i>	SS = 2	
<i>extreme</i>	SS = 1	
<i>unknown</i>	propagate as unknown throughout	

Figure 40 Discrete system susceptibility values

Part 1

The likelihood of failure is now reported as being one of the discrete values shown in Figure 41 for each frequency range in the global frequency range set. As can be seen from the figure, the discrete level assigned to a frequency range is dependent on a failure index variable denoted FI. This FI variable is calculated for a susceptible node by subtracting the total system susceptibility of a node from the total propagated ambient field from all other emitting nodes in the electromagnetic topology. That is:

$$\mathbf{FI} = \mathbf{PAF} - \mathbf{SS}$$

and then the likelihood of failure is then assigned a value according to Figure 41.

<i>extreme</i>	if $\mathbf{FI} \geq 1.5$
<i>high</i>	if $0.5 \leq \mathbf{FI} < 1.5$
<i>marginal</i>	if $-0.5 \leq \mathbf{FI} < 0.5$
<i>low</i>	if $-1.5 \leq \mathbf{FI} < -0.5$
<i>very low</i>	if $-2.5 \leq \mathbf{FI} < -1.5$
<i>nil</i>	$\mathbf{FI} < -2.5$ or associated with a non-susceptible nodes
<i>unknown</i>	if either susceptibility or disturbance are <i>unknown</i>

Figure 41 Likelihood of failure discrete levels

If the likelihood of failure of any suspector is too great, then parameters in one or all of the three constraining factors must be modified at one or more locations in the topology in order to reduce the likelihood of failure. That is, the electromagnetic disturbance located at a node may be reduced (if one has control of the emitter), the susceptibility of the receptor may need to be decreased, and/or the shielding effectiveness of specific surfaces may be increased. There will usually exist more than one way to reduce the likelihood of failure at a specific suspector, each having its own advantages and

Part 1

disadvantages. This is where the traces which were developed for the worst PAF will help. Also for the worst PAF the critical path is stored with a trace of lowest to highest SE thus giving the most probable surface to enhance in the topology.

Visually it is convenient to refer to Figure 42 to understand how the likelihood of failure is determined. Notice how the calculated FI is not uniquely determined by the *reported* PAF and system susceptibility. For example a PAF reported as *very-low* may be stored numerically as from -1.5 to 1.0 and produce either a *nil* to *marginal* likelihood of failure for an *extreme* susceptibility. This example is highlighted in Figure 42 below.

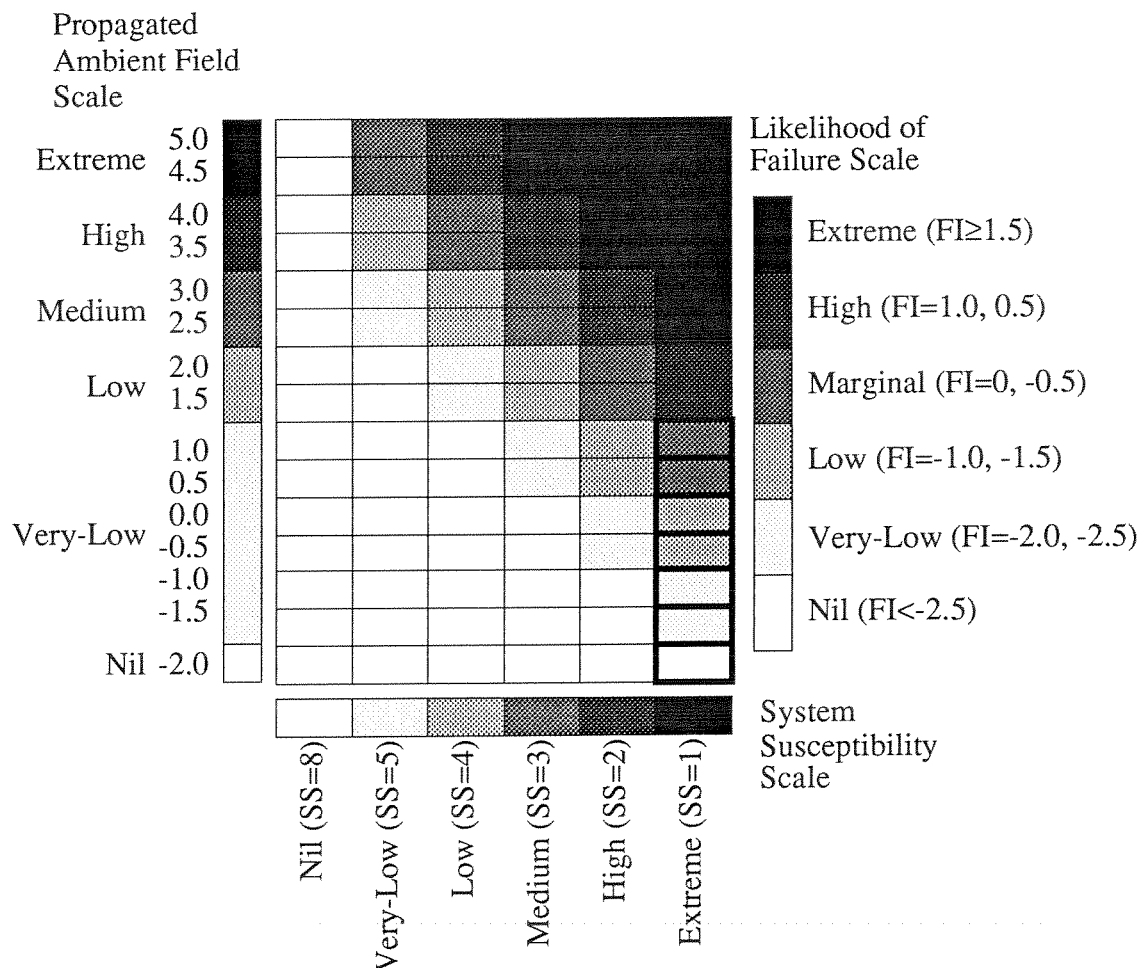


Figure 42 Likelihood of Failure Chart

5.6.1 Justification of Failure Index Determination

The procedure for determining the likelihood of failure described above can be justified heuristically by an understanding of what each of the FI levels represents. Recall that the disturbance levels of Figure 17 and Figure 18 (here referred to as ambient field levels) as well as the susceptibility levels of Figure 24 were defined to correspond to the same power levels. Thus the ambient field ranges can be plotted on a graph of the susceptibility levels as shown below in Figure 43.

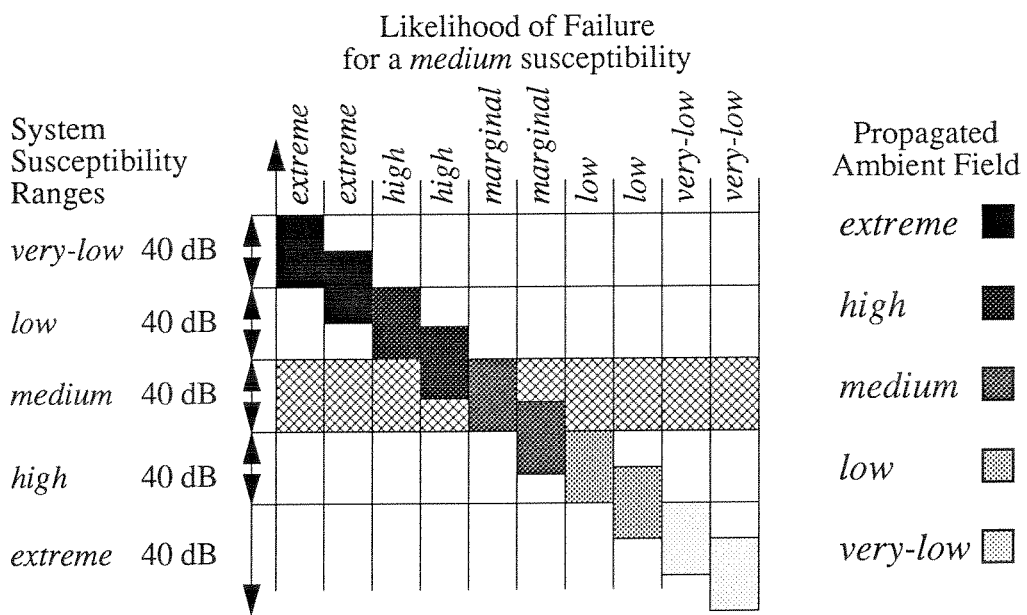


Figure 43 Overlap of PAF ranges with SS ranges to determine FI

The likelihood of failure results for a system susceptibility of *medium* are shown across the top of the diagram. Note that there are two ambient field ranges for each level shown in the propagated ambient field key at the right of the figure. This is again due to the 20 dB discretization of the shielding effectiveness data. Any time there is an overlap between the PAF distribution and the SS distribution the likelihood of failure is said to be *high* or *marginal*; *high* if the PAF distribution overlaps above the SS distribution. When the

Part 1

PAF distribution lies totally above the SS distribution then the likelihood of failure is said to be *high* or *extreme* depending on how much higher the distribution lies. Alternatively the likelihood of failure is determined as *low*, *very-low* or *nil* depending on how much lower the PAF distribution is than the SS distribution.

5.7 Grouping of Electromagnetic Volume Nodes

Previously it was shown how a set of nodes in a graph could be grouped together and represented in the graph as a *grouped node*. Recall that not just any set of nodes could be grouped together but that they must form a valid grouping (see discussion about grouping nodes associated with Figure 9 in the section *Some Graph Theory Definitions and Techniques* on page 24). The advantage of grouping is that the size of the graph is reduced markedly and all of the grouped nodes are removed from the search space when finding worst case shielding paths. The procedure for representing the attributes of the grouped node based on the individual attributes of the nodes being grouped is presented below.

In order for the grouped node to accurately represent the subgraph from which it was formed it must derive its attributes from the subgraph attributes. This is accomplished by determining the *single source minimal spanning tree* for the subgraph in terms of shielding effectiveness with the cut-node as the root node. The susceptibility as well as the ambient field attributes of each node in the subgraph are then propagated to the root node and added in parallel along with the self attributes of the cut-node to form a new grouped system susceptibility and ambient field for the grouped node.

The propagation of the individual susceptibility values is accomplished by using the discrete system susceptibility numbers of Figure 40 and subtracting from these the total shielding effectiveness value SE (see Figure 35) for the worst case shielding path to the root node. The propagation of the ambient fields is performed in the same manner as discussed previously in the section *Propagation of Electromagnetic Disturbance* on page 80.

Part 1

For example, Figure 44 shows a subgraph to be grouped into the cut-node v_1 . The attributes of the individual nodes are also shown to the right of the figure for a specific frequency range in the global frequency ranges. Notice that node V_3 has no ambient field while node V_2 has neither susceptibility nor ambient field. The shielding effectiveness of the individual paths is shown on the subgraph and the worst case minimal spanning tree is highlighted

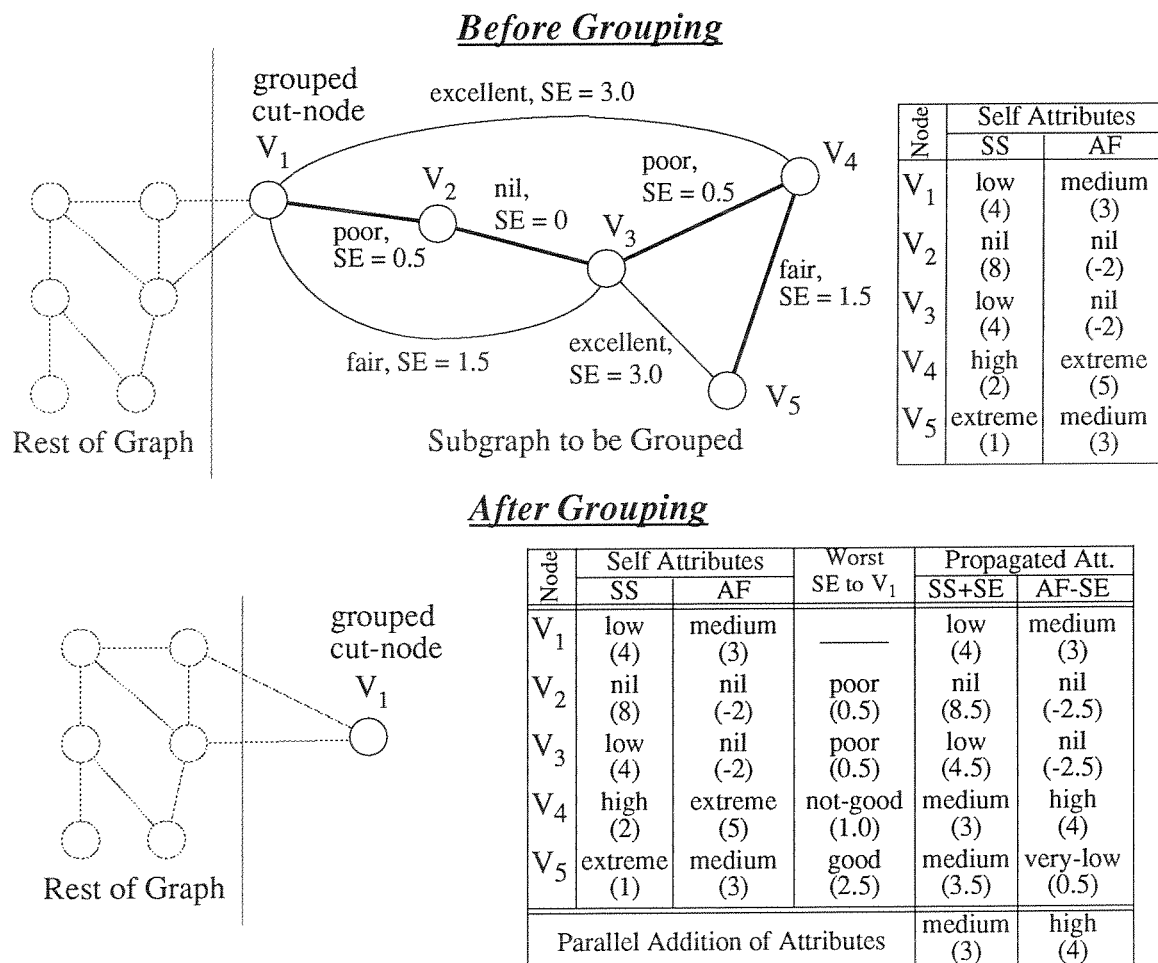


Figure 44 Example of grouping a subgraph in a cut-node
(attributes are shown for a specific frequency range)

Part 1

After grouping, only node V_1 is left with a grouped system susceptibility of *medium* and a grouped ambient field of *high*. Notice that parallel addition effectively takes the worst case of both attributes. Thus, even if attributes of nodes in other parts of the graph change or even if the topology of the rest of the graph changes, the minimal spanning tree search for this particular subgraph does not need to be repeated. Similarly, if attributes or the topology of the grouped nodes change, the minimal spanning tree of the rest of the graph (assuming that the cut-node is still a valid cut-node) will not change. Note that although the minimal spanning trees of either graph components (i.e. the grouped node component or the rest of the graph component) do not change, the likelihood of failures of the individual nodes therein *may* change.

In order that information is not lost about which node might be failing when the likelihood of failure of a grouped node is calculated, a *trace* is kept of the node in the group contributing the most to the grouped node susceptibility attribute. Thus, if the likelihood of failure is determined to be *high* in a certain frequency range, then the trace of the susceptibility attribute will list, in order from worst SS to best SS, the nodes contributing to the grouped SS. Similarly a record of the worst propagated ambient fields is kept in the form of a *trace*.

As an example, for the grouped nodes of Figure 44 the trace of the grouped SS attribute would be represented as the list $[V_4, V_5, V_1, V_3, V_2]$ while the grouped AF trace would be held as $[V_4, V_1, V_5, V_2, V_3]$. From these traces one can immediately determine which nodes' SS to increase or which nodes' AF to decrease if an interaction problem exists within the grouped node.

Chapter 6

Implementation

The heuristic techniques and procedures described in the previous chapters have been implemented in the form of an *Electromagnetic Interaction Advisor* on a Sun Microsystem's SPARCstation 1™ (see LoVetri *et al* in [LoVetri 89] and [LoVetri 90a,b]). The implementation consists of two main parts; a smart topology drawing tool referred to as *HardDraw* (see Taylor [Taylor 90]), and an electromagnetic interactions expert system referred to as *HardSys*.

6.1 HardDraw: Smart Topology Drawing Tool

The purpose of *HardDraw* is to give the user of the software an easy way to input the electromagnetic topology of systems. The smart topology drawing tool is implemented on top of four existing development tools. These are: NeWS™ (see [Arden 89] and [X11/NeWS 89]; GoodNeWS [van Hoff 89a]; HyperNeWS [van Hoff 89b]; and Quintus Prolog™ [Quintus 88]). The *multiple stack* interface of HardDraw runs under HyperNeWS/GoodNeWS, which run under the Sun Microsystems *Network Windowing System* (NeWS™). A brief description of the GoodNeWS and HyperNeWS environments follows in order to clarify the workings of the software implementation.

6.1.1 GoodNeWS

GoodNeWS is a NeWS-based window interface that has been developed at the Turing Institute in Glasgow, Scotland [van Hoff 89a]. It is written in C and PostScript (see [Adobe 85,87] and makes use of NeWS graphics primitives. GoodNeWS provides a complete windowing environment which includes terminal emulation, graphics drawing tools (colour and black and white), use of captured images and a LaTeX previewer. It is an extension of the NeWS environment implying downward compatibility with existing NeWS software.

6.1.2 HyperNeWS

HyperNeWS is a general user interface designing tool written in Postscript. The programming philosophy is *object-oriented* and is based on *parallel stacks*; each stack consisting of a number of cards. Individual objects may be created and attached to individual cards or stacks. These objects may take the form of buttons, sliders, text, and a number of other types including user designed buttons via the GoodNeWS drawing tool. Messages can be passed between objects as well as between objects and a client program running in a terminal window. There exists an interfacing capability to the C, Prolog, and Lisp programming languages. Thus, as will be described latter, a Prolog client program can be interfaced to one or many stacks running in HyperNeWS.

6.1.3 HardDraw as a Stack

The smart topology drawing tool is implemented as a stack in HyperNeWS. On the stack, a user can draw named electromagnetic volumes which overlap each other. The overlapping volumes represent surfaces between the individual volumes. As the user draws the volumes the surfaces are automatically calculated and the corresponding graphical representation of the electromagnetic topology is created in another stack. Changes can be made to the topology using the various drawing options provided. Also, a drawing produced in the GoodNeWS drawing tool can be copied onto an electromagnetic volume

Part 1

thereby providing a visual queue for the volume. A stack based menu system is also used to change the electromagnetic attributes of any of the volume nodes. This is done by first selecting a component either on the volume topology stack or the graph stack and then modifying the attributes via the attribute editor stack. The attributes associated with a surface can be modified by selecting two volumes or two nodes and then using the attribute editor.

The above has been a very brief description of some of the capabilities of the *HardDraw* tool. For further details see the preliminary document produced by Taylor [Taylor 90]. An example of what the user's screen would look like during a session is shown below in Figure 45.

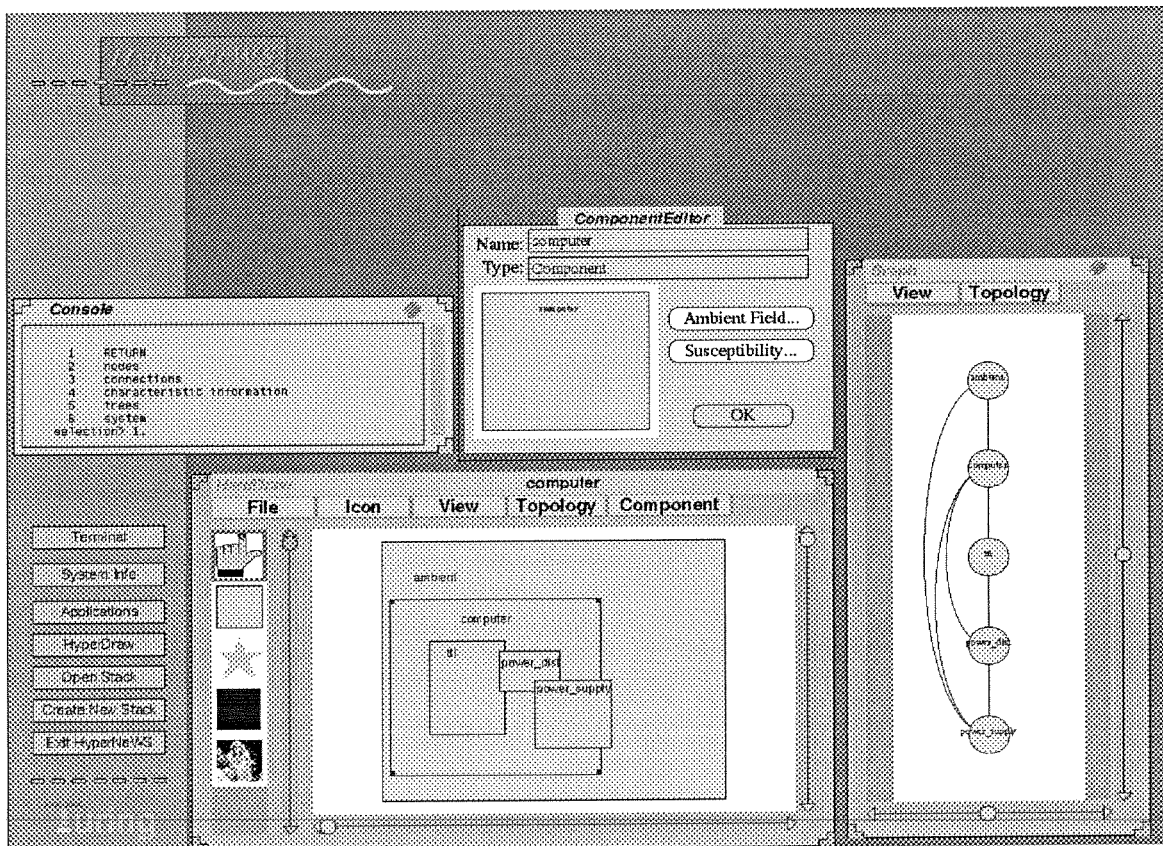


Figure 45 Example HardDraw session

6.2 HardSys: Electromagnetic Interaction Expert System

Once the electromagnetic topology has been entered and the volume/surface node attributes have been defined, reasoning about the possible interactions therein is performed by HardSys, an expert system written in Prolog (see [Clocksin 84], [Sterling 86], and [Quintus 88]). An *object-oriented knowledge representation* approach is taken based on that of Stabler (see [Stabler 86]). A predicate was added for modifying an object's methods. A description of how the methodology presented in previous chapters is implemented as objects now follows.

6.2.1 Electromagnetic Volume Nodes as Objects

Electromagnetic volume nodes are implemented as *objects* with *methods* describing the attributes associated with the volume. Any *name* can be used to label an object; the object is then referenced using *node(name)* as the object name. When a node is created it is created with many methods for storing the attributes or constraints which will be imposed. Some of the methods are shown below; specific methods required to implement the interface with HardDraw are not shown.

1) Node Identification Methods

- *node_name(Name)* - holds the name of the node.
- *description(' ... ')* - any description the user wants to associate with the node.
- *type(internal or grouped)* - whether it is a grouped node or an individual volume node.

2) Electromagnetic Disturbance Methods

- *af_components([Self_af_components])* - holds the list of specific disturbances (i.e. [type, sub-type]) as defined in the currently loaded knowledge base.
- *af_value([Self_af_values])* - holds the value of the self disturbance after *frequency normalization* and *parallel addition* algorithms are applied to components in the list of af_components.

Part 1

- af_trace([... [Self_af_trace] ...]) - list of self disturbance traces, that is a list of af_components in worst to best order for each frequency in the global frequency range.
- af_update_flag(false or true) - indicates whether af_value requires to be updated, that is whether or not any new af_components have been added.

3) System Susceptibility Methods

- ss_components([Self_ss_components]) - holds the list of specific system susceptibilities (i.e. [type, sub-type]) as defined in the currently loaded knowledge base.
- ss_value([Self_ss_values]) - holds the value of the self system susceptibility after *frequency normalization* and *parallel addition* algorithms are applied to components in the list of ss_components.
- ss_trace([... [Self_ss_trace] ...]) - list of self susceptibility traces, that is a list of ss_components in worst to best order for each frequency in the global frequency range.
- ss_update_flag(false or true) - indicates whether ss_value requires to be updated, that is whether or not any new ss_components have been added.

4) Group Node Methods

- group_components([Group_nodes]) - the nodes belonging to this grouped node.
- group_af_value([Group_af_values]) - same as af_value but holds the composite grouped af_value for the grouped nodes.
- group_af_trace([... [Group_af_trace] ...]) - the trace due to the parallel addition of the grouped nodes total af_values.
- group_ss_value([Group_ss_values]) - same as ss_value but holds the composite grouped ss_value for the grouped nodes.
- group_ss_trace([... [Group_ss_trace] ...]) - the trace due to the parallel addition of the grouped nodes total af_values.

Part 1

- `total_af_value([Total_af_values])` - parallel addition of group_af_value and af_value lists, that is total disturbance emitted from node.
- `total_af_trace([... [Total_af_trace] ...])` - trace associated with total_af_value for the node.
- `total_ss_value(Total_ss_value)` - parallel addition of group_ss_value and ss_value lists, that is total system susceptibility of grouped node.
- `total_ss_trace([... [Total_ss_trace] ...])` -trace associated with total_ss_value for the node.

6.2.2 Surface Nodes as Objects

In a similar way the surfaces between electromagnetic volume nodes are represented as objects. A specific surface is identified as a unidirectional connection between two nodes in the topology. For example, the shielding effectiveness of a path from `node(v1)` to `node(v2)` would be stored in the methods of the object called *connections(node(v₁), node(v₂))*. Some of the methods stored in a typical connections object are shown below.

1) Connection Identification Methods

- `type(link or hidden_link)` - hidden if grouped into a grouped node.
- `description(' ... ')` - any description the user wants to associate with the node.

2) Shielding Effectiveness Methods

- `se_components([Se_characteristics])` - holds the list of specific shielding effectivenesses (i.e. [type, sub-type]) as defined in the currently loaded knowledge base.
- `se_value([Se_values])` - holds the value of the shielding effectiveness after *frequency normalization* and *parallel addition* algorithms are applied to components in the list of se_components.

Part 1

- `se_trace([... [Se_trace] ...])` - list of shielding effectiveness traces, that is a list of `se_components` in worst to best order for each frequency in the global frequency range.
- `se_update_flag(true or false)` - indicates whether `se_value` is required to be updated, that is whether or not any new `se_components` have been added.

6.2.3 Spanning Tree Calculations

The minimal spanning tree can be calculated for any or all nodes defined in the electromagnetic topology. Recall that the minimal spanning tree for a root node must be calculated for all frequency ranges in global frequency range set and will, in general, be different for each frequency range.

The search is performed for each susceptible node. That is, each node for which the total system susceptibility is not *unknown*, using Dijkstra's algorithm as given in Figure 6 on page 28. The algorithm searches the graph in order, starting with the nodes with worst shielding effectiveness from the root node. The search is stopped when one of the two goals shown below in Figure 46 has been achieved.

- 1) *All the nodes left in the search space do not have ambient fields associated with them. That is, they are not emitting nodes, and thus they will have no effect on the likelihood of failure of the root node;*
- 2) *or when the total current shielding in the search has produced a $SE \geq 10$, thus the next node search will have an SE of at least 10 from the current root node.*

Figure 46 Two heuristics to stop the MST search

For example, using the first heuristic, if only one emitting node exists in the topology then the search only has to proceed until the shielding effectiveness to this node has been determined. The second heuristic provides for the concept of *neighborhoods* to be introduced; any nodes with a shielding effectiveness of less than 10 to a root node are said

Part 1

to be in the neighborhood of the root node. Thus, when a change is made in the topology attributes, knowledge about the nodes which will be affected by this change can be immediately determined by knowledge of the nodes included in the neighborhood where the change took place. In this way the search time can be greatly reduced.

The minimal spanning tree information is also stored as an object referenced as *spantree(environment)* where environment is a predicate of the form:

- *environ(Root, Frequency_range)* - where Root is the root node of the tree and Frequency_range is a frequency range in the global frequency range list.

Some methods associated with this object are:

- *type(tree)* - specifies that this is a minimal spanning tree.
- *description (' ... ')* - for future use to hold the conditions under which the search was performed.
- *tree_vertices([Nodes])* - list of nodes in the minimal spanning tree
- *tree_edges([Connections])* - list of connection objects which make up the edges of the tree.

With this representation it is easy to access information about any minimal spanning tree calculations which have been performed.

6.3 Future Implementation Issues

Speed is the major concern at the present time. The knowledge representation scheme used herein is general enough to make incremental modifications to the methods used. Techniques such as keeping information used in previous searches to speed up new searches required when changes are made to the topology can be implemented in the current knowledge representation scheme. For information regarding some recent research on these techniques see the work by Ahuja [Ahuja 90] and Dechter [Dechter 90].

Chapter 7

An Application: Helicopter EMI

7.1 NEMP Hardening of Typical Helicopter

The EMI prediction concepts discussed in the previous chapters were applied to data obtained for a typical helicopter (see LoVetri *et al* [LoVetri 90c]). This was done in order to validate the paradigm established herein for the approximate understanding of electromagnetic interactions. The use of the topological approach helps also in defining a general view of shielding and filtering requirements at the design stages of a project.

7.1.1 Specific Electromagnetic Topology Used

The topology of the helicopter was decomposed into basic surfaces: the aircraft skin; the equipment shield; and the interconnecting cables. The data obtained pertaining to the electromagnetic topology was coarse since the helicopter design was at the initial stages; that is, contractor specifications were in the process of being written. These design specifications include EMI/EMC requirements for each sub-component in the helicopter. Thus it is at this stage that one would like to try different hardening approaches to the design of the complete system. The specific topology used is shown below in Figure 47. The associated bipartite graph is shown in Figure 48. Note that in Figure 48 the circuit nodes are shaded while the field nodes are not. The smaller solid nodes represent the surfaces where the shielding effectiveness data is stored.

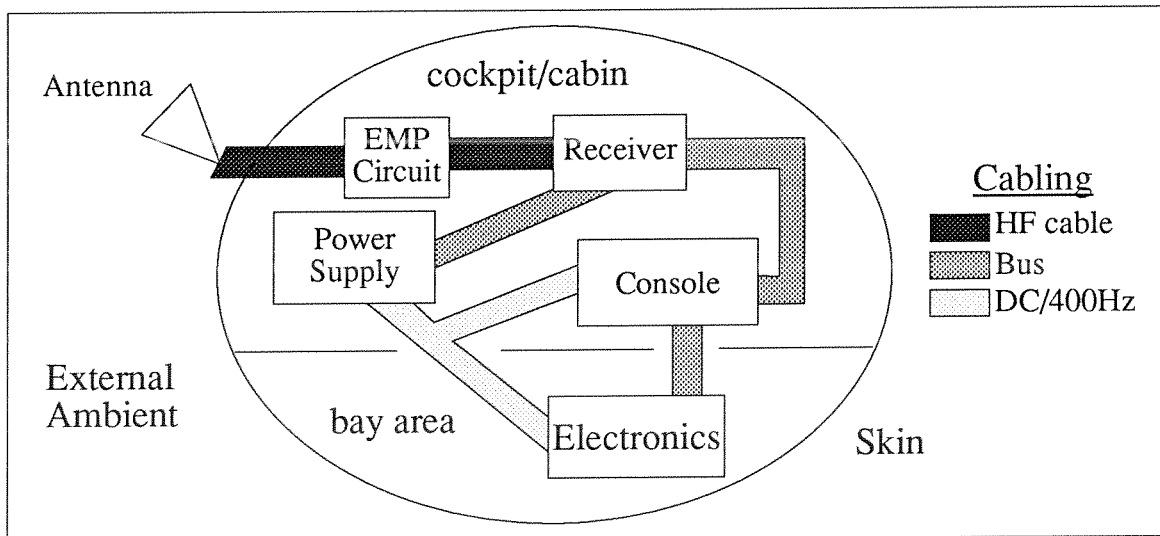
Part 1

Figure 47 Simplified helicopter electromagnetic topology

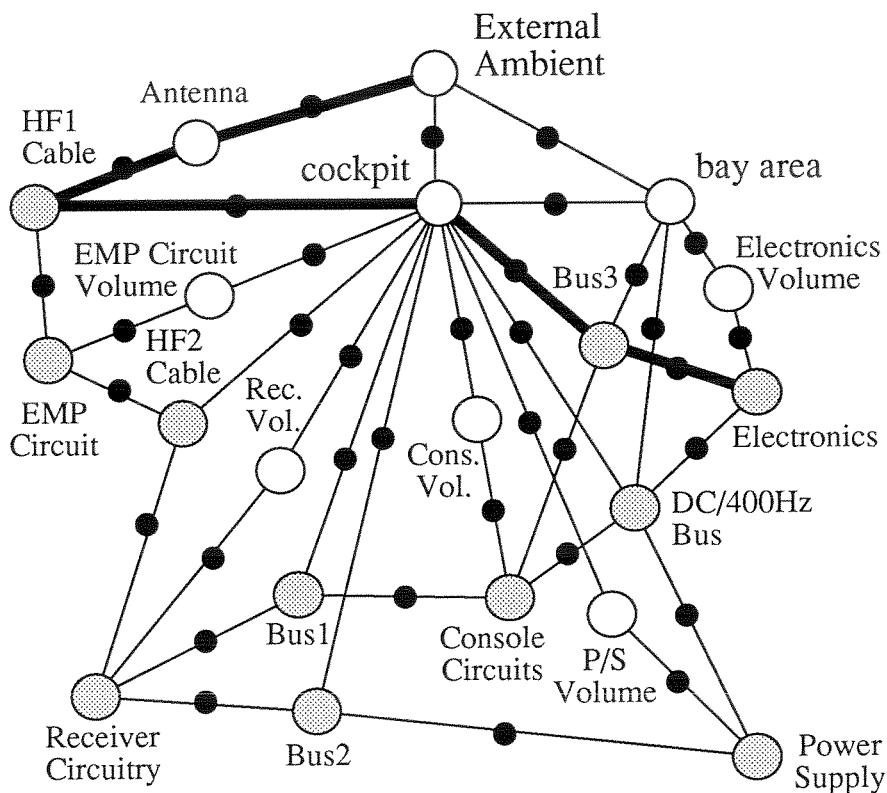


Figure 48 Equivalent bipartite graph for helicopter topology

Part 1

7.1.2 Electromagnetic Disturbance

The major electromagnetic disturbances which were of concern were the *nuclear and lightning electromagnetic pulse* (NEMP and LEMP) as well as isolated continuous wave *microwave threats* located in the ambient field volume of Figure 47. A similar combination of threats was used by Podgorski as a *composite threat* (see [Podgorski 90a]) to describe the external electromagnetic threat produced by a combination of lightning, NEMP, and microwave threats (note that Podgorski adds the individual threats with units of [V/m] which he obtains by multiplying with frequency). The data for the individual threats was entered individually into HardSys which in turn constructed the composite threat based on the parallel addition and frequency normalization procedures previously described. The individual threats used are shown below in Figure 49. The global frequency range set used can also be seen in the figure.

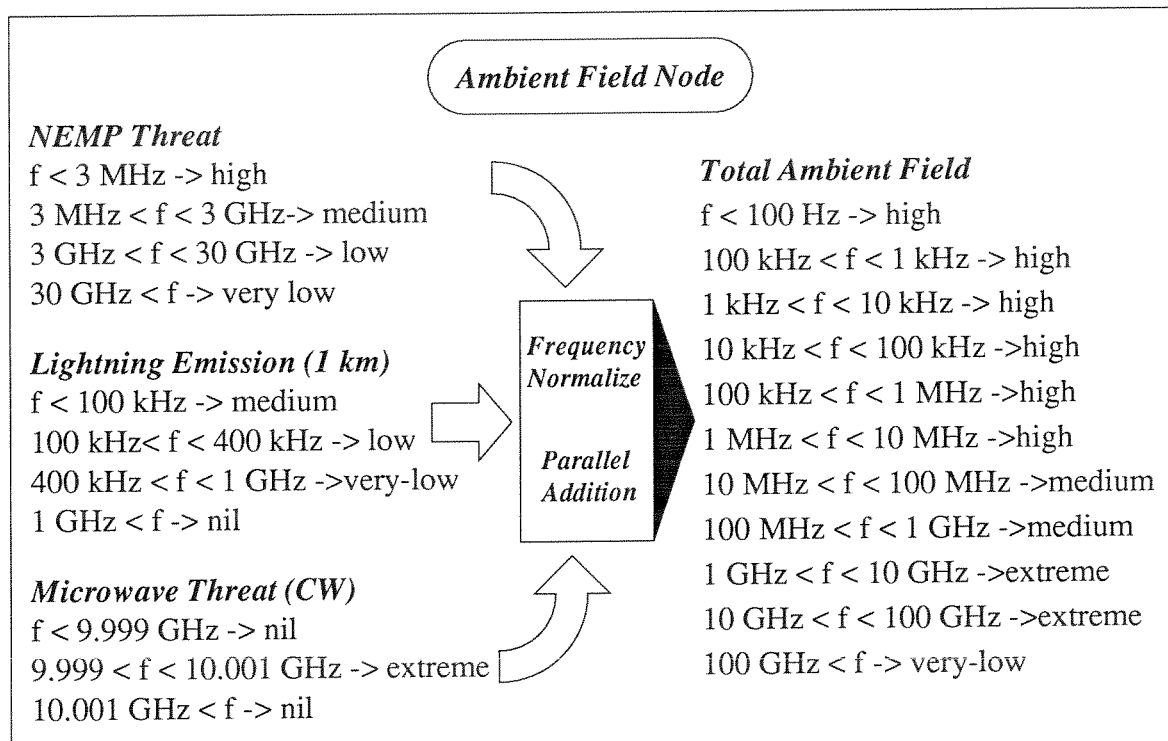


Figure 49 Approximation of the electromagnetic threats used

Part 1

Notice that, although the frequency ranges are quite fine, they produce some bad approximations in the 1 GHz to 100 GHz range due to the *microwave threat* at 10 GHz. Ideally, a finer frequency range should be used in this area. Of course, if this produces a high likelihood of failure then the traces available in the system would reveal this coarse approximation; if no high likelihood of failure was produced then one can be assured that a worst case approximation has been taken and further frequency refinement is not required.

Now although a single ambient field is propagated the trace of the parallel addition provides the information about which of the three fields is the determining factor in a certain frequency range. Each threat can be deleted individually in order to determine a new likelihood of failure at the susceptible nodes, thus providing information about what the susceptible node will withstand in terms of disturbance before failure.

7.1.3 System Susceptibility

Information obtained for the susceptible systems of the helicopter were converted into a representation which HardSys could handle. This information consisted of the specific technologies used in each subcomponent in the helicopter. Sensitivity analysis of the analogue and digital circuits was based on analysis of MOS and TTL technology respectively (see [McDonnel 78]). As for the case of the ambient fields, the susceptibilities for each node were entered individually and HardSys determined the composite susceptibility at each node.

For example, the power supply was assumed to consist of TTL, analogue op-amps, and comparator type electronics. The susceptibility for each of these was taken from the knowledge-base and combined to produce a single total susceptibility for the power supply node. This procedure is shown for the *electronics node* in Figure 50.

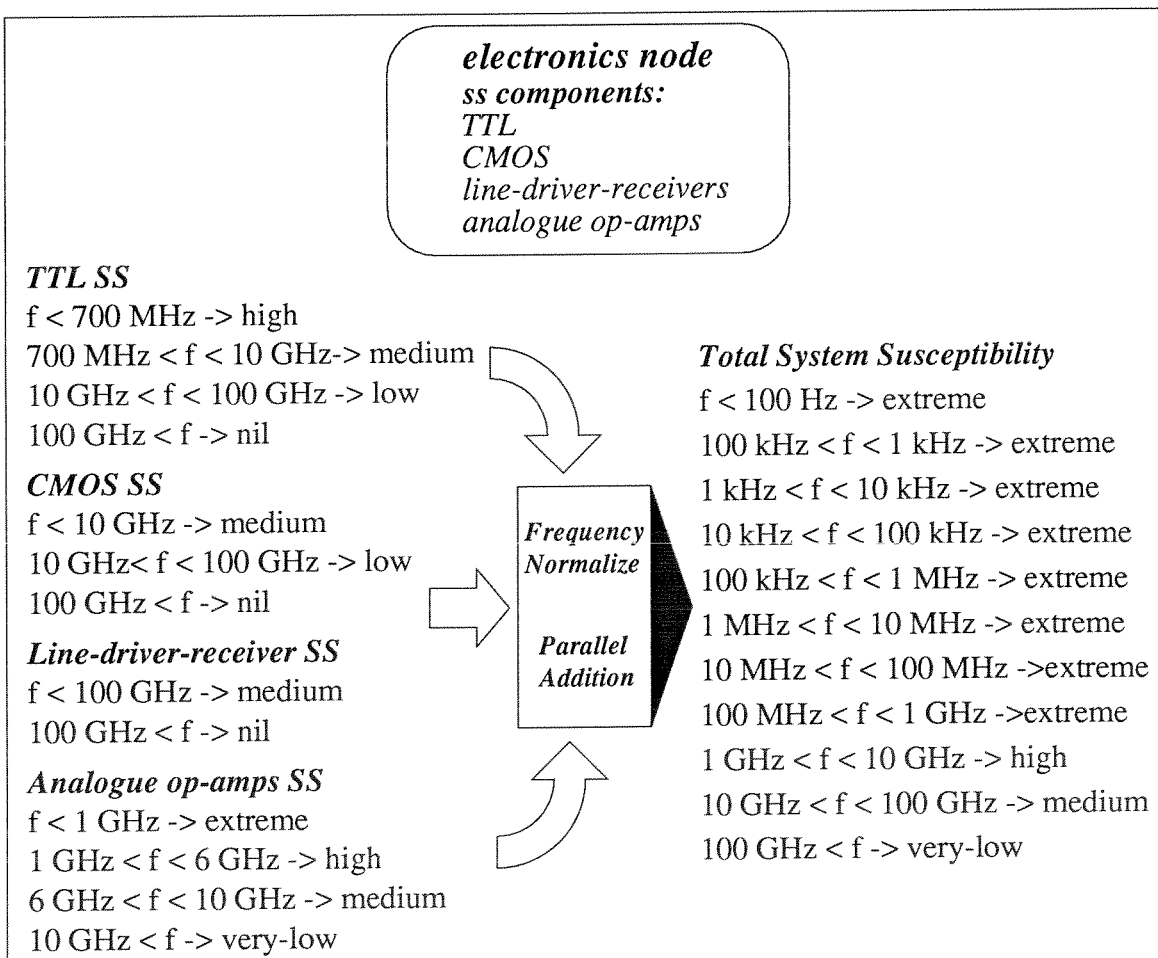
Part 1

Figure 50 System susceptibility for electronics node

As can be seen from the above figure the determining factor in *almost* all of the frequency ranges is the system susceptibility for the *analogue op-amp*. Thus a means of isolating this device in the case where the likelihood of failure for the node is not acceptable is to create a node for the op-amp itself. Physically, this may consist of placing the op-amp circuitry in a module of its own with its own *shielding surface*. In this manner, as long as the likelihood of failure due to the other components in the electronics node is acceptable no further shielding would be required on the electronics node. This may produce a savings in either weight or cost; both very important for this type of system.

7.1.4 Shielding Effectiveness of Surfaces

The shielding properties of the helicopter shell and equipment cabinets with the associated cabling were also entered in the appropriate form. The shielding effectiveness of the helicopter skin was assumed to be negligible above 10 GHz and drastically reduced by large windows and doors below 10 MHz. The SE of the *external ambient/antenna* path was assumed to be *nil* in the HF and UHF bands while set to *excellent* outside these bandwidths. The coupling to the printed circuit boards was based on an average size printed circuit board of 1x1 ft.² and assuming short connector runs. For example, the SE from a field node to a circuit node was approximated by that of a half-wave dipole as given by equation (4.31) and equation (4.32). As was discussed in *Section 4.4.1.3 on page 68*, this approximation has been found to be good for frequencies ranging from 100 MHz to 10 GHz (see McDonnel Douglas report [McDonnel 78]). For lower frequencies a maximum effective aperture of $A_{em} = 1$ is appropriate.

For the case of coupling to shielded cables, a *transfer impedance* can be defined which relates the differential-mode voltage produced on a cable to the current induced on the surface of a shielded cable by an external electromagnetic field (see Smith [Smith 77] and Vance [Vance 78]). The transfer impedance is a function of frequency $\omega = 2\pi f$ and the cable geometry. If the transfer impedance is denoted as $Z_t(\omega)$ then:

$$dV(z, \omega) = Z_t(\omega) \times I_s(z, \omega) dz \quad (7.1)$$

where $I_s(z, \omega)$ is the shield current at position z along the cable and $V(z, \omega)$ is the voltage induced inside the cable. Analytical expressions for $Z_t(\omega)$ and $I_s(z, \omega)$ can be found in many publications such as [Smith 77] and [Vance 78]. A comparison between experimental and analytic predictions has been done by Guo [Guo 86] where plots of the induced voltage at a load connected to a coaxial cable due to an incident electric field for both experimental and analytic cases are provided. Results were given for a 4m length of RG-58C/U coaxial cable above a finite ground plane. From these plots, approximate data can be derived for

Part 1

use in the HardSys knowledge-base. Two sets of data for a short (2m) and a long (4m) cable are shown below in Figure 51.

<i>Shielding Effectiveness for Cables</i>	
<i>Short Cable (2m)</i>	<i>Long Cable (4m)</i>
$f < 50 \text{ MHz}$ -> good	$f < 25 \text{ MHz}$ -> good
$50 \text{ MHz} < f < 55 \text{ MHz}$ -> poor	$25 \text{ MHz} < f < 30 \text{ MHz}$ -> poor
$55 \text{ MHz} < f < 150 \text{ MHz}$ -> good	$30 \text{ MHz} < f < 50 \text{ MHz}$ -> good
$150 \text{ MHz} < f < 155 \text{ MHz}$ -> poor	$50 \text{ MHz} < f < 55 \text{ MHz}$ -> poor
$155 \text{ MHz} < f < 250 \text{ MHz}$ -> good	$55 \text{ MHz} < f < 75 \text{ MHz}$ -> good
$250 \text{ MHz} < f < 255 \text{ MHz}$ -> poor	$75 \text{ MHz} < f < 80 \text{ MHz}$ -> poor
$255 \text{ MHz} < f < 350 \text{ MHz}$ -> good	$80 \text{ MHz} < f < 100 \text{ MHz}$ -> good
$350 \text{ MHz} < f < 355 \text{ MHz}$ -> poor	$100 \text{ MHz} < f < 105 \text{ MHz}$ -> poor
$355 \text{ MHz} < f < 450 \text{ MHz}$ -> good	$105 \text{ MHz} < f < 125 \text{ MHz}$ -> good
$450 \text{ MHz} < f < 455 \text{ MHz}$ -> poor	$125 \text{ MHz} < f < 130 \text{ MHz}$ -> poor
$455 \text{ MHz} < f < 550 \text{ MHz}$ -> good	$130 \text{ MHz} < f < 150 \text{ MHz}$ -> good
$550 \text{ MHz} < f < 555 \text{ MHz}$ -> poor	$150 \text{ MHz} < f < 155 \text{ MHz}$ -> poor
$555 \text{ MHz} < f < 1 \text{ GHz}$ -> fair	$155 \text{ MHz} < f < 1 \text{ GHz}$ -> fair
$1 \text{ GHz} < f < 10 \text{ GHz}$ -> good	$1 \text{ GHz} < f < 10 \text{ GHz}$ -> good
$10 \text{ GHz} < f$ -> excellent	$10 \text{ GHz} < f$ -> excellent

Figure 51 Approximations for cable shielding

As can be seen from the above figure *resonances* occur in the shielding effectiveness of the finite length cables. Of course, unless a sufficiently fine global frequency range is used, these resonances will be spread out over a larger frequency range.

As well as the above mentioned shielding paths, other shielding characteristics such as for *honey-comb* cooling vents, power-line filters, viewing screen filters (for the console monitor) and other typical shielding components were used to fill the attributes of each surface node. The intent here is not to come up with precise approximations for all path attributes but to include a sufficient number such that the usefulness of the software can be determined. More wide ranging data can be collected in the future.

7.1.5 Results and Software Performance

HardSys provides the *critical path* through the topology for each susceptible node; this is the path which causes the greatest likelihood of failure for a node. In the present case there are five critical paths from the external ambient node to the five susceptible nodes. These are highlighted on the HardDraw graph stack. For example, in the 10 MHz to 100 MHz frequency range the worst case path from the external ambient to the electronic circuits in the bay area is highlighted (in bold) in Figure 48. This path caused a *marginal* likelihood of failure in the 10 MHz to 100 MHz frequency range. Other global frequency ranges would produce different critical paths.

As well as the graphical information, HardSys outputs the likelihood of failure in tabular form over the global frequency ranges. An example of the likelihood of failure for the electronics node is shown below.

<i>Frequency Range</i>	<i>Failure Risk</i>	<i>Frequency Range</i>	<i>Failure Risk</i>
>0 Hz to 100 Hz	low	10 MHz to 100 MHz	marginal
100 Hz to 1 kHz	very_low	100 MHz to 1 GHz	marginal
1 kHz to 10 kHz	very_low	1 GHz to 10 GHz	very_low
10 kHz to 100 kHz	very_low	10 GHz to 100 GHz	very_low
100 kHz to 1 MHz	very_low	>100 GHz	nil
1 MHz to 10 MHz	very_low		

Figure 52 Tabular output of likelihood of failure information

The program took only about 5 minutes of CPU time per susceptible node to complete the search, which is reasonably efficient considering this graph contains 20 volume nodes and 70 surface nodes (2 times 35 directional nodes).

Chapter 8

Conclusions and Future Plans for the EMI Advisor

Work on the *Electromagnetic Interactions Advisor* is ongoing in order to bring it to the level of a usable commercial software tool. The future plans in this development can be described as falling under three categories:

- 1) knowledge representation and search technique enhancements;
- 2) user interface enhancements; and
- 3) knowledge acquisition and validation.

The search technique used thus far is the *theoretically* most efficient (see Ahuja [Ahuja 90]) although implementation techniques to improve efficiency can be applied. For example, automatic grouping of nodes by the advisor is a possibility to be examined. Such a technique, called *cut-set decomposition*, has been studied by Rina Dechter [Dechter 90]. Changes in the knowledge representation may also yield better search times.

Currently the advisor works in the *analysis mode*, that is, the physical topology along with the associated node attributes are first entered and the system then determines if any interaction problems exist. In the *design mode* the advisor would be given some global constraints to satisfy and it would be free to choose or design the system within these constraints. For example, a global constraint may be a weight and cost limit. The system

Part 1

would then choose subcomponents from a database with each having unique cost and weight attributes as well as system susceptibilities and electromagnetic emissions. Shielding components may also be chosen in a similar way. Of course, in such a process, more than one solution would exist; thus heuristic guided design would be appropriate.

The user interface, HardDraw, will be enhanced in terms of better menus and easier creation of electromagnetic topologies. For example, presently the topology can only be created and modified on the *volume topology stack*. In future versions modification of the topology should be possible on the *graph stack*. User interface *is* important in the acceptance of any software tool — if it cannot be used easily it will not be used.

Knowledge acquisition is the problem of how to acquire accurate EMI data from the many sources available (see for instance the six volumes of White [White 73]) and how to categorize it so that it can be presented to the user in a logical and efficient manner. Validation of the knowledge base, once created, is a process which will take many years and will only be accomplished by the EMI community's *acceptance* of the tool; for it can only be validated on practical systems.

The concepts used in the advisor are fundamental to all electromagnetic interaction phenomena and thus *HardDraw* and *HardSys* as educational tools can be very instructive. Hopefully the art of electromagnetic hardening will be better understood, for in the future, its importance in our technologically based world *will grow*.



Algorithmic Techniques

In this part algorithmic techniques for solving electromagnetic interaction problems are investigated. Numerical methods for solving partial differential equations have progressed very rapidly in the past twenty years; not only in the field of electromagnetics, but also in other applied fields such as computational fluid dynamics. Computers and software capable of implementing these procedures have also advanced. Furthermore graphics software for displaying the computed results are readily available on most computer systems. These tools make the visualization and the understanding of the electromagnetic physics easier.

Chapter 9

Introduction to Numerical Methods

The physical phenomenon of electromagnetic interactions is described by Maxwell's equations. These equations can be expressed in a variety of mathematical forms, each having its own advantages and disadvantages. For example, they may be formulated as a system of partial differential equations over space and time domains or, as is often done in the engineering literature, the partial differential equations may be immediately cast in the frequency domain by assuming time harmonic excitations (see [Harrington 61]). Time domain responses are then calculated by a linear superposition of the individual harmonic solutions. Other formulations consist of defining vector and scalar potentials which are related to the electric and magnetic fields by some vector differential operators (see [Stratton 41]). Still others make use of integral relations, in either time or frequency domains, for either potential fields or the electric and magnetic fields directly. These usually result from using the integral form of Maxwell's equations or solving the differential equations analytically for some *fundamental sources*, in the form of a Green's function, and then formulating integral relations for the general source problem using the Green's function (see [Tai 71] and [Eyes 80]).

Once the equations have been formulated, many algorithmic techniques exist to produce the required solution. *Finite difference* and *finite element* methods (*i.e.* including the *method of moments*) form the majority of these techniques for all the different types of formulations encountered (see [Lapidus 82] and [Mitchell 80]). Depending on the chosen

Part 2

formulation each algorithmic method has its own advantages and disadvantages. Issues which arise in the use of numerical techniques are *accuracy* of the resulting solution, as well as *efficiency* and *stability* of the algorithm (especially for time domain problems). In general, no one algorithm is robust enough to account for all the physical and formulation variations encountered in solving electromagnetic field problems. Therefore, it is prudent to have an understanding of a variety of algorithms.

Practical issues such as memory requirements, efficiency, and overall speed of calculation are also of concern when numerical methods are implemented on a computer. Also, to allow easy study of interaction phenomena, the output from a numerical method must be presented in some visual form (i.e. using graphics software). A summary of all these concerns is depicted in Figure 53.

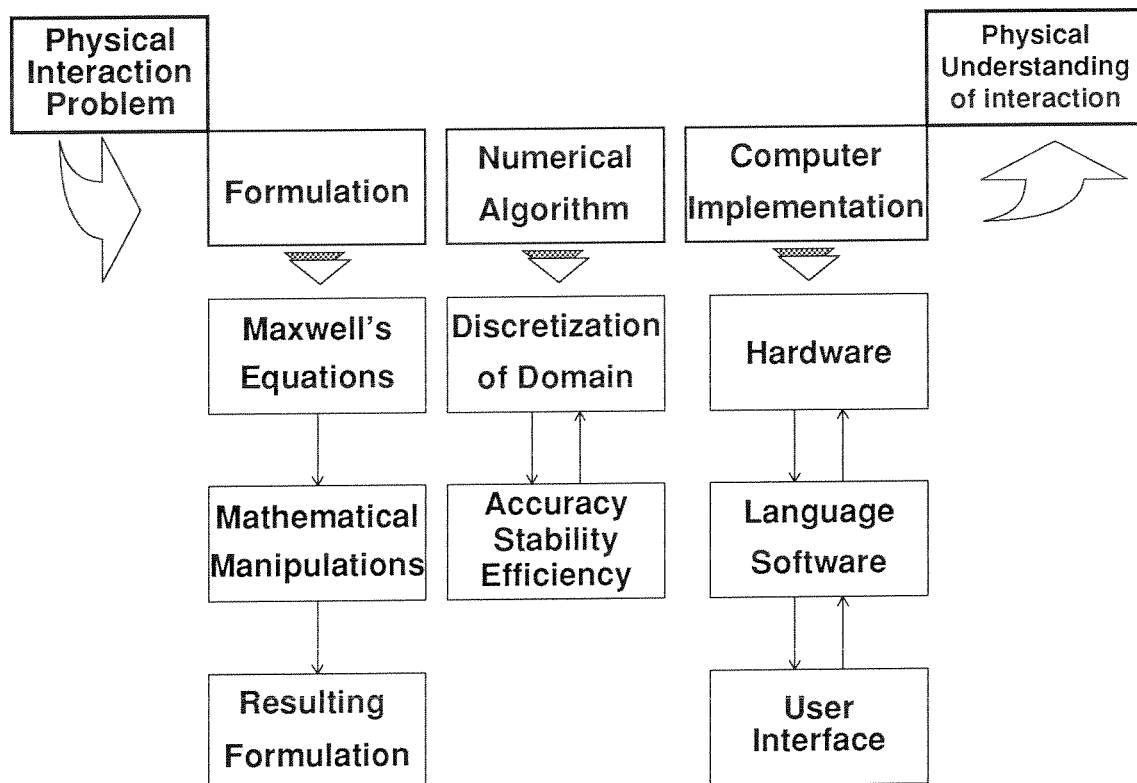


Figure 53 Numerical methods issues

Part 2

In the following chapters, an investigation is made of current numerical techniques based on the differential form of the time domain Maxwell's equations. Time-domain finite difference techniques based on Maxwell's equations written in *conservation law* form are implemented. The code is written in the C language and runs on a Sun workstation. Results are shown for the electromagnetic fields associated with plane wave propagation which varies in time. A comparison is made between different methods of formulating the finite difference form of the partial differential equations.

A two-dimensional time-domain application of a general finite element mathematical package, IMSL:PDE/PROTRAN (see [PDE 86], [Sewell 85]), is also considered. The software runs on the IBM 3090 main frame computer. A two-dimensional shielding problem is formulated via the *magnetic vector potential*. Results are presented in the form of vector plots.

Chapter 10

Maxwell's Equations

In the most general terms, *macroscopic* electromagnetic phenomena are described by Maxwell's equations which are partial differential equations relating the five vector fields $\mathbf{E}(\mathbf{x}, t)$, $\mathbf{D}(\mathbf{x}, t)$, $\mathbf{H}(\mathbf{x}, t)$, $\mathbf{B}(\mathbf{x}, t)$, and $\mathbf{J}(\mathbf{x}, t)$, as well as one scalar field $\rho(\mathbf{x}, t)$. These are most easily stated in differential form as (see [Stratton 41], chapter 1)

$$\nabla \times \mathbf{E} = -\left(\frac{\partial \mathbf{B}}{\partial t}\right), \quad (10.1)$$

$$\nabla \times \mathbf{H} = \left(\frac{\partial \mathbf{D}}{\partial t}\right) + \mathbf{J}, \quad (10.2)$$

$$\nabla \cdot \mathbf{J} = -\left(\frac{\partial \rho}{\partial t}\right), \quad (10.3)$$

where: $\mathbf{E}(\mathbf{x}, t)$ is the electric field intensity with units of volts/meter,
 $\mathbf{H}(\mathbf{x}, t)$ is the magnetic field intensity with units of amperes/meter,
 $\mathbf{D}(\mathbf{x}, t)$ is the electric flux density with units of coulombs/meter²,
 $\mathbf{B}(\mathbf{x}, t)$ is the magnetic flux density with units of webers/meter²,
 $\mathbf{J}(\mathbf{x}, t)$ is electric current density with units of amperes/meter², and
 $\rho(\mathbf{x}, t)$ is the electric charge density in units of coulombs/meter³.

Part 2

Although Maxwell's equations are most easily stated in the above differential form they are more general when expressed in integral form where the differentiability of the fields is not required. In other words, equations (10.1) to (10.3) require that the fields represented by $\mathbf{E}(\mathbf{x}, t)$, $\mathbf{D}(\mathbf{x}, t)$, $\mathbf{H}(\mathbf{x}, t)$, $\mathbf{B}(\mathbf{x}, t)$, and $\mathbf{J}(\mathbf{x}, t)$ be continuous functions of space and time, and that the scalar field $\rho(\mathbf{x}, t)$ be continuous in time. The integral forms are

$$\oint_C (\mathbf{E} \cdot d\mathbf{l}) = -\frac{d}{dt} \left(\int_S (\mathbf{B} \cdot \mathbf{n}) ds \right), \quad (10.4)$$

$$\oint_C (\mathbf{H} \cdot d\mathbf{l}) = \frac{d}{dt} \left(\int_S (\mathbf{D} \cdot \mathbf{n}) ds \right) + \mathbf{I}, \quad (10.5)$$

and

$$\oint_S (\mathbf{J} \cdot \mathbf{n}) ds = -\frac{d}{dt} \left(\int_V \rho dv \right) = -\frac{dQ}{dt}, \quad (10.6)$$

where $Q(t)$ is the total charge in the volume V enclosed by S , $I(t)$ is the total current passing through the surface S , C is the contour enclosing the surface S , ds is the surface element of the surface S , dv is the volume element of V , and $d\mathbf{l}$ is the vector line element in the direction appropriate for a right-handed system with the surface normal \mathbf{n} . These are more general than the differential form and in fact, it is this form which was originally formulated as the result of experimental evidence. These experimental laws are Faraday's law (equation (10.4)), Ampere's law (equation (10.5)) to which Maxwell added his displacement current $\partial\mathbf{D}/\partial t$, and the continuity equation (equation (10.6)).

To the above equations are added the constitutive equations and Ohm's law. The constitutive equations relate \mathbf{D} to \mathbf{E} and \mathbf{B} to \mathbf{H} , while Ohm's law relates \mathbf{J} to \mathbf{E} . These are stated as

$$\mathbf{D} = \epsilon \mathbf{E}, \quad (10.7)$$

Part 2

$$\mathbf{B} = \mu \mathbf{H}, \quad (10.8)$$

and

$$\mathbf{J} = \sigma \mathbf{E}, \quad (10.9)$$

where $\epsilon(\mathbf{x}, t)$ is the permittivity, $\mu(\mathbf{x}, t)$ is the permeability, and $\sigma(\mathbf{x}, t)$ is the conductivity of the medium. These quantities are tensors, which relate two vectors.

Thus equations (10.1) to (10.3) or equations (10.4) to (10.6) along with equations (10.7) to (10.9) form a set of 16 independent equations, while the vector functions $\mathbf{E}(\mathbf{x}, t)$, $\mathbf{D}(\mathbf{x}, t)$, $\mathbf{H}(\mathbf{x}, t)$, $\mathbf{B}(\mathbf{x}, t)$, $\mathbf{J}(\mathbf{x}, t)$, along with the scalar function $\rho(\mathbf{x}, t)$ are the 16 unknowns which can be solved for.

From equations (10.1) to (10.3) the familiar divergence equations can be derived. These are

$$\nabla \cdot \mathbf{D} = \rho, \quad (10.10)$$

$$\nabla \cdot \mathbf{B} = 0, \quad (10.11)$$

or in integral form,

$$\oint_S (\mathbf{D} \cdot \mathbf{n}) ds = \int_V \rho dv = Q, \quad (10.12)$$

$$\oint_S (\mathbf{B} \cdot \mathbf{n}) ds = 0, \quad (10.13)$$

where equation (10.12) can be recognized as the Gauss law. These equations are dependent on the previous and will not be required.

Chapter 11

Hyperbolic Systems of Conservation Laws

The mathematical theory involved in solving *hyperbolic systems of conservation laws* is fundamental in many areas of the physical sciences. A concise exposition of this theory for one dimensional systems was given by P. D. Lax [Lax 73]. The equations of *fluid dynamics* can be cast as a system of hyperbolic conservation laws. In fact, much of the mathematical theory of fluid dynamics has resulted from work in the area of hyperbolic systems. Some of the fundamental concepts and relations of this theory will be given here with the goal of applying the methods to Maxwell's equations. For other more complete discussions see Lax [Lax 73], Courant and Hilbert [Courant 62] and Garabedian [Garabedian 64].

11.1 Hyperbolic Conservation Laws

Conservation laws state the physical principle that the rate of change of the total amount of substance, say $\mathbf{u}(\mathbf{x}, t) = (u^1(\mathbf{x}, t) \dots u^j(\mathbf{x}, t) \dots u^n(\mathbf{x}, t))^T$, contained in a fixed domain V is equal to the *flux* of that substance, say $\mathbf{f} = (f^1(\mathbf{u}) \dots f^j(\mathbf{u}) \dots f^n(\mathbf{u}))^T$, across the boundary of V (i.e. S) with outward normal \mathbf{n} . This can be stated in integral form as

$$\oint_S (\mathbf{f}^j \cdot \mathbf{n}) ds = -\frac{d}{dt} \int_V u^j dv, \quad j = 1, \dots, n, \quad (11.1)$$

Part 2

where ds is the surface element of S while u^j and f^j are components of $\{u\}$ and $\{f\}$ which are column vectors of length n . Thus equation (11.1) represents a system of n conservation laws.

At a point where all partial derivatives of $\{u\}$ and $\{f\}$ are continuous, the *divergence theorem* can be applied in order to obtain the differential conservation law

$$u_t^j + \nabla \cdot f^j = 0; j = 1, \dots, n. \quad (11.2)$$

If f^j has spatial components given by $f^j = E^j \hat{x} + F^j \hat{y} + G^j \hat{z}$, then equation (11.2) can be written as

$$u_t^j + \frac{\partial E^j}{\partial x} + \frac{\partial F^j}{\partial y} + \frac{\partial G^j}{\partial z} = 0, j = 1, \dots, n. \quad (11.3)$$

This can also be written as a first order system of quasi-linear partial differential equations given by

$$u_t + \sum_x A_i u_{x_i} = 0, x = (x_1, x_2, x_3), \quad (11.4)$$

where $A_i = \nabla_u f_i$ are the Jacobian matrices associated with each flux f_i in the coordinate direction x_i . The above system is *hyperbolic* if each matrix $A_i(u)$ is diagonalizable and has real eigenvalues over the range of u .

11.2 Formulation of Maxwell's Equations in Conservation Law Form

The motivation for the study of conservation laws is that it can be easily shown (see [Shankar 89, 90],[Mitchell 80] pp. 180-181) that Maxwell's equations (10.1) - (10.2) and the constitutive relations, equations (10.7) - (10.9), can be written in the form of equation (11.3). In this form, the solution vector $\{u\}$ is given by

Part 2

$$\{u(x, t)\} = \begin{bmatrix} B_x \\ B_y \\ B_z \end{bmatrix} \begin{bmatrix} D_x \\ D_y \\ D_z \end{bmatrix}^T = \begin{bmatrix} \mathbf{B} \\ \mathbf{D} \end{bmatrix}, \quad (11.5)$$

and the flux vectors $\{E\}$, $\{F\}$, and $\{G\}$ are given as

$$\{E(x, t)\} = \begin{bmatrix} 0 \\ (-D_z) \\ (D_y) \end{bmatrix} \begin{bmatrix} 0 \\ (\frac{B_z}{\mu}) \\ (-\frac{B_y}{\mu}) \end{bmatrix}^T = \begin{bmatrix} \hat{x} \times \mathbf{E} \\ -\hat{x} \times \mathbf{H} \end{bmatrix} = \begin{bmatrix} \hat{x} \times e\mathbf{D} \\ -\hat{x} \times m\mathbf{B} \end{bmatrix}, \quad (11.6)$$

$$\{F(x, t)\} = \begin{bmatrix} (D_z) \\ 0 \\ (-D_x) \end{bmatrix} \begin{bmatrix} (-\frac{B_z}{\mu}) \\ 0 \\ (\frac{B_x}{\mu}) \end{bmatrix}^T = \begin{bmatrix} \hat{y} \times \mathbf{E} \\ -\hat{y} \times \mathbf{H} \end{bmatrix} = \begin{bmatrix} \hat{y} \times e\mathbf{D} \\ -\hat{y} \times m\mathbf{B} \end{bmatrix}, \quad (11.7)$$

$$\{G(x, t)\} = \begin{bmatrix} (-D_y) \\ (D_x) \\ 0 \end{bmatrix} \begin{bmatrix} (\frac{B_y}{\mu}) \\ (-\frac{B_x}{\mu}) \\ 0 \end{bmatrix}^T = \begin{bmatrix} \hat{z} \times \mathbf{E} \\ -\hat{z} \times \mathbf{H} \end{bmatrix} = \begin{bmatrix} \hat{z} \times e\mathbf{D} \\ -\hat{z} \times m\mathbf{B} \end{bmatrix}. \quad (11.8)$$

In order to represent the current density term $\mathbf{J}(x, t)$ in equation (11.3) a source term needs to be added (see [Shankar 89, 90]),

$$u_t^j + \frac{\partial E^j}{\partial x} + \frac{\partial F^j}{\partial y} + \frac{\partial G^j}{\partial z} = S^j, \quad j = 1, \dots, n, \quad (11.9)$$

Part 2

where

$$\{ \mathbf{S}(\mathbf{x}, t) \} = \begin{bmatrix} 0 \\ 0 \\ 0 \end{bmatrix} \begin{bmatrix} -\mathbf{J}_x \\ -\mathbf{J}_y \\ -\mathbf{J}_z \end{bmatrix}^T = \begin{bmatrix} 0 \\ -\mathbf{J} \end{bmatrix}. \quad (11.10)$$

It can be easily checked that equation (11.9) represents Maxwell's curl equations. The divergence relations, equations (10.10) - (10.11), will be automatically satisfied as long as they are satisfied by the initial conditions.

11.3 Systems in One Space Dimension and Time

A hyperbolic system of conservation laws in one space dimension is written as

$$\mathbf{u}_t + \mathbf{f}_x = 0 \quad (11.11)$$

or in quasi-linear form as

$$\mathbf{u}_t + \mathbf{A}\mathbf{u}_x = 0 \quad (11.12)$$

where \mathbf{u} is a column vector of size n and \mathbf{A} is an $n \times n$ Jacobian matrix of the flux \mathbf{f} . The eigenvalues are real since the system is hyperbolic and it is assumed that they can be written in ascending order as

$$\lambda_1 \leq \lambda_2 \leq \dots \leq \lambda_n, \quad (11.13)$$

with \mathbf{r}_k and \mathbf{l}_k being the right and left eigenvectors corresponding to the eigenvalue λ_k . In general, the eigenvalues are a function of the solution vector \mathbf{u} . If the k^{th} eigenvalue λ_k is a nonconstant function of \mathbf{u} and if the gradient of λ_k is not orthogonal to \mathbf{r}_k , then the k^{th} field is said to be *genuinely nonlinear*. This can be succinctly written as

Part 2

$$\mathbf{r}_k \cdot \nabla_{\mathbf{u}} \lambda_k = 1, \quad (11.14)$$

where \mathbf{r}_k has been normalized in order to make the right hand side of equation (11.14) equal to 1. If this is not the case then the k^{th} field is said to be *linearly degenerate*, that is

$$\mathbf{r}_k \cdot \nabla_{\mathbf{u}} \lambda_k = 0. \quad (11.15)$$

It can be shown that across a surface $s(t)$ where the solution vector is discontinuous, each of the n conservation laws defined by equation (11.11) must satisfy the *Rankine-Hugoniot* jump relation given as

$$S [u_j] = [f_j]. \quad (11.16)$$

In the above equation, S denotes the speed of propagation, $S = \dot{s}(t)$, of the discontinuous surface $s(t)$. The square brackets denote the jump in the quantity, that is $[g] = g_R - g_L$ where g_R and g_L denote the value of the quantity on the right and left side of the discontinuity.

In the $x-t$ plane there exist n *characteristic lines*, denoted Γ_j , defined by the ordinary differential equations

$$\Gamma_j \leftarrow \frac{dx}{dt} = \lambda_j, \quad j = 1, \dots, n, \quad (11.17)$$

In general, the waves described by the conservation laws propagate along these characteristics and thus they form part of the solution procedure for the equations.

Since discontinuous solutions or, in general, non differentiable solutions exist for the solution vector \mathbf{u} the equations are solved for the class of generalized functions. In order to achieve uniqueness of solution for this class P. D. Lax (see [Lax 73]) proposed that the solution must satisfy the so-called *entropy condition*. This condition is written as the pair of inequalities

Part 2

$$\lambda_k(\mathbf{u}_L) > S(t) > \lambda_k(\mathbf{u}_R), \quad (11.18)$$

$$\lambda_{k-1}(\mathbf{u}_L) < S(t) < \lambda_{k+1}(\mathbf{u}_R), \quad (11.19)$$

for some k , $1 \leq k \leq n$. This condition is sufficient to guarantee that the solution to the conservation law, given unique initial values of \mathbf{u} , is unique. Since the eigenvalues have been assumed to be ordered, the above inequalities may be combined to yield

$$\lambda_1(\mathbf{u}_L) \leq \lambda_2(\mathbf{u}_L) \leq \dots \leq \lambda_{k-1}(\mathbf{u}_L) < S(t) < \lambda_k(\mathbf{u}_L), \quad (11.20)$$

$$\lambda_k(\mathbf{u}_R) < S(t) < \lambda_{k+1}(\mathbf{u}_R) \leq \lambda_{k+2}(\mathbf{u}_R) \leq \dots \leq \lambda_n(\mathbf{u}_R), \quad (11.21)$$

which imply that $n+1$ of the $2n$ characteristic lines on either side of the discontinuity intersect the discontinuous surface $s(t)$. The discontinuous surface $s(t)$ for which the entropy condition is satisfied is called a *k-shock*.

Now if the k field is linearly degenerate then equality holds in equation (11.18) and the speed of propagation of the discontinuous solution is $S(t) = \lambda_k(\mathbf{u})$ which when put in the Rankine-Hugoniot jump relation produces

$$\lambda_k[\mathbf{u}_k] = [f_k]. \quad (11.22)$$

Now, via a theorem due to P. D. Lax, there is a path connecting \mathbf{u}_L to \mathbf{u}_R through intermediate constant states separated by k -waves [Lax 73] (see also Osher [Osher 82] and Harten [Harten 83]). If each of the k -waves are linearly degenerate then equation (11.22) may be used to represent the solution vector at the end points of each path. This is the approach taken to solve the linear *Riemann Problem*. That is, equation (11.12) with initial conditions

$$\mathbf{u}(x, 0) = \begin{cases} \mathbf{u}_L, & x < 0 \\ \mathbf{u}_R, & x > 0 \end{cases}. \quad (11.23)$$

Part 2**11.4 Maxwell's Equations in One Space Dimension and Time**

It is useful to study solutions of Maxwell's time domain equations in one space dimension in order to understand certain properties which they exhibit. If it is assumed that the solution vector $\mathbf{u}(\mathbf{x}, t)$ is independent of the x and y space directions (i.e. $\mathbf{u} = \mathbf{u}(z, t)$) then Maxwell's equations can be written as

$$u_t^j + \frac{\partial G^j}{\partial z} = S^j; \quad j = 1, \dots, n \quad (11.24)$$

which form the four systems of partial differential equations

$$\frac{\partial D_z}{\partial t} + \frac{\sigma}{\epsilon} D_z = 0 \quad (11.25)$$

$$\frac{\partial B_z}{\partial t} = 0 \quad (11.26)$$

$$\left. \begin{aligned} \frac{\partial D_x}{\partial t} + \frac{\partial}{\partial z} (m B_y) &= -e \sigma D_x \\ \frac{\partial B_y}{\partial t} + \frac{\partial}{\partial z} (e D_x) &= 0 \end{aligned} \right\} \quad (11.27)$$

$$\left. \begin{aligned} \frac{\partial D_y}{\partial t} - \frac{\partial}{\partial z} (m B_x) &= -e \sigma D_y \\ \frac{\partial B_x}{\partial t} - \frac{\partial}{\partial z} (e D_y) &= 0 \end{aligned} \right\} \quad (11.28)$$

where $e = 1/\epsilon$ and $m = 1/\mu$.

Part 2

In a homogeneous isotropic medium, solutions to equation (11.25) can easily be obtained as an exponentially decaying field with initial value being given. That is, if the initial field component $D_z(z, t=0) = D_{z0}(z)$ then equation (11.25) has the solution

$$D_z(z, t) = D_{z0}(z)e^{-e\sigma t} \quad (11.29)$$

for times $t > 0$.

Solutions to equation (11.26) can also easily be found as any function of space which is constant in time. Thus if initially (at time $t = 0$) a magnetic field $B_z = B_z(z)$ is given then this field distribution will stay constant in time.

The final two equations governing electromagnetic waves in one space dimension are similar in form, thus only equations (11.28) will be considered. These equations will now be solved for the non-dissipative case of $\sigma = 0$ by the *method of characteristics* and for the case where $\sigma > 0$ by the *Laplace transform method*.

11.4.1 Wave equation in a non-dissipative medium ($\sigma = 0$)

In a homogeneous region of space the system of equations (11.28) can be written as

$$\mathbf{u}_t + A \mathbf{u}_z = 0 \quad (11.30)$$

where the matrix A is given by

$$A = \begin{bmatrix} 0 & -m \\ -e & 0 \end{bmatrix} \quad (11.31)$$

and \mathbf{u} is the column vector $\mathbf{u} = \{D \ B\}^T$ where here D and B represent D_y and B_x of equations (11.28). The system of equation (11.30) can be diagonalized by pre-multiplication with the matrix T where

Part 2

$$T = \begin{bmatrix} \mu & 1 \\ \frac{1}{2} & \frac{2c}{2c} \\ \frac{1}{2c} & -\frac{\epsilon}{2} \end{bmatrix} \quad (11.32)$$

with corresponding inverse

$$T^{-1} = \begin{bmatrix} m & c \\ c & -e \end{bmatrix} \quad (11.33)$$

where $c^2 = me$. Thus it can be easily shown that $TAT^{-1} = \text{diag}(\lambda_i) = \Lambda$ where λ_i are the eigenvalues of the matrix A , that is

$$\text{diag}(\lambda_i) = \begin{bmatrix} -c & 0 \\ 0 & c \end{bmatrix} = \Lambda. \quad (11.34)$$

Before pre-multiplication with T , the substitution $\mathbf{u} = T^{-1}\mathbf{v}$ where

$$\mathbf{v} = T\mathbf{u} = \begin{bmatrix} v_1 \\ v_2 \end{bmatrix} = \begin{bmatrix} \frac{D}{2m} + \frac{B}{2c} \\ \frac{D}{2c} - \frac{B}{2e} \end{bmatrix} \quad (11.35)$$

is made in equation (11.30). If e and m are constants in time as well as the region of space being considered then this substitution produces

$$v_t + \Lambda v_z = 0 \quad (11.36)$$

which represents a set of two *uncoupled* partial differential equations in the *characteristic variables* v .

In order to solve equations (11.36) it is convenient to use the fact that both equations are of the form

Part 2

$$\frac{\partial v}{\partial t} + \lambda \frac{\partial v}{\partial z} = 0 \quad (11.37)$$

which is equivalent to the pair of simultaneous ordinary differential equations (see Ince [Ince 56])

$$\frac{dt}{1} = \frac{dz}{\lambda} = \frac{dv}{0} \quad (11.38)$$

which produces $dv_1 = 0$ on the *characteristic line* defined by

$$\Gamma_1 \leftarrow \frac{dz}{dt} = -c \quad (11.39)$$

and for the second equation, $dv_2 = 0$ on the characteristic line defined by

$$\Gamma_2 \leftarrow \frac{dz}{dt} = c. \quad (11.40)$$

In regions of homogeneous permittivity and permeability Γ_1 and Γ_2 represent straight lines with negative and positive slopes in the $z-t$ plane, respectively. These are shown below in Figure 54.

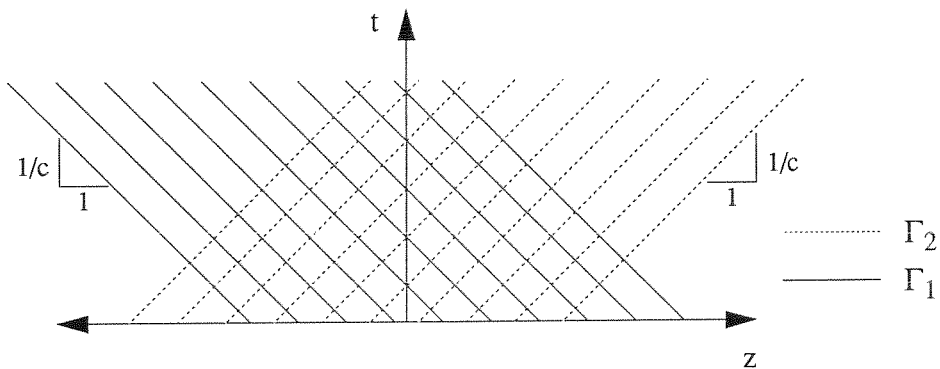


Figure 54 Characteristic lines for wave equation

Part 2

Now if initial conditions are imposed on \mathbf{u} at time $t = 0$ (i.e. along the z axis) then the corresponding initial conditions will define \mathbf{v} as

$$\mathbf{v}_0 = \mathbf{v}(z, 0) = T\mathbf{u}(z, 0) = T\mathbf{u}_0 \quad (11.41)$$

where T is given in equation (11.32). Solutions anywhere in the $z-t$ plane can be found by the fact that v_1 and v_2 will be constants along each characteristic line Γ_1 and Γ_2 respectively. That is, at any point (ζ, τ) in the $z-t$ plane v_1 and v_2 can be written as

$$v_1(\zeta, \tau) = v_{10}(\zeta + c\tau) \quad (11.42)$$

$$v_2(\zeta, \tau) = v_{20}(\zeta - c\tau) \quad (11.43)$$

where v_1 represents a left moving wave and v_2 a right moving wave. Thus from equation (11.33) D and B can be determined at any point (ζ, τ) as

$$D(\zeta, \tau) = mv_{10}(\zeta + c\tau) + cv_{20}(\zeta - c\tau) \quad (11.44)$$

$$B(\zeta, \tau) = cv_{10}(\zeta + c\tau) - ev_{20}(\zeta - c\tau) \quad (11.45)$$

and finally in terms of the initial conditions D_0 and B_0 as

$$D(\zeta, \tau) = \frac{1}{2} (D_0(\zeta + c\tau) + D_0(\zeta - c\tau)) + \frac{1}{2} \sqrt{\frac{\epsilon}{\mu}} (B_0(\zeta + c\tau) - B_0(\zeta - c\tau)) \quad (11.46)$$

$$B(\zeta, \tau) = \frac{1}{2} (B_0(\zeta + c\tau) + B_0(\zeta - c\tau)) + \frac{1}{2} \sqrt{\frac{\mu}{\epsilon}} (D_0(\zeta + c\tau) - D_0(\zeta - c\tau)) \quad (11.47)$$

where equations (11.41) have been used.

It should be noted that the above equations are valid even if the initial data is discontinuous. Thus an initial rectangular pulse breaks up into two rectangular pulses of one-half amplitude; one travelling along the negative z -axis and the other travelling along the positive z -axis.

Part 2

The interesting point about the form of the solution given by equation (11.46) and equation (11.47) is that they can easily be applied over a discretized z-t space. Again assuming that the space is homogeneous it can be discretized with the indices (j, n) denoting the point ($j\Delta z$, $n\Delta t$). Now as long as the ratio $\Delta z/\Delta t = c$, then the field at any point (j, n) can be calculated *exactly* from the initial distribution $D_j^n = D_0(j\Delta z)$ and $B_j^n = B_0(j\Delta z)$ by the equations

$$D_j^{n+1} = \frac{1}{2} \left[(D_{j+1}^n + D_{j-1}^n) + \sqrt{\frac{\epsilon}{\mu}} (B_{j+1}^n - B_{j-1}^n) \right] \quad (11.48)$$

$$B_j^{n+1} = \frac{1}{2} \left[(B_{j+1}^n + B_{j-1}^n) + \sqrt{\frac{\mu}{\epsilon}} (D_{j+1}^n - D_{j-1}^n) \right] \quad (11.49)$$

where $D_j^n = D(j\Delta z, n\Delta t)$ and $B_j^n = B(j\Delta z, n\Delta t)$.

Thus far it has been assumed that the z-t space where the initial electromagnetic disturbance occurs is homogeneous, that is ϵ and μ are not functions of time nor space. If a discrete boundary exists separating the space into a region 1 and a region 2 with permittivity and permeability given as ϵ_1, μ_1 and ϵ_2, μ_2 respectively, as shown in Figure 55, then the equations derived thus far are invalid and equation (11.28) cannot be written as equation (11.30).

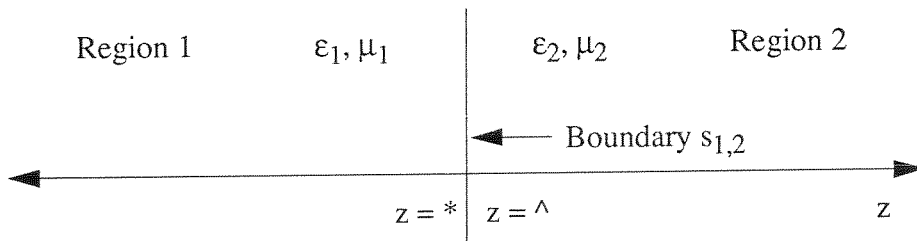


Figure 55 Region with abrupt boundary

Part 2

If the boundary is described by the surface $s(t) = \text{constant}$, then the *Rankine-Hugoniot* jump relation for the boundary is written as

$$-S[u^j] + [f^j] = 0 \quad (11.50)$$

where $S = \dot{s}(t)$ is the speed of propagation of the discontinuous surface and f denotes the corresponding flux. For the present case $f = \{-mB \ -eD\}^T$ and since the discontinuous boundary is stationary, $S = 0$ and the jump condition becomes

$$[f^j] = 0. \quad (11.51)$$

For the one-dimensional Maxwell equations this produces

$$\begin{bmatrix} m_1 B_1 \\ e_1 D_1 \end{bmatrix} = \begin{bmatrix} H_1 \\ E_1 \end{bmatrix} = \begin{bmatrix} H_2 \\ E_2 \end{bmatrix} = \begin{bmatrix} m_2 B_2 \\ e_2 D_2 \end{bmatrix}. \quad (11.52)$$

These are easily recognized as the standard boundary conditions between two regions of space (see Stratton [Stratton 41]). Thus in homogeneous regions equations (11.30) apply while at points of discontinuity equations (11.52) apply.

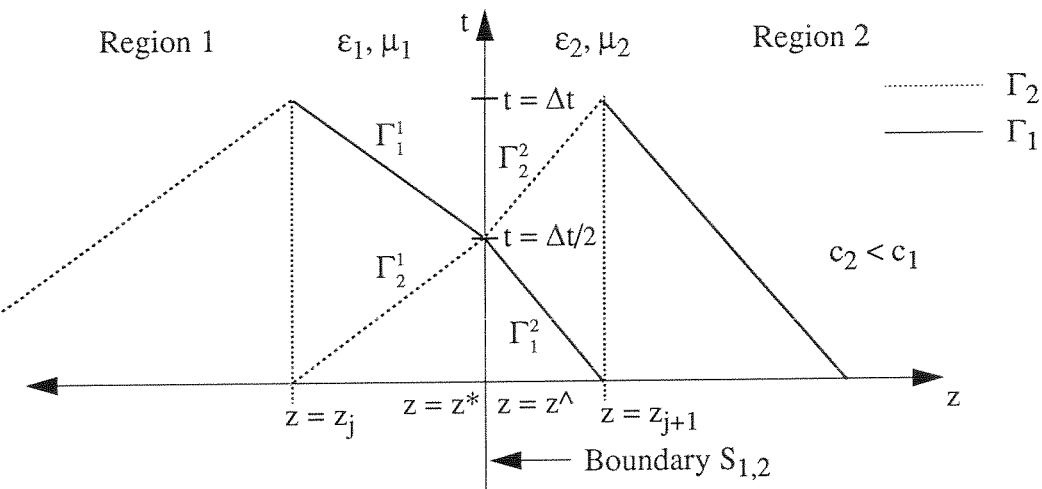


Figure 56 Characteristic theory for boundary problem

Part 2

In the presence of a boundary the characteristic lines Γ_1 and Γ_2 defined by equations (11.39) and (11.40) can be drawn in the z-t plane as shown in Figure 56. Note that the characteristic lines are products of the differential equations and therefore must stop at a discontinuous boundary where the jump condition applies.

Denoting the solution as \mathbf{u}_j^1 at $z = z_j$ in region 1 and \mathbf{u}_{j+1}^1 at $z = z_{j+1}$ in region 2 and $\mathbf{u}_*^1, \mathbf{u}_\wedge^1$ at $z = z_*$ and $z = z_\wedge$ respectively then the condition that v_2^1 is constant on Γ_2^1 and v_1^2 is constant on Γ_1^2 produces the equations

$$v_{2j}^1 = v_{2*}^1 \rightarrow \frac{D_j^1}{2m_j^1} - \frac{B_j^1}{2c_j^1} = \frac{D_*^1}{2m_j^1} - \frac{B_*^1}{2c_j^1} \quad (11.53)$$

$$v_{1,j+1}^2 = v_{1,\wedge}^2 \rightarrow \frac{D_{j+1}^2}{2m_{j+1}^2} + \frac{B_{j+1}^2}{2c_{j+1}^2} = \frac{D_*^2}{2m_{j+1}^2} - \frac{B_*^2}{2c_{j+1}^2}. \quad (11.54)$$

These can be simplified and re-written without the superscript as

$$c_j(D_* - D_j) = m_j(B_* - B_j) \quad (11.55)$$

$$c_{j+1}(D_\wedge - D_{j+1}) = -m_{j+1}(B_\wedge - B_{j+1}) \quad (11.56)$$

since it is obvious from the subscript which region is being denoted. The *jump relation* at the boundary produces the equations

$$e_j D_* = e_{j+1} D_\wedge \quad (11.57)$$

$$m_j B_* = m_{j+1} B_\wedge. \quad (11.58)$$

Thus the above four equations can be solved for the field values D_* , D_\wedge , B_* and B_\wedge to produce the boundary fluxes

Part 2

$$e_j D_* = \frac{(c_{j+1} D_{j+1} + m_{j+1} B_{j+1}) + (c_j D_j - m_j B_j)}{(c_j/e_j + c_{j+1}/e_{j+1})} = (f^2)_{j+1/2}^{n+1/2} \quad (11.59)$$

$$m_j B_* = \frac{(e_{j+1} D_{j+1} + c_{j+1} B_{j+1}) + (c_j B_j - e_j D_j)}{(e_j/c_j + e_{j+1}/c_{j+1})} = (f^1)_{j+1/2}^{n+1/2} \quad (11.60)$$

$$e_{j+1} D_\wedge = \frac{(c_{j+1} D_{j+1} + m_{j+1} B_{j+1}) + (c_j D_j - m_j B_j)}{(c_j/e_j + c_{j+1}/e_{j+1})} = (f^2)_{j+1/2}^{n+1/2} \quad (11.61)$$

$$m_{j+1} B_\wedge = \frac{(e_{j+1} D_{j+1} + c_{j+1} B_{j+1}) + (c_j B_j - e_j D_j)}{(e_j/c_j + e_{j+1}/c_{j+1})} = (f^1)_{j+1/2}^{n+1/2}. \quad (11.62)$$

The field values at z_j and z_{j+1} can now be determined from equations (11.48) and (11.49) using the field values defined at the boundary between two neighboring cells. That is, a numerical procedure, which is exact, can be produced using the above defined boundary fluxes. The procedure is exact *only if* the cells corresponding to each space point $z = z_j$ is of the correct size such that the characteristics of each two neighboring cells meet at the one-half time point $t = \Delta t/2$. This is shown pictorially below in Figure 57.

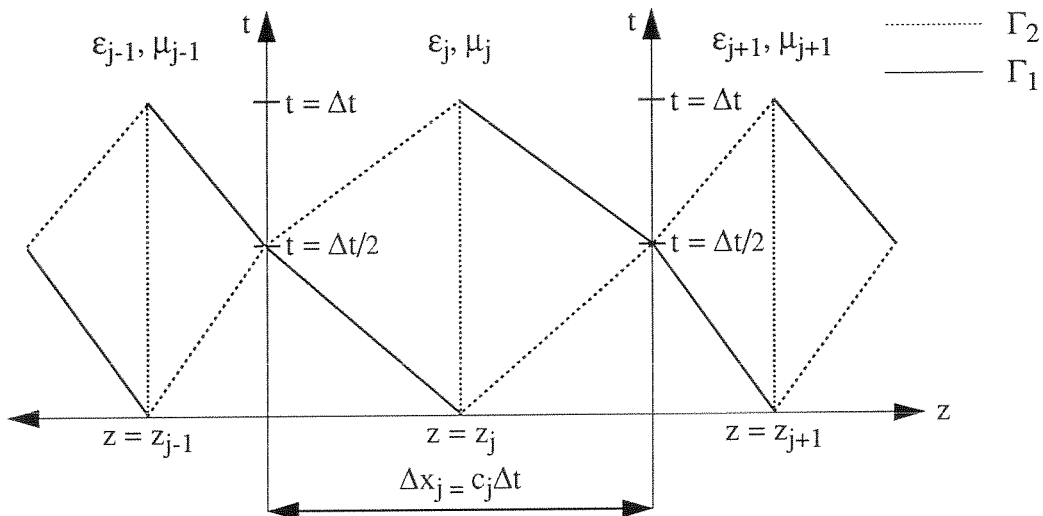


Figure 57 Exact numerical procedure for layered medium

Part 2

The exact numerical procedure on the above grid can thus be written as

$$D_j^{n+1} = \frac{\epsilon_j}{2} \left((f^2)_{j+1/2}^{n+1/2} + (f^2)_{j-1/2}^{n+1/2} \right) + \frac{1}{2c_j} \left((f^1)_{j+1/2}^{n+1/2} - (f^1)_{j-1/2}^{n+1/2} \right) \quad (11.63)$$

$$B_j^{n+1} = \frac{\mu_j}{2} \left((f^1)_{j+1/2}^{n+1/2} + (f^1)_{j-1/2}^{n+1/2} \right) + \frac{c_j}{2} \left((f^2)_{j+1/2}^{n+1/2} - (f^2)_{j-1/2}^{n+1/2} \right) \quad (11.64)$$

where the flux, $\mathbf{f} = \{f^1 \ f^2\}$, at the half-time and half-space points is determined from equations (11.59) to (11.62). The time and space discretization is made with prior knowledge of the constitutive parameters of the space. That is, the space dimension is discretized based on the speed of propagation in each finite homogeneous region. The time step is kept constant in order that the characteristic method can be applied.

It should be noted that the flux values determined from equations (11.59) to (11.62) are identical to those derived by Shankar et al [Shankar 89] but that no restriction is given on the space discretization in that work. Thus the numerical procedure derived therein is not exact.

11.4.2 Wave equation in a dissipative medium ($\sigma \neq 0$)

For the case of a dissipative medium where the conductivity (σ) is not equal to zero the solution to the wave equation becomes much more difficult. A testimony to this fact is the series of articles by Harmuth [Harmuth 86a, b] along with subsequent letters to the editor of IEEE EMC Transactions by various authors, notably Gray *et al* [Gray 88] and Barrett [Barrett 89a, b].

Part 2

In this case the one dimensional system to be solved is

$$\mathbf{u}_t + A \mathbf{u}_x = \mathbf{s} \quad (11.65)$$

where the matrix A is given by equation (11.31) and $\mathbf{s} = \{-\sigma D/\epsilon, 0\}^T$. Diagonalization by the matrices T and T^{-1} given in equations (11.32) and (11.33) then produces

$$\mathbf{v}_t + \Lambda \mathbf{v}_x = Ts \quad (11.66)$$

where $\mathbf{v} = Tu$ is given by equation (11.35) and Ts can be written in terms of \mathbf{v} as

$$Ts = \begin{bmatrix} -e\sigma \\ -\frac{2m}{2c}D \\ -\frac{e\sigma}{2c}D \end{bmatrix} = \begin{bmatrix} -e\sigma & -e\sigma c \\ \frac{2}{2} & \frac{2m}{2} \\ -c\sigma & -e\sigma \end{bmatrix} v \quad (11.67)$$

where the two partial differential equations are now no longer uncoupled. That is, they are coupled by the source term Ts . Thus the characteristic variables v are no longer constant on the characteristics defined by equations (11.39) and (11.40) and this approach to solving equation (11.65) is no longer the best one.

The two partial differential equations (11.65) can be transformed to a single second order equation written as

$$\frac{\partial^2 \psi}{\partial x^2} - \mu \epsilon \frac{\partial^2 \psi}{\partial t^2} - \mu \sigma \frac{\partial \psi}{\partial t} = 0 \quad (11.68)$$

where ψ is either D or B (i.e. they satisfy the same equation).

Given the initial conditions $D(x, 0) = g_D(x)$, $B(x, 0) = 0$, implying that

$$\left. \frac{\partial D}{\partial t} \right|_{t=0} = -\sigma e D(x, 0) = -\sigma e g_D(x) = G_D(x), \quad (11.69)$$

Part 2

the electric displacement D can be calculated at any time along the x axis as

$$D(x, t) = e^{-bt} \left\{ \frac{1}{2} g_D(x + ct) + \frac{1}{2} g_D(x - ct) - \right. \\ \left. \frac{1}{2c} \int_{(x-ct)}^{(x+ct)} b g_D(\beta) J_0 \left(\frac{b}{c} \sqrt{(x-\beta)^2 - c^2 t^2} \right) d\beta + \right. \\ \left. \frac{1}{2c} \int_{(x-ct)}^{(x+ct)} g_D(\beta) \frac{\partial}{\partial t} J_0 \left(\frac{b}{c} \sqrt{(x-\beta)^2 - c^2 t^2} \right) d\beta \right\} \quad (11.70)$$

where $b = \frac{\sigma}{2\epsilon}$ and $c = \frac{1}{\sqrt{\mu\epsilon}}$ as given by Stratton [Stratton 41]. The magnetic displacement can be found by solving equation (11.68) for the same initial conditions. That is $B(x, 0) = 0 = g_B(x)$, and

$$\frac{\partial B}{\partial t} \Big|_{t=0} = G_B(x) = \frac{\partial}{\partial x}(eD) = \frac{\partial}{\partial x}(eg(x)). \quad (11.71)$$

Thus, the magnetic displacement is given as

$$B(x, t) = \frac{1}{2c} \int_{(x-ct)}^{(x+ct)} (G_B(\beta) J_0 \left(\frac{b}{c} \sqrt{(x-\beta)^2 - c^2 t^2} \right)) d\beta. \quad (11.72)$$

Note that in his example, Stratton chooses $G_D(x) = 0$. This implies that $B(x, 0)$ is not equal to zero. These equations will be integrated numerically in the next chapter in order to compare the results with solutions derived via the finite difference method.

Chapter 12

Finite Difference Methods

The numerical solution of initial-boundary value problems using finite difference techniques is discussed. The initial-boundary value problems are in the form of hyperbolic conservation laws as discussed in the previous chapter. In order to keep the equations manageable, the standard difference operator notation is used (see for example Dahlquist [Dahlquist 74] and Lapidus [Lapidus 82]).

<i>Linear Finite Difference Operators</i>		
Operator	Symbol	Operation
Forward Difference	Δ	$\Delta u_r = u_{r+1} - u_r$
Backward Difference	∇	$\nabla u_r = u_r - u_{r-1}$
Central Difference	δ	$\delta u_r = u_{r+1/2} - u_{r-1/2}$
Forward Shift	E_+	$E_+ u_r = u_{r+1}$
Backward Shift	E_-	$E_- u_r = u_{r-1}$
Average	μ	$\mu u_r = 1/2(u_{r+1/2} + u_{r-1/2})$
Differentiation	D	$D u_r = du/dx _r = u_x _r$

Figure 58 Table of linear finite difference operators

Part 2

The standard finite difference techniques are described first for systems of conservation laws in one space dimension. More accurate *upwind* schemes which use numerical fluxes defined via the method of characteristics are then presented. Generalization to more space dimensions is then described.

12.1 Some Finite Difference Terminology

One advantage of the conservation law formulation of Maxwell's equations is that the finite difference procedures become simpler to write and to analyze (see for example Richtmyer and Morton [Richtmyer 67], Sod [Sod 85], and Strikwerda [Strikwerda 89]). Given, as the initial value problem, the one-dimensional system of n conservation laws

$$\mathbf{u}_t + \mathbf{f}_x = 0, \quad (12.1)$$

with initial conditions $\mathbf{u}(x, 0) = \mathbf{g}(x)$ an approximate solution $\mathbf{u}_j^n = \mathbf{u}(x_j, t^n)$ is sought on a rectangular lattice

$$\Omega_{jn} = \{ (x, t) \mid (x_{j-1/2} \leq x \leq x_{j+1/2}), (t^n \leq t \leq t^{n+1}) \}, \quad (12.2)$$

where $x_j = j\Delta x$, $t^n = n\Delta t$ and j, n are integers. The initial conditions are approximated on Ω_{j0} by

$$\mathbf{u}_j^0 = \mathbf{g}_j = \mathbf{g}(x_j), \quad (12.3)$$

and a finite difference procedure is used to determine the solution at a new time $t = t^{n+1}$. A general finite difference scheme can be written as

$$\mathbf{u}_j^{n+1} = Q(\mathbf{u}_j^n), \quad (12.4)$$

for $n \geq 0$ where Q is a polynomial in the backward and forward shift operators E_- and E_+ .

Part 2

Important qualities of a finite difference scheme are its *stability*, whether it is *consistent* with the partial differential equation being approximated, and whether it is a *convergent* scheme. Only heuristic definitions of these concepts will be given here. For the mathematical definitions consult Strikwerda [Strikwerda 89].

Consistency

A finite difference scheme is *consistent* with the partial differential equation being approximated if the difference between the partial differential equation and finite difference operators applied to any smooth function tends to zero as the time step and the space step tend to zero. In other words, the *truncation error*, when the finite difference scheme is derived via *Taylor's expansion*, must tend to zero as Δt and Δx tend to zero for the scheme to be consistent.

Convergence

A finite difference scheme is *convergent in a norm*, relative to the initial value problem being approximated, if the norm of the difference between the solution produced by the scheme and that produced by the initial value problem tends to zero as Δt and Δx tend to zero.

Stability

A finite difference scheme is stable if the growth produced in a norm of the solution at a certain time step is limited to the growth at the previous time step multiplied by a constant. That is, growth which is exponential in n , where n is the time step, would be unstable. This ensures that any local error is not amplified indefinitely as the time stepping is performed.

Now consistency and stability restrictions are usually relatively easy to derive for a finite difference approximation; convergence, on the other hand, is more difficult. Consistency follows immediately from the derivation of a scheme using Taylor's

Part 2

expansion. Stability of a scheme can be determined easily using the von Neuman condition and harmonic analysis of a linearized problem (see for example Lapidus [Lapidus 82]).

Fortunately the following theorem proposed by Lax and Richtmyer alleviates the difficulties in proving convergence.

Lax-Richtmyer Equivalence Theorem

For a well posed initial value problem, a consistent finite difference approximation to the partial differential equation is convergent if and only if the scheme is stable.

Thus if the finite difference scheme is known to be stable and consistent, it can be used with full knowledge that the resulting solution converges to the solution of the initial value problem.

Now in the present case, what is needed is a finite difference scheme to approximate the system of conservation laws given by equation (12.1). In the general case this system is non-linear, and the required solution must be taken from the, possibly infinity, *weak solutions* satisfying the weak form of the conservation law. The weak form of the initial value problem given by equation (12.1) and the initial conditions $\mathbf{u}(x, 0) = \mathbf{g}(x)$ can be written as

$$\int_{-\infty}^{\infty} \int_{-\infty}^{\infty} (\mathbf{u} \cdot \Phi_t + \mathbf{f} \cdot \Phi_x) dx dt + \int_{-\infty}^{\infty} (\mathbf{g} \cdot \Phi(x, 0)) dx = 0 \quad (12.5)$$

where Φ is a vector valued *test function* having the same number of components as \mathbf{u} . That is, Φ is a vector of n scalar test functions $\phi_j \in C_0^\infty$ (*i.e.* smooth with compact support, see R. D. Richtmyer [Richtmyer 78]).

The finite difference scheme given in equation (12.4) is said to be in *conservation form* if it can be expressed in the form

Part 2

$$\mathbf{u}_j^{n+1} = \mathbf{u}_j^n - \rho (\mathbf{h}_{j+1/2}^n - \mathbf{h}_{j-1/2}^n), \quad (12.6)$$

where $\rho = \Delta t / \Delta x$ and \mathbf{h} is a *consistent numerical flux*

$$\mathbf{h}_{j+1/2}^n = \mathbf{h}(\mathbf{u}_{j+1}^n, \dots, \mathbf{u}_j^n, \dots, \mathbf{u}_{j-m}^n), \quad (12.7)$$

$$\mathbf{h}(\mathbf{u}, \mathbf{u}, \dots, \mathbf{u}) = \mathbf{f}(\mathbf{u}). \quad (12.8)$$

The requirement that the numerical flux be consistent with the physical flux, that is equation (12.8), is necessary in order that the scheme be consistent with the conservation law. The importance of making sure a finite difference scheme is in conservation form is exemplified by the following theorem due to Lax and Wendroff (see Sod [Sod 85] and Harten [Harten 83]).

Lax-Wendroff Theorem

If a finite difference scheme which is in conservation form is convergent then the solution $\mathbf{u}_n^i \rightarrow \mathbf{u}(x_i, t^n)$ derived from the difference scheme converges to a weak solution of the conservation law as Δt and Δx tend to zero.

12.2 Classical Finite Difference Schemes

Now that some of the terminology associated with finite difference techniques has been established, some specific schemes will be presented. The first to be presented is the Lax-Wendroff scheme which can be written for equation (12.1) in one step form as

$$\mathbf{u}_j^{n+1} = \mathbf{u}_j^n - \frac{\rho}{2} A (\Delta_x + \nabla_x) \mathbf{u}_j^n + \frac{\rho^2}{2} A^2 \delta_x^2 \mathbf{u}_j^n \quad (12.9)$$

where A , which is assumed constant, is the Jacobian matrix, $\nabla_u f$, of the flux vector f and $\rho = \Delta t / \Delta x$. For the inhomogeneous case, where a source function s is included in the conservation law, that is

Part 2

$$\mathbf{u}_t + \mathbf{f}_x = \mathbf{s}, \quad (12.10)$$

the Lax-Wendroff method can be written as

$$\begin{aligned} \mathbf{u}_j^{n+1} &= \mathbf{u}_j^n - \frac{\rho}{2} A (\Delta_x + \nabla_x) \mathbf{u}_j^n + \frac{\rho^2}{2} A^2 \delta_x^2 \mathbf{u}_j^n + \\ &\quad \frac{\Delta t}{2} (s_{j+1}^n + s_j^n) - \frac{\rho \Delta t}{4} A (\Delta_x + \nabla_x) \mathbf{s}_j^n \end{aligned} \quad (12.11)$$

where $s_j^n = s(x_j, t^n)$. The simplest way to account for a Jacobian matrix which is not constant is to write the above equations in *two step* form as

$$\mathbf{u}_{j+1/2}^{\overline{n+1}} = \mu_x \mathbf{u}_{j+1/2}^n - \frac{\rho}{2} \Delta_x \mathbf{f}_j^n, \quad (12.12)$$

$$\mathbf{u}_j^{n+1} = \mathbf{u}_j^n - \rho \delta_x \mathbf{f}_{j+1/2}^{\overline{n+1}} + \frac{\Delta t}{2} \Delta_t \mathbf{s}_j^n - \frac{\rho \Delta t}{4} (\Delta_x + \nabla_x) A \mathbf{s}_j^n, \quad (12.13)$$

where $\mathbf{f}_{j+1/2}^{\overline{n+1}} = \mathbf{f}(\mathbf{u}_{j+1/2}^{\overline{n+1}})$. This scheme is stable with a *Courant number* of 1, that is

$$\rho \lambda_{\max} \leq 1, \quad (12.14)$$

where λ_{\max} is the largest eigenvalue of A . This scheme is consistent with the partial differential equation

$$\mathbf{u}_t + \mathbf{f}_x = \frac{\Delta t}{2} \mathbf{f}_{xx} + \mathbf{s}, \quad (12.15)$$

which is therefore consistent with equation (12.10) as Δt tends to zero. It can also be shown that the Lax-Wendroff scheme is second order accurate in both time and space. That is, the truncation error is $O(\Delta t^2)$ and $O(\Delta x^2)$. The use of equation (12.15) is another way of ensuring that the numerical solution converges to the correct physical solution (see Harten [Harten 83]). The term $((\Delta t)/2) \mathbf{f}_{xx}$ is called an artificial viscosity term and it adds

Part 2

dissipation to the scheme. Note also that in this scheme every component of the solution vector is defined at each grid point in the lattice.

An alternate classical method of approximating the partial differential equation (12.10), which does not add any artificial dissipation, is via centered differences for both time and space. The scheme, known as the leap-frog method, is written very simply as

$$\mathbf{u}_j^{n+1} = \mathbf{u}_j^{n-1} - \rho (\mathbf{f}_{j+1}^n - \mathbf{f}_{j-1}^n) + \Delta t (\mathbf{s}_j^{n+1} + \mathbf{s}_j^{n-1}) \quad (12.16)$$

which is also stable for a Courant number of 1 and is second order accurate in both time and space. This scheme is a *two-step* method in that it requires initial conditions at t^0 and t^1 before it can be used for time stepping. Note also that, in this scheme, the solution vector is calculated on two interlaced meshes which are independent of each other. This is depicted in Figure 59.

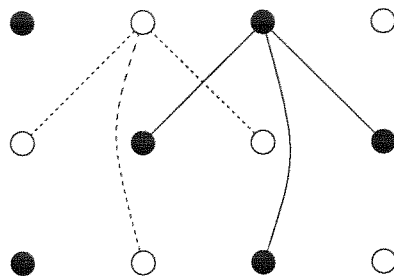


Figure 59 Computational molecule for leap-frog scheme

It is natural to keep only one of the meshes, and to execute the scheme on a staggered mesh. Also, a closer look at Maxwell's equations in one dimension (and later in higher dimensions) reveals that if equation (12.16) is used, the component D_j^{n+1} is dependent on D_j^{n-1} , B_{j+1}^n , and B_{j-1}^n . Thus it is also natural to interlace the components on the staggered mesh. That is, the discrete solution vector can be defined as

Part 2

$$\mathbf{u}_j^n = \begin{bmatrix} D_j^n \\ B_{j+1/2}^{n-1/2} \end{bmatrix}, \quad (12.17)$$

and equation (12.16) can be rewritten as

$$D_j^{n+1} = D_j^n - \rho (f_j^n - f_{j-1}^n) + \Delta t (s_j^{n+1} + s_j^n), \quad (12.18)$$

$$B_{j+1/2}^{n+1/2} = B_{j+1/2}^{n-1/2} - \rho (f_{j+1}^n - f_j^n) + \Delta t (s_j^{n+1} + s_j^n). \quad (12.19)$$

This is the classical interlaced staggered mesh introduced by Yee (see [Yee 66]). The components of the solution vector \mathbf{u} are updated at alternate half time steps and the computational molecule becomes as that shown in Figure 60.

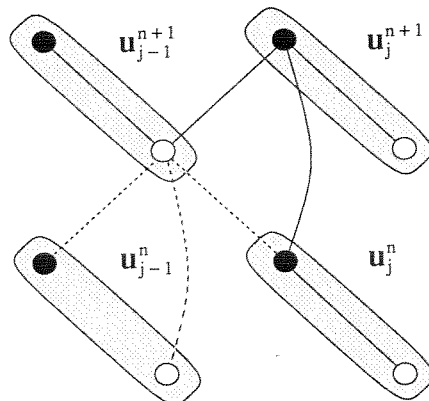


Figure 60 Interlaced mesh for leap-frog

12.3 Schemes Based on Upwinding and Flux-Splitting Techniques

The concept of an upwinding difference scheme is based on the fact that a finite difference scheme is stable for wave type equations if the *domain of dependence* of the numerical method is greater than that of the physical phenomenon being modelled. The domain of dependence of a discrete method can be easily found from the computational molecule depicting the scheme. The domain of dependence of the physical problem can be

Part 2

defined as the domain in x - t space which has influence on the disturbance at a specific point in the plane. This is best explained by the example of the *one-way scalar wave equation* defined by the partial differential equation

$$u_t + au_x = 0 \quad (12.20)$$

which has solution $u(x, t) = f(x - at)$ where $f(x) = u(x, 0)$ is the initial condition for the problem. This equation represents a wave moving to the right with *velocity* given by a (if a is negative then the wave moves to the left, *i.e.* right with negative velocity). Thus the domain of dependence at a point (ξ, τ) for the physical problem is the characteristic line of slope $1/a$ passing through the point and for times less than τ . In order for the numerical scheme to be stable, its domain of dependence must encompass this characteristic. This is shown in Figure 61. Thus for the one way wave equation, centered space differences are not required for stability.

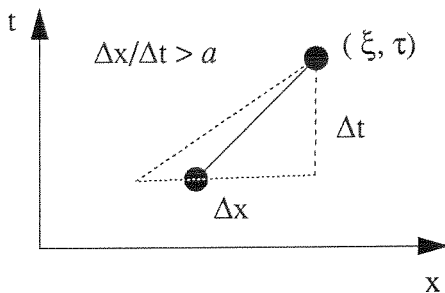


Figure 61 Domain of dependence of physical and numerical problem

This was taken advantage of in the formulation of the classical *upwind method* by Courant, Isaacson, and Rees [Courant 52]. This scheme which approximates equation (12.20), where it is assumed that $a = a(x)$, is written as

$$u_j^{n+1} = u_j^n - \begin{cases} \rho a(x_j) \Delta_x u_j^n, & a(x_j) < 0 \\ \rho a(x_j) \nabla_x u_j^n, & a(x_j) > 0 \end{cases} \quad (12.21)$$

Part 2

and is stable with Courant number of 1. It can be shown that it is first order accurate in both space and time.

For systems of conservation laws given by equation (12.1), a scheme which is second order accurate in both space and time and also makes use of upwind differencing is the *predictor-corrector* scheme of Warming and Beam (see [Warming 76]). They based their analysis on the *MacCormack scheme* which is written as

$$\bar{\mathbf{u}}_j^{n+1} = \mathbf{u}_j^n - \rho \nabla_x \mathbf{f}_j^n \quad (12.22)$$

$$\mathbf{u}_j^{n+1} = \frac{1}{2} (\mathbf{u}_j^n + \bar{\mathbf{u}}_j^{n+1}) - \frac{\rho}{2} \Delta_x \bar{\mathbf{f}}_j^{n+1}. \quad (12.23)$$

From this the fully upwind scheme is produced by modifying the corrector of equation (12.23) to

$$\mathbf{u}_j^{n+1} = \frac{1}{2} (\mathbf{u}_j^n + \bar{\mathbf{u}}_j^{n+1}) - \frac{\rho}{2} \nabla_x \mathbf{f}_j^{n+1} - \frac{\rho}{2} \nabla_x^2 \bar{\mathbf{f}}_j^{n+1} \quad (12.24)$$

where $\bar{\mathbf{f}}_j^{n+1} = \mathbf{f}(\mathbf{u}_j^{n+1})$. This scheme is only stable for systems having a Jacobian matrix A with all positive eigenvalues. It can be converted to handle a system with all negative eigenvalues by replacing ∇ by Δ in equations (12.21) and (12.23).

For the general case, where the eigenvalues of A are both positive and negative, a *flux vector splitting technique* must be used if a stable upwinding scheme is desired (see Steger and Warming [Steger 81]). In this method the flux vector is split into two parts as

$$\mathbf{f} = \mathbf{f}^+ + \mathbf{f}^- \quad (12.25)$$

where \mathbf{f}^+ corresponds to the positive eigenvalues and thus the positive flowing waves, and \mathbf{f}^- to the negative eigenvalues of the negative flowing waves. This splitting is accomplished by recalling that, by definition of a hyperbolic system, the Jacobian matrix can be

Part 2

diagonalized by a matrix T , and T^{-1} , where T is made up of the right eigenvectors and T^{-1} of the left eigenvectors such that

$$\mathbf{f} = \mathbf{A}\mathbf{u} = T\Lambda T^{-1}\mathbf{u} \quad (12.26)$$

where $\Lambda = \text{diag}(\lambda_j)$ is the diagonal matrix of the corresponding eigenvalues of A . The matrix Λ can be split into the sum of two matrices Λ^+ and Λ^- as

$$\Lambda = \Lambda^+ + \Lambda^- \quad (12.27)$$

where Λ^+ contains only positive eigenvalues λ^+ and Λ^- contains only negative eigenvalues λ^- . Thus the splitting of the flux vector \mathbf{f} can be achieved by using equation (12.27) in equation (12.26) as

$$\mathbf{f} = T(\Lambda^+ + \Lambda^-)T^{-1}\mathbf{u} = (A^+ + A^-)\mathbf{u} = \mathbf{f}^+ + \mathbf{f}^- \quad (12.28)$$

Once the flux vector has been split it can be used in the second order accurate Warming and Beam scheme given by equations (12.22) and (12.23). These become

$$\bar{\mathbf{u}}_j^{n+1} = \mathbf{u}_j^n - \rho \nabla_x (\mathbf{f}_j^+)^n - \rho \Delta_x (\mathbf{f}_j^-)^n \quad (12.29)$$

$$\begin{aligned} \mathbf{u}_j^{n+1} = & \frac{1}{2} (\mathbf{u}_j^n + \bar{\mathbf{u}}_j^{n+1}) - \frac{\rho}{2} (\nabla_x (\mathbf{f}_j^+)^{n+1} + \nabla_x^2 (\mathbf{f}_j^+)^{\overline{n+1}}) \\ & + \frac{\rho}{2} (\Delta_x^2 (\mathbf{f}_j^-)^{\overline{n+1}} - \Delta_x (\mathbf{f}_j^-)^{n+1}) \end{aligned} \quad (12.30)$$

which can be shown to be stable with a *Courant number of 2* (see Steger and Warming [Steger 81]). The above equations form the basis of the difference technique used by Shankar for the electromagnetic equations [Shankar 90]. The method of determining the backward and forward flux differences still remains to be discussed in order that the scheme can be implemented.

Part 2

In general, the fluxes at the cell interfaces (i.e. $x_{j+1/2}$) are not known and some method of approximation must be determined. Since these are approximations, they are referred to as *numerical* fluxes, denoted by $\mathbf{h}_{j+1/2}$, and are defined as in equations (12.7) and (12.8). Now in terms of these numerical fluxes, the forward and backward differences of the negative and positive fluxes may be defined as those defined by Sweby [Sweby 84]

$$\nabla \mathbf{f}_j^+ = \delta \mathbf{f}_{j-1/2}^+ = -(\mathbf{h}_{j-1/2} - \mathbf{f}(x_j)) \quad (12.31)$$

$$\Delta \mathbf{f}_j^- = \delta \mathbf{f}_{j+1/2}^- = (\mathbf{h}_{j+1/2} - \mathbf{f}(x_j)). \quad (12.32)$$

When these are substituted into the predictor of equation (12.22) it becomes

$$\overline{\mathbf{u}_j^{n+1}} = \mathbf{u}_j^n - \rho (\mathbf{h}_{j+1/2} - \mathbf{h}_{j-1/2}) \quad (12.33)$$

and the corrector becomes

$$\mathbf{u}_j^{n+1} = \frac{1}{2} (\mathbf{u}_j^n + \overline{\mathbf{u}_j^{n+1}}) - \frac{\rho}{2} (\mathbf{h}_{j+1/2}^{n+1} - \mathbf{h}_{j-1/2}^{n+1}) \quad (12.34)$$

$$\begin{aligned} \mathbf{u}_j^{n+1} &= \frac{1}{2} (\mathbf{u}_j^n + \overline{\mathbf{u}_j^{n+1}}) - \frac{\rho}{2} (\overline{\mathbf{h}_{j+1/2}^{n+1}} - \overline{\mathbf{h}_{j-1/2}^{n+1}}) \\ &\quad - \frac{\rho}{2} (\delta_x (\mathbf{f}^+)_{j-1/2}^{\overline{n+1}} - \delta_x (\mathbf{f}^+)_{j-3/2}^{n+1}) \\ &\quad + \frac{\rho}{2} (\delta_x (\mathbf{f}^-)_{j+3/2}^{\overline{n+1}} - \delta_x (\mathbf{f}^-)_{j+1/2}^{n+1}) \end{aligned} \quad (12.35)$$

after substitution. The above predictor-corrector form given by equations (12.34) and (12.35) are identical to those given by Shankar [Shankar 90].

12.4 Numerical Flux Determination

The final task before the upwind scheme can be used is to determine the appropriate numerical fluxes. There are many ways in which the flux at the interface between two cells can be approximated (i.e. $\mathbf{h}_{j+1/2}$). The usual procedure is to determine the numerical fluxes

Part 2

by solving a *Riemann problem* (see Roe [Roe 81] and Osher [Osher 84]). The Riemann problem is specified by the conservation law with initial conditions given by equation (11.23). In the case of the finite difference approximations the solution is assumed constant in each cell. Therefore, at a cell interface located at $x_{j+1/2}$, the left solution of the Riemann problem would correspond to \mathbf{u}_j and the right to \mathbf{u}_{j+1} .

Maxwell's equations for the one dimensional case can be written as equation (12.10) with

$$\mathbf{u}(x, t) = \begin{bmatrix} \mathbf{B} \\ \mathbf{D} \end{bmatrix}, \quad (12.36)$$

$$\mathbf{f}(x, t) = \begin{bmatrix} \hat{\mathbf{x}} \times e\mathbf{D} \\ -\hat{\mathbf{x}} \times m\mathbf{B} \end{bmatrix}, \quad (12.37)$$

$$\mathbf{s}(x, t) = \begin{bmatrix} 0 \\ -\mathbf{J} \end{bmatrix} = \begin{bmatrix} 0 \\ -e\sigma\mathbf{D} \end{bmatrix}, \quad (12.38)$$

where the fields have been left in vector form for ease of manipulation. Since all the fields in the Maxwell's equations are linearly degenerate, equation (11.22) becomes

$$\lambda[\mathbf{u}] = [\mathbf{f}], \quad (12.39)$$

and may be used to solve the Riemann problem. This can easily be seen by replacing \mathbf{f} in equation (11.16) with $A\mathbf{u}$ which then becomes

$$S[\mathbf{u}] = [\mathbf{f}] = A[\mathbf{u}] \quad (12.40)$$

$$(A - SI)[\mathbf{u}] = 0 \quad (12.41)$$

which has non-trivial solutions only for the speed of propagation equal to an eigenvalue of A , that is $S = \lambda$. For the above case, the eigenvalues are $\lambda = \pm c = \pm (me)^{1/2}$.

Part 2

The solution vector just to the left of the cell boundary is denoted as \mathbf{u}^* and just to the right of the boundary as \mathbf{u}^\wedge , similar to the notation of Figure 56. The solution at the point x_j can then be related to the solution at x^* by equation (12.39) using the negative eigenvalue, and the solution at x^\wedge to the solution at x_{j+1} using the positive eigenvalue. This produces the equations

$$-c_j (\mathbf{u}^* - \mathbf{u}_j) = (\mathbf{f}^* - \mathbf{f}_j), \quad (12.42)$$

$$c_{j+1} (\mathbf{u}_{j+1} - \mathbf{u}^\wedge) = (\mathbf{f}_{j+1} - \mathbf{f}^\wedge), \quad (12.43)$$

while at the boundary, \mathbf{f}^* and \mathbf{f}^\wedge are related by

$$\mathbf{f}^* = \mathbf{f}^\wedge. \quad (12.44)$$

These are now solved for \mathbf{f}^* and \mathbf{f}^\wedge in terms of \mathbf{u}_{j+1} and \mathbf{u}_j . For the individual components, equations (12.42) and (12.43) can be written as

$$-c_j (\mathbf{B}^* - \mathbf{B}_j) = (\hat{\mathbf{x}} \times (\mathbf{e}\mathbf{D})^* - \hat{\mathbf{x}} \times (\mathbf{e}\mathbf{D})_j), \quad (12.45)$$

$$-c_j (\mathbf{D}^* - \mathbf{D}_j) = -(\hat{\mathbf{x}} \times (\mathbf{m}\mathbf{B})^* - \hat{\mathbf{x}} \times (\mathbf{m}\mathbf{B})_j), \quad (12.46)$$

and

$$c_{j+1} (\mathbf{B}_{j+1} - \mathbf{B}^\wedge) = (\hat{\mathbf{x}} \times (\mathbf{e}\mathbf{D})_{j+1} - \hat{\mathbf{x}} \times (\mathbf{e}\mathbf{D})^\wedge), \quad (12.47)$$

$$c_{j+1} (\mathbf{D}_{j+1} - \mathbf{D}^\wedge) = -(\hat{\mathbf{x}} \times (\mathbf{m}\mathbf{B})_{j+1} - \hat{\mathbf{x}} \times (\mathbf{m}\mathbf{B})^\wedge), \quad (12.48)$$

while equation (12.44) becomes

$$\hat{\mathbf{x}} \times \mathbf{e}_j \mathbf{D}^* = \hat{\mathbf{x}} \times \mathbf{e}_{j+1} \mathbf{D}^\wedge, \quad (12.49)$$

and

Part 2

$$\hat{x} \times m_j \mathbf{B}^* = \hat{x} \times m_{j+1} \mathbf{B}^\wedge. \quad (12.50)$$

Now taking the cross-product of equations (12.46) and (12.48) with \hat{x} ,

$$-c_j (\hat{x} \times \mathbf{D}^* - \hat{x} \times \mathbf{D}_j) = -\hat{x} \times (\hat{x} \times m_j \mathbf{B}^* - \hat{x} \times (m \mathbf{B})_j), \quad (12.51)$$

and

$$c_{j+1} (\hat{x} \times \mathbf{D}_{j+1} - \hat{x} \times \mathbf{D}^\wedge) = -\hat{x} \times (\hat{x} \times (m \mathbf{B})_{j+1} - \hat{x} \times (m \mathbf{B})^\wedge), \quad (12.52)$$

which, using equation (12.49), becomes

$$c_{j+1} (\hat{x} \times \mathbf{D}_{j+1} - \hat{x} \times \frac{e_j}{e_{j+1}} \mathbf{D}^*) = -\hat{x} \times (\hat{x} \times (e \mathbf{B})_{j+1} - \hat{x} \times (m_j \mathbf{B}^*)). \quad (12.53)$$

Adding equations (12.51) and (12.53) yields

$$\begin{aligned} \hat{x} \times e_j \mathbf{D}^* \left(\frac{c_{j+1}}{e_{j+1}} + \frac{c_j}{e_j} \right) &= \hat{x} \times \{ [(c \mathbf{D})_{j+1} + \hat{x} \times (m \mathbf{B})_{j+1}] \\ &\quad + [(c \mathbf{D})_j - \hat{x} \times (m \mathbf{B})_j] \}. \end{aligned} \quad (12.54)$$

A similar procedure produces

$$\begin{aligned} \hat{x} \times m_j \mathbf{B}^* \left(\frac{e_{j+1}}{c_{j+1}} + \frac{e_j}{c_j} \right) &= \hat{x} \times \{ [(c \mathbf{B})_{j+1} - \hat{x} \times (e \mathbf{D})_{j+1}] \\ &\quad + [(c \mathbf{B})_j + \hat{x} \times (e \mathbf{D})_j] \}. \end{aligned} \quad (12.55)$$

Note that equations (12.54) and (12.55) are the same as that derived by Shankar [Shankar 90] without the generalization of the resistive sheet. Also note that the form of these equations is identical to those of equations (11.59) to (11.62).

The above equations can now be used for the numerical flux definition required in the two step upwind scheme of equations (12.34) and (12.35).

12.5 Comparison of Schemes for 1-D Electromagnetics

Numerical results for the finite difference schemes presented in the previous two sections are compared for the solution of Maxwell's equations in one dimensional space. These are also compared to the exact solution given in the section *Maxwell's Equations in One Space Dimension and Time* on page 121.

The first test case is that of a incident square \mathbf{D} pulse on a perfectly conducting boundary as shown in Figure 62. Here the results due to the different finite difference schemes are labeled in the figures themselves. Note that the scheme given by equations (11.63) and (11.64) is referred to as the semi-analytic scheme. The perfectly reflecting boundary is implemented using the *image principle*. That is, a numerical mesh point is located to the right of the boundary (x_{k+1}) and its solution (\mathbf{u}_{k+1}) is calculated using

$$\mathbf{D}_{k+1} = -\mathbf{D}_k, \quad (12.56)$$

and

$$\mathbf{B}_{k+1} = \mathbf{B}_k. \quad (12.57)$$

Notice that all the schemes perform exceptionally well since ρ is set at the Courant limit for all the schemes. Thus, the upwind scheme requires half the number of time steps for this and all remaining test cases.

The next test case is that of a square initial \mathbf{D} pulse impinging on a dielectric boundary shown in Figure 63. The relative dielectric constant of the second region is chosen as $\epsilon_r = 10$. Thus the wave speed in this region is $10^{1/2}$ times slower than in the region where the pulse originated. The oscillations seen in the dielectric region are due to the fact that ρ is set constant for all schemes except for the semi-analytic scheme where ρ is dictated by the scheme. As can be seen, a great loss of accuracy occurs when ρ is reduced from the Courant limit.

Part 2

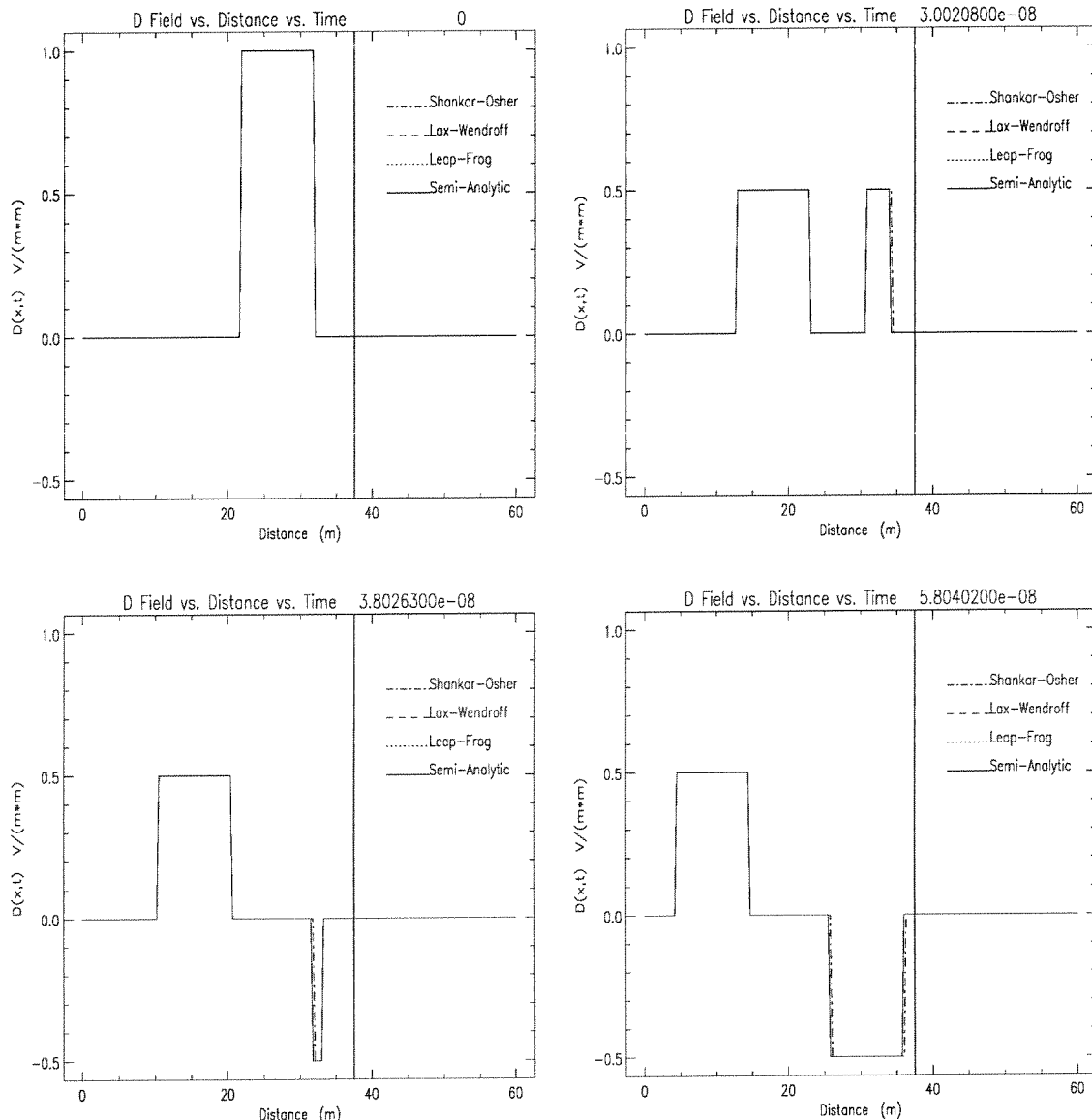


Figure 62 1-D electromagnetic solutions for a perfectly conducting boundary (initial electric displacement D = square pulse)

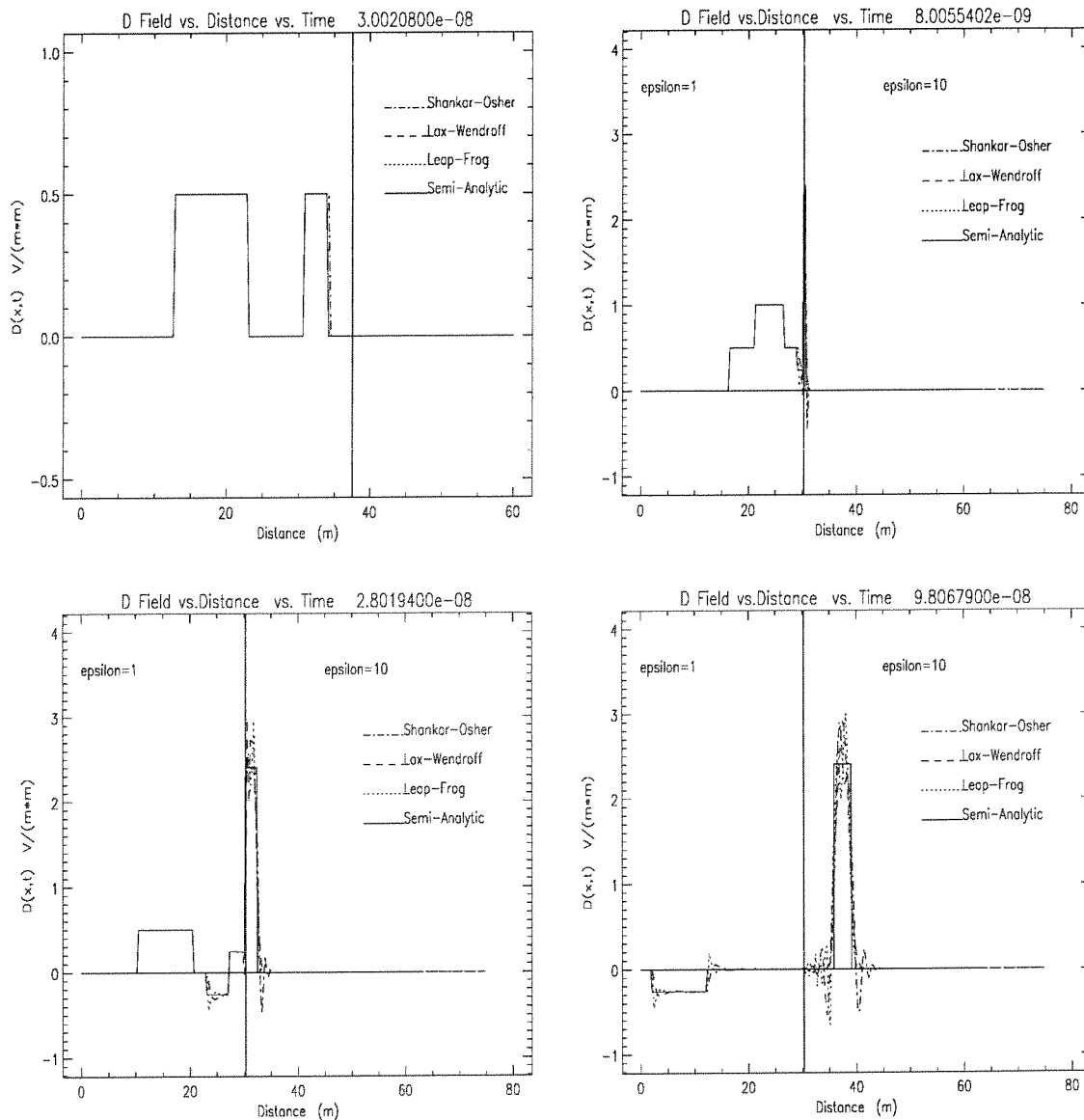
Part 2


Figure 63 1-D electromagnetic solutions for dielectric boundary
(initial electric displacement D = square pulse)

Part 2

The next test case is for an incident square \mathbf{D} pulse on a partially conducting boundary as shown in Figure 64. The partially conducting region has a dielectric constant of $\epsilon_r = 10$ and a conductivity of $\sigma = 0.001$. In this case the semi-analytic solution is modified by multiplying the boundary fluxes by

$$e^{-\frac{e\sigma}{2}\Delta t}, \quad (12.58)$$

and by adding the term s_j^n to equations (11.63) and (11.64). These addition terms make the scheme non-exact.

The final two test cases are that of a Gaussian and square initial \mathbf{D} pulse in a homogeneous conducting medium with $\sigma = 0.001$, as shown in Figure 65 and Figure 66 respectively. For these cases the numerical schemes are compared to the analytical solution found via equations (11.70) and (11.72). These equations were integrated using Simpson's rule where a *series* approximation was used for the Bessel function.

Notice that the negative tail shown in these plots, as opposed to the positive tail of Stratton (see [Stratton 41] pp 307, Figure 53a), as the pulse splits and travels to the right and the left is due to different initial conditions being imposed in the two cases. This was discussed at the end of section 11.4.2 on page 130. In general, all of the numerical schemes are less accurate in the presence of the conductivity, especially for the high frequency components present in the square initial pulse.

In order to see the differences more clearly, separate plots are presented for the case of the square initial pulse in the conducting medium for each of the numerical schemes used. These are shown in Figure 67 for one specific time. As can be seen from the figure, all the methods produce *oscillations* or *ripples*.

Part 2

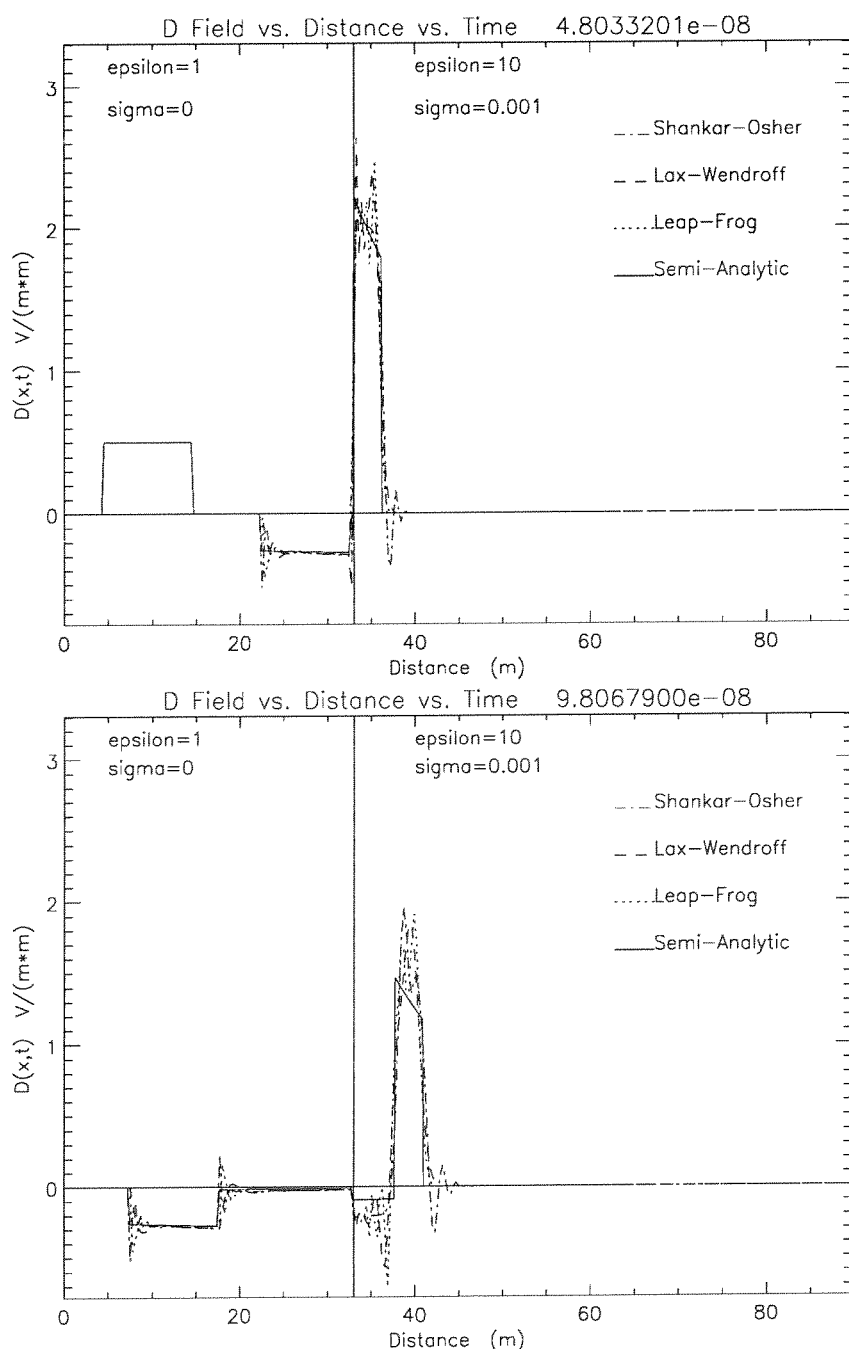


Figure 64 1-D electromagnetic solutions for dielectric conducting boundary
(initial electric displacement D = square pulse)

Part 2

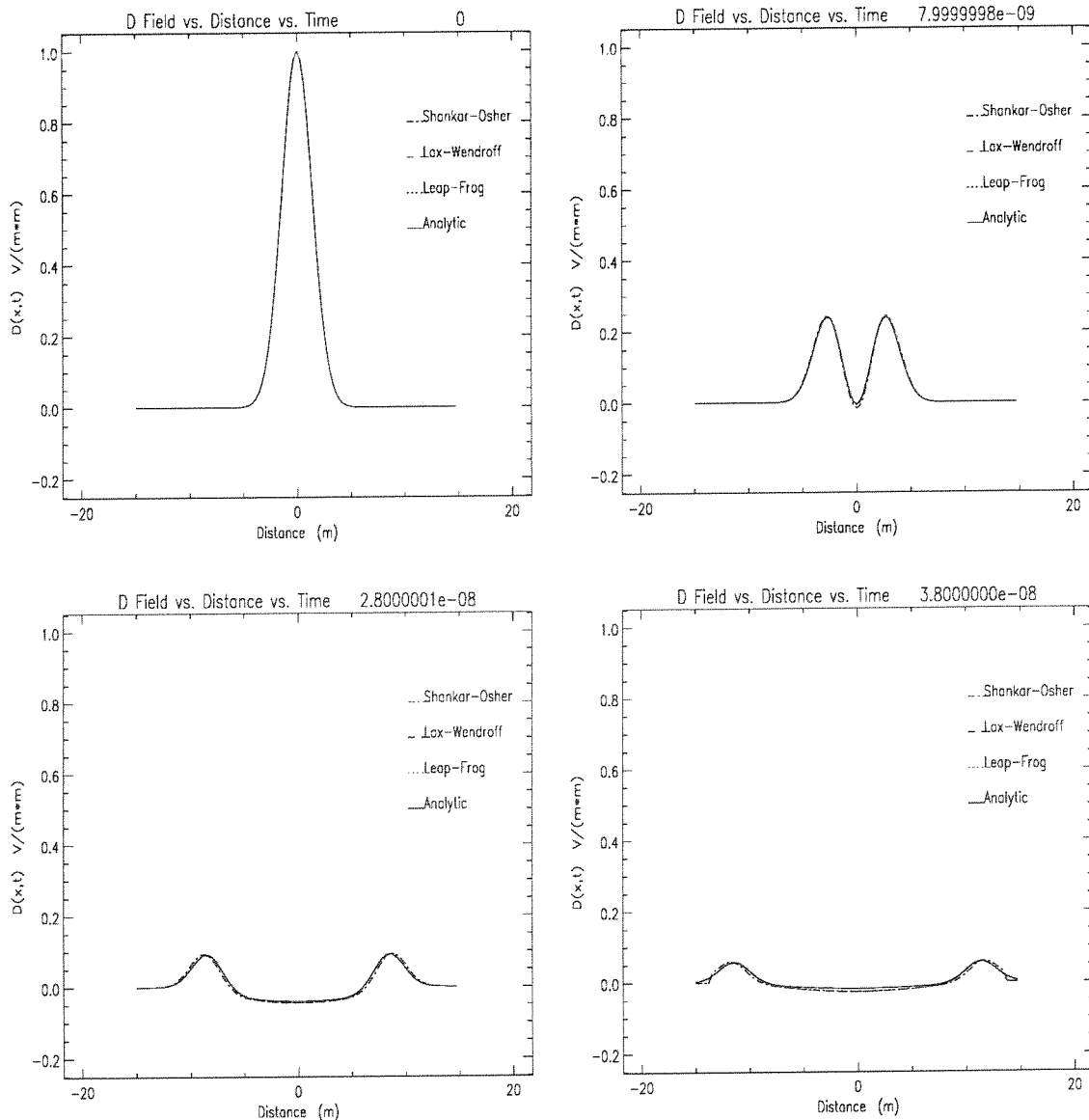


Figure 65 1-D electromagnetic solutions for conducting medium
(initial electric displacement D = Gaussian pulse)

Part 2

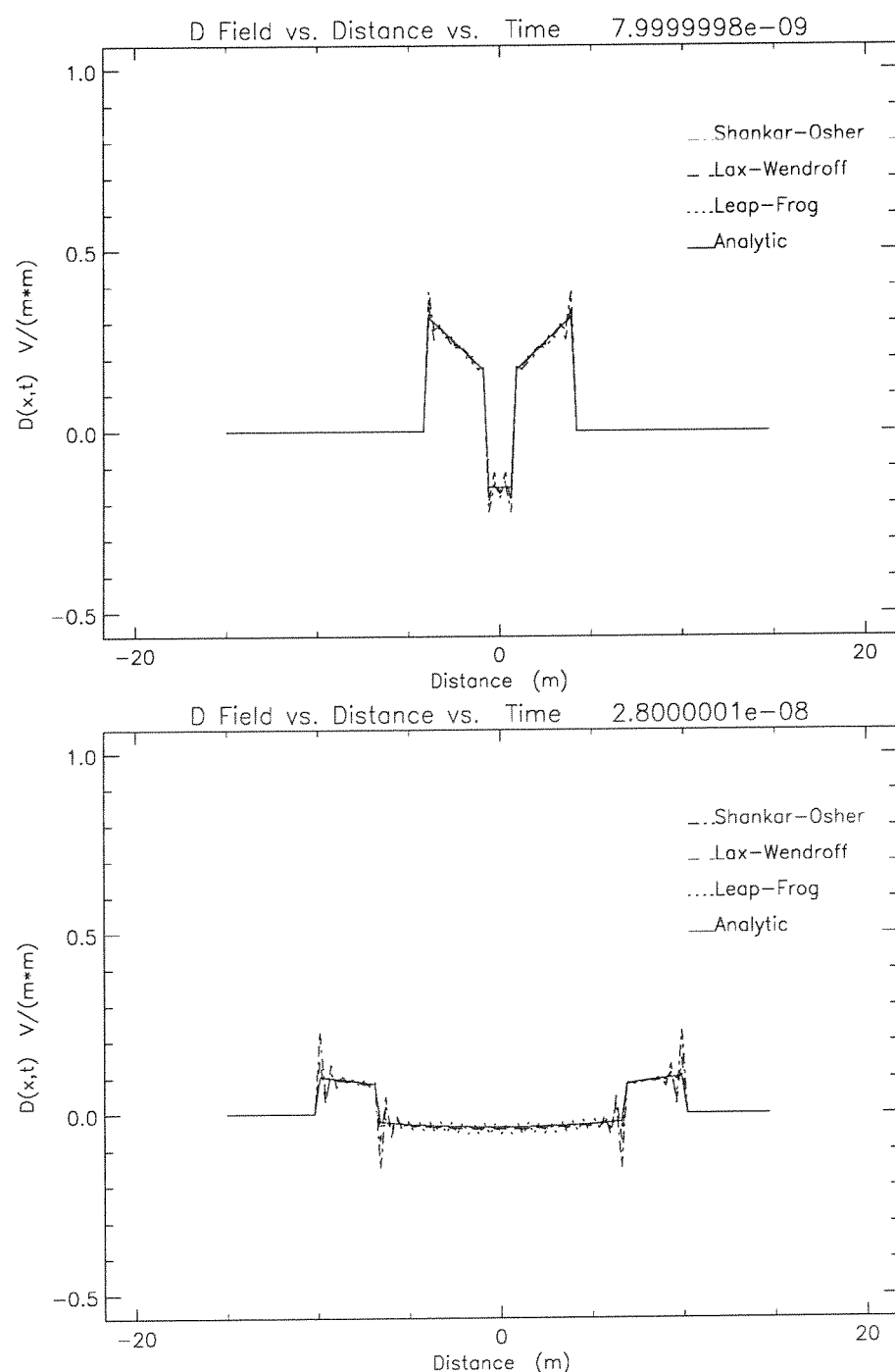


Figure 66 1-D electromagnetic solutions for conducting medium
(initial electric displacement D = square pulse)

Part 2

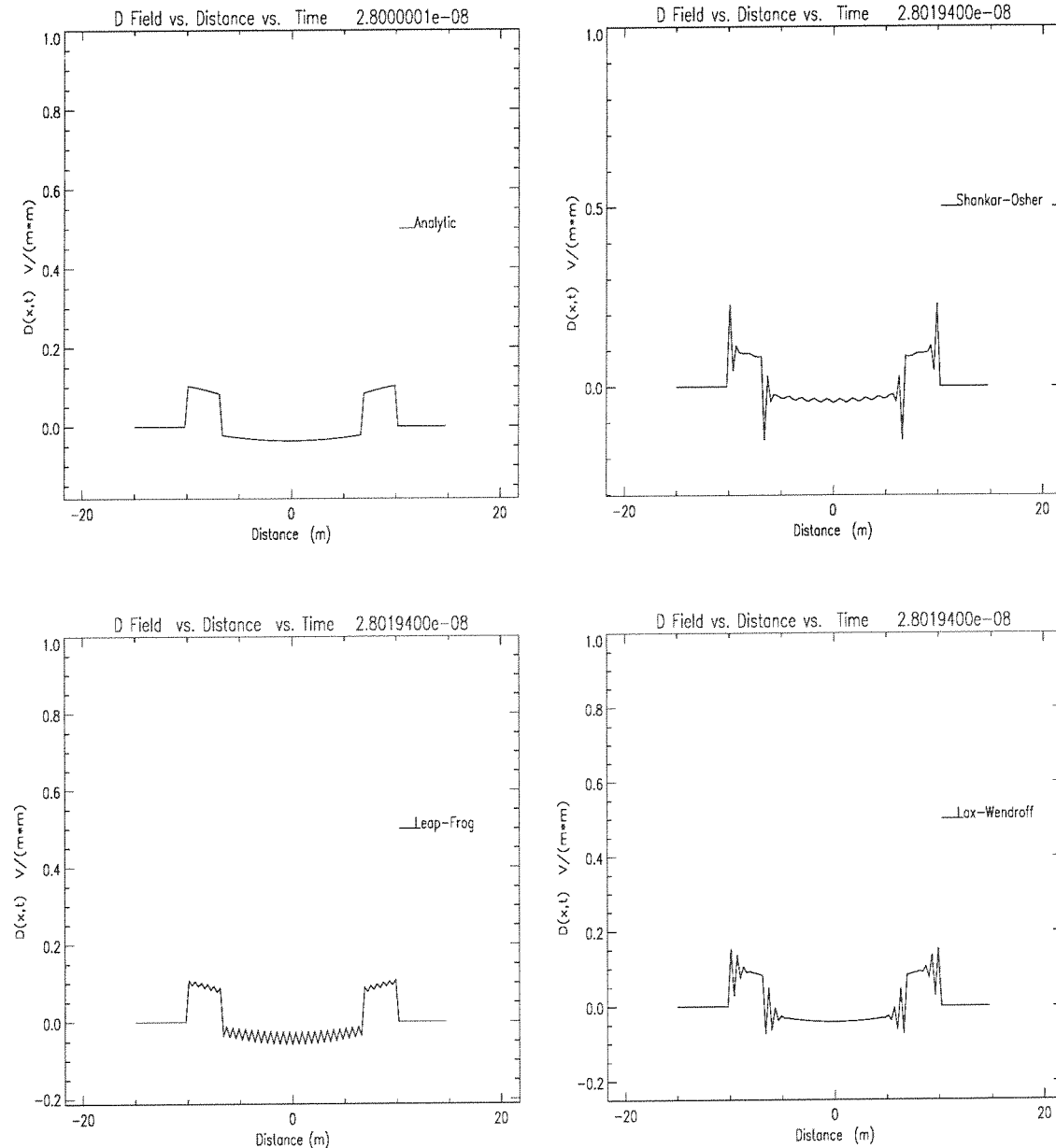


Figure 67 Separate plots for square initial \mathbf{D} in conducting medium

Chapter 13

Finite Differences in Higher Dimensions

The finite difference schemes previously presented for hyperbolic conservation laws in one space dimension are now generalized to two and three dimensions. The convenience of describing Maxwell's equations in conservation law form will become evident. An approximate solution to the general three dimensional conservation law,

$$\mathbf{u}_t + \mathbf{E}_x + \mathbf{F}_y + \mathbf{G}_z = \mathbf{S}, \quad (13.1)$$

with initial conditions $\mathbf{u}(x, y, z, 0) = \mathbf{g}(x, y, z)$ is sought on the rectangular lattice

$$\Omega_{jkl} = \left\{ (x, y, z, t) \mid \begin{array}{l} x_{j-1/2} \leq x \leq x_{j+1/2} \\ y_{k-1/2} \leq y \leq y_{k+1/2} \\ z_{l-1/2} \leq z \leq z_{l+1/2} \\ t^n \leq t \leq t^{n+1} \end{array} \right\}, \quad (13.2)$$

where $x_j = j\Delta x$, $y_k = k\Delta y$, $z_l = l\Delta z$, $t^n = n\Delta t$ and j, k, l , and n are integers. The initial conditions are approximated on Ω_{jkl0} by

$$\mathbf{u}_{jkl}^0 = \mathbf{g}_{jkl} = \mathbf{g}(x_j, y_k, z_l), \quad (13.3)$$

and a finite difference procedure is used to determine the solution at a new time $t = t^{n+1}$. The general finite difference scheme can be written as in the previous chapter as

Part 2

$$\mathbf{u}_{jkl}^{n+1} = Q(\mathbf{u}_{jkl}^n), \quad (13.4)$$

for $n \geq 0$ where Q is now a polynomial in the backward and forward shift operators E_- and E_+ for each space dimension. The qualities of *consistency*, *stability*, and *convergence* are still used to describe a specific difference scheme.

13.1 Leap-frog: Yee Algorithm

The simplest scheme to understand and implement is the leap-frog scheme formulated by Yee [Yee 66]. This is a two step scheme on an interlaced mesh. The interlacing of the solution vector components is easy to see in one-dimension (Figure 60). It is a bit more difficult to visualize in two and three dimensions. Note that this interlacing is specific to Maxwell's equations and may not occur for other equations.

Following the procedure of the previous chapter, the solution vector may be written as

$$\mathbf{u}_{jkl}^n = \begin{bmatrix} \mathbf{B}_{jkl}^n \\ \mathbf{D}_{jkl}^n \end{bmatrix} = \begin{bmatrix} (\mathbf{B}_x)_{j, k+1/2, l+1/2}^{n-1/2} \\ (\mathbf{B}_y)_{j+1/2, k, l+1/2}^{n-1/2} \\ (\mathbf{B}_z)_{j+1/2, k+1/2, l}^{n-1/2} \end{bmatrix} \begin{bmatrix} (\mathbf{D}_x)_{j+1/2, k, l}^n \\ (\mathbf{D}_y)_{j, k+1/2, l}^n \\ (\mathbf{D}_z)_{j, k, l+1/2}^n \end{bmatrix}^T, \quad (13.5)$$

and the scheme becomes

$$\begin{aligned} \mathbf{D}_{jkl}^{n+1} &= \mathbf{D}_{jkl}^n + \frac{\Delta t}{2} (\mathbf{s}_{jkl}^{n+1} + \mathbf{s}_{jkl}^n) \\ &\quad - \rho_x (\mathbf{E}_j^n - \mathbf{E}_{j-1}^n) \\ &\quad - \rho_y (\mathbf{F}_k^n - \mathbf{F}_{k-1}^n) \\ &\quad - \rho_z (\mathbf{G}_l^n - \mathbf{G}_{l-1}^n), \end{aligned} \quad (13.6)$$

and

Part 2

$$\begin{aligned}
 \mathbf{B}_{jkl}^{n+1} = & \mathbf{B}_{jkl}^n + \frac{\Delta t}{2} (\mathbf{s}_{jkl}^{n+1} + \mathbf{s}_{jkl}^n) \\
 & - \rho_x (\mathbf{E}_{j+1}^n - \mathbf{E}_j^n) \\
 & - \rho_y (\mathbf{F}_{k+1}^n - \mathbf{F}_k^n) \\
 & - \rho_z (\mathbf{G}_{l+1}^n - \mathbf{G}_l^n)
 \end{aligned} \tag{13.7}$$

where \mathbf{B}_{jkl}^n implies \mathbf{u}_{jkl}^n for any of the \mathbf{B} components and \mathbf{D}_{jkl}^n implies \mathbf{u}_{jkl}^n for any of the \mathbf{D} components and $\rho_\xi = \Delta t / \Delta \xi$. The notation for the flux vectors \mathbf{E} , \mathbf{F} , and \mathbf{G} is determined by

$$\mathbf{E}_j^n = \mathbf{E}(\mathbf{u}_{jkl}^n) = \left[\begin{array}{c} 0 \\ \left(\frac{-D_z}{\epsilon} \right)_j^n \\ \left(\frac{D_y}{\epsilon} \right)_j^n \end{array} \right] \left[\begin{array}{c} 0 \\ \left(\frac{B_z}{\mu} \right)_{j+1/2}^{n-1/2} \\ \left(\frac{-B_y}{\mu} \right)_{j+1/2}^{n-1/2} \end{array} \right]^T, \tag{13.8}$$

$$\mathbf{F}_k^n = \mathbf{F}(\mathbf{u}_{jkl}^n) = \left[\begin{array}{c} \left(\frac{D_z}{\epsilon} \right)_{j,k,1+1/2}^n \\ 0 \\ \left(\frac{-D_x}{\epsilon} \right)_{j+1/2,k,1}^n \end{array} \right] \left[\begin{array}{c} \left(\frac{-B_z}{\mu} \right)_{j+1/2,k+1/2,1}^{n-1/2} \\ 0 \\ \left(\frac{B_x}{\mu} \right)_{j+k+1/2,1+1/2}^{n-1/2} \end{array} \right]^T, \tag{13.9}$$

$$\mathbf{G}_l^n = \mathbf{G}(\mathbf{u}_{jkl}^n) = \left[\begin{array}{c} \left(\frac{-D_y}{\epsilon} \right)_{j,k+1/2,1}^n \\ \left(\frac{D_x}{\epsilon} \right)_{j+1/2,k,1}^n \\ 0 \end{array} \right] \left[\begin{array}{c} \left(\frac{B_y}{\mu} \right)_{j+1/2,k,1+1/2}^{n-1/2} \\ \left(\frac{-B_x}{\mu} \right)_{j,k+1/2,1+1/2}^{n-1/2} \\ 0 \end{array} \right]^T. \tag{13.10}$$

Part 2

The component locations as defined by equation (13.5) are depicted in Figure 68.

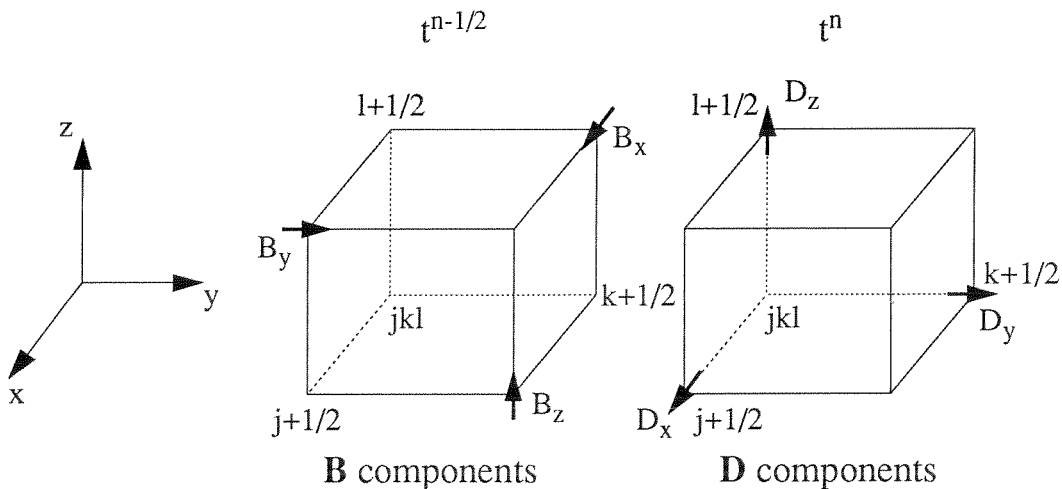


Figure 68 Location of components for leap-frog scheme

In two dimensions the scheme is obvious and will not be given explicitly here, except to recall that Maxwell's equations uncouple into two independent sets of three partial differential equations. These are the *TE case* where only the B_z , D_x , and D_y components exist, and the *TM case* where only the D_z , B_x , and B_y components exist. Note that these two cases correspond to either the components at the bottoms of the cubes in Figure 68 (i.e. TE case) or at the tops of the cubes (i.e. TM case).

In order to start the time marching, when either the initial \mathbf{B} or the initial \mathbf{D} is given in the initial condition, the first step will be a half time step ($\Delta t^0 = \Delta t/2$) if the other component is assumed to be zero. For example, if $\mathbf{B}(x, 0)$ is given as the initial condition, then equations (13.6) are used to update the \mathbf{D} fields assuming that the previous \mathbf{D} fields are zero, and using a time step of $\Delta t/2$. Alternatively, if $\mathbf{D}(x, 0)$ is given then equations (13.7) are used first with a time step of $\Delta t/2$. From this point on equations (13.7) and equations (13.6) are used alternately with a Δt time step.

Part 2

The boundary conditions for a perfectly conducting medium are easily implemented by imposing that the tangential electric field be equal to zero on this boundary. Thus, when a perfectly conducting body is placed in the mesh, the boundaries of the body should line up with mesh points containing tangential \mathbf{E} field components.

The stability of the scheme has been established by many authors (see for example [Taflove 90]). The scheme is stable for

$$\Delta t \leq \frac{1}{\left(\frac{1}{\Delta x^2} + \frac{1}{\Delta y^2} + \frac{1}{\Delta z^2} \right)^{1/2} c_{\max}} \quad (13.11)$$

where if $\Delta x = \Delta y = \Delta z$ this corresponds to a Courant number of $1/(\sqrt{3})$. In two dimensions, $\Delta z = \infty$ and the Courant number becomes $1/(\sqrt{2})$.

13.2 Lax-Wendroff: Two Step Method

In higher space dimensions there are many ways to write the Lax-Wendroff scheme (see [Lapidus 82]). The formulation of the Lax-Wendroff method in two step form was first presented by Richtmyer [Richtmyer 67] and thus the different versions of the scheme have become his namesake. The analysis of these schemes has been investigated by Wilson [Wilson 72] and are written below using the notation defined in Figure 58

i) *Richtmyer Scheme (3-D) (also Two-step Lax-Wendroff)*

$$\mathbf{u}_{jkl}^{n*} = \frac{(\mu_x + \mu_y + \mu_z)}{3} \mathbf{u}_{jkl}^n - \frac{[\rho_x \delta_x \mathbf{E}_{jkl}^n + \rho_y \delta_y \mathbf{F}_{jkl}^n + \rho_z \delta_z \mathbf{G}_{jkl}^n]}{2} \quad (13.12)$$

$$\mathbf{u}_{jkl}^{n+1} = \mathbf{u}_{jkl}^{n*} - [\rho_x \delta_x \mathbf{E}_{jkl}^{n*} + \rho_y \delta_y \mathbf{F}_{jkl}^{n*} + \rho_z \delta_z \mathbf{G}_{jkl}^{n*}]$$

Part 2

ii) Modified Richtmyer Scheme (3-D)

$$\mathbf{u}_{jkl}^{n*} = (\mu_x \mu_y \mu_z) \mathbf{u}_{jkl}^n - \frac{[\rho_x \delta_x E_{jkl}^n + \rho_y \delta_y F_{jkl}^n + \rho_z \delta_z G_{jkl}^n]}{2}$$

$$\mathbf{u}_{jkl}^{n+1} = \mathbf{u}_{jkl}^{n*} - [\rho_x \delta_x E_{jkl}^{n*} + \rho_y \delta_y F_{jkl}^{n*} + \rho_z \delta_z G_{jkl}^{n*}] \quad (13.13)$$

iii) Rotated Richtmyer Scheme (3-D)

$$\mathbf{u}_{jkl}^{n*} = (\mu_x \mu_y \mu_z) \mathbf{u}_{jkl}^n$$

$$- \frac{[\rho_x \mu_y \mu_z \delta_x E_{jkl}^n + \rho_y \mu_x \mu_z \delta_y F_{jkl}^n + \rho_z \mu_x \mu_y \delta_z G_{jkl}^n]}{2}$$

$$\mathbf{u}_{jkl}^{n+1} = \mathbf{u}_{jkl}^{n*} - [\rho_x \mu_y \mu_z \delta_x E_{jkl}^{n*} + \rho_y \mu_x \mu_z \delta_y F_{jkl}^{n*} + \rho_z \mu_x \mu_y \delta_z G_{jkl}^{n*}] \quad (13.14)$$

where $E_{jkl}^n = E(\mathbf{u}_{jkl}^n)$, $E_{jkl}^{n*} = E(\mathbf{u}_{jkl}^{n*})$, with similar relations for the flux vectors F , and

G , and $\rho_x = \frac{\Delta t}{\Delta x}$, $\rho_y = \frac{\Delta t}{\Delta y}$, $\rho_z = \frac{\Delta t}{\Delta z}$. The two dimensional versions of these

schemes can be easily obtained from the above equations by dropping the flux vector G and all finite difference operators in the z -coordinate direction. Thus they can be written as follows.

i) Richtmyer Scheme (2-D)

$$\mathbf{u}_{jk}^{n*} = \frac{(\mu_x + \mu_y)}{2} \mathbf{u}_{jk}^n - \frac{[\rho_x \delta_x E_{jk}^n + \rho_y \delta_y F_{jk}^n]}{2} \quad (13.15)$$

$$\mathbf{u}_{jk}^{n+1} = \mathbf{u}_{jk}^{n*} - [\rho_x \delta_x E_{jk}^{n*} + \rho_y \delta_y F_{jk}^{n*}]$$

Part 2

ii) Modified Richtmyer Scheme (2-D)

$$\mathbf{u}_{jk}^{n*} = (\mu_x \mu_y) \mathbf{u}_{jk}^n - \frac{[\rho_x \delta_x E_{jk}^n + \rho_y \delta_y F_{jk}^n]}{2} \quad (13.16)$$

$$\mathbf{u}_{jk}^{n+1} = \mathbf{u}_{jk}^{n*} - [\rho_x \delta_x E_{jk}^{n*} + \rho_y \delta_y F_{jk}^{n*}]$$

iii) Rotated Richtmyer Scheme (2-D)

$$\mathbf{u}_{jk}^{n*} = (\mu_x \mu_y) \mathbf{u}_{jk}^n - \frac{[\rho_x \mu_y \delta_x E_{jk}^n + \rho_y \mu_x \delta_y F_{jk}^n]}{2} \quad (13.17)$$

$$\mathbf{u}_{jk}^{n+1} = \mathbf{u}_{jk}^{n*} - [\rho_x \mu_y \delta_x E_{jk}^{n*} + \rho_y \mu_x \delta_y F_{jk}^{n*}]$$

The computational molecules for these schemes are shown in Figure 69.

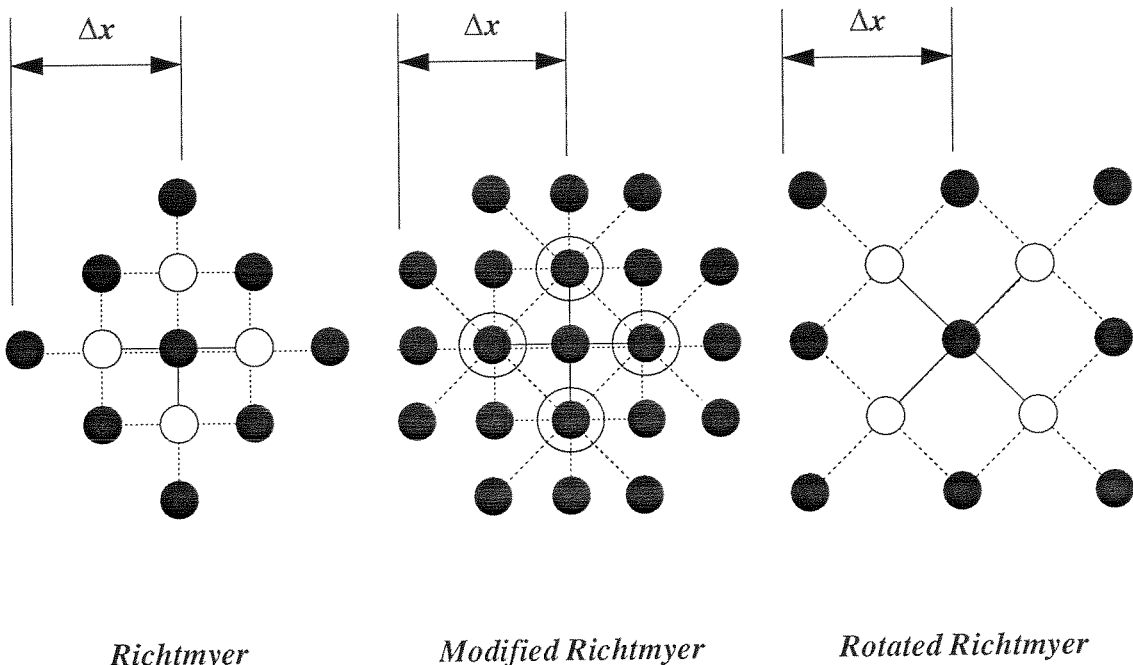


Figure 69 Computational molecules for 2-D Richtmyer schemes

Part 2

Note that in these schemes every component of the solution vector \mathbf{u} is represented at each lattice point. Thus it is simpler to introduce material boundaries into the mesh. The Rotated Richtmyer scheme is the simplest on which to impose boundary conditions due to its square computational boundary. It also has the largest Courant number. The Courant numbers for the Richtmyer schemes, corresponding to the case where $\Delta x = \Delta y = \Delta z$, are given in Figure 70 (see [Wilson 72]).

<i>Scheme</i>	<i>2-D Courant No.</i>	<i>3-D Courant No.</i>
Richtmyer	$\frac{1}{\sqrt{2}}$	$\frac{1}{\sqrt{3}}$
Modified Richtmyer	$\frac{1}{\sqrt{2}}$	$\frac{1}{\sqrt{3}}$
Rotated Richtmyer	1	1

Figure 70 Courant numbers for Richtmyer schemes

13.3 Upwind Schemes

The upwind difference methods based on the schemes of Warming and Beam (see [Warming 76] and the flux vector splitting techniques of Steger and Warming (see [Steger 81]) presented in section 12.3 on page 140 are now generalized to higher space dimensions. The flux vector splitting can be performed on each of the flux vectors \mathbf{E} , \mathbf{F} , and \mathbf{G} individually based on the Jacobian matrices of each. Thus the split vectors can be written as

$$\mathbf{E} = T_E (\Lambda_E^+ + \Lambda_E^-) T_E^{-1} \mathbf{u} = (A_E^+ + A_E^-) \mathbf{u} = \mathbf{E}^+ + \mathbf{E}^-, \quad (13.18)$$

$$\mathbf{F} = T_F (\Lambda_F^+ + \Lambda_F^-) T_F^{-1} \mathbf{u} = (A_F^+ + A_F^-) \mathbf{u} = \mathbf{F}^+ + \mathbf{F}^-, \quad (13.19)$$

$$\mathbf{G} = T_G (\Lambda_G^+ + \Lambda_G^-) T_G^{-1} \mathbf{u} = (A_G^+ + A_G^-) \mathbf{u} = \mathbf{G}^+ + \mathbf{G}^-, \quad (13.20)$$

Part 2

where, as before, the + superscript denotes a positive flowing flux and the - superscript denotes a negative flowing flux.

The Warming and Beam scheme predictor can now be written as

$$\begin{aligned} \bar{\mathbf{u}}_{jkl}^{n+1} = & \mathbf{u}_{jkl}^n - \rho_x \nabla_x (\mathbf{E}_j^+)^n - \rho_x \Delta_x (\mathbf{E}_j^-)^n \\ & - \rho_y \nabla_y (\mathbf{F}_k^+)^n - \rho_y \Delta_y (\mathbf{F}_k^-)^n \\ & - \rho_z \nabla_z (\mathbf{G}_l^+)^n - \rho_z \Delta_z (\mathbf{G}_l^-)^n, \end{aligned} \quad (13.21)$$

and the corrector as

$$\begin{aligned} \mathbf{u}_{jkl}^{n+1} = & \frac{1}{2} (\mathbf{u}_{jkl}^n + \bar{\mathbf{u}}_{jkl}^{n+1}) - \frac{\rho_x}{2} (\nabla_x (\mathbf{E}_j^+)^{n+1} + \nabla_x^2 (\mathbf{E}_j^+)^{\overline{n+1}}) \\ & + \frac{\rho_x}{2} (\Delta_x^2 (\mathbf{E}_j^-)^{\overline{n+1}} - \Delta_x (\mathbf{E}_j^-)^{n+1}) \\ & - \frac{\rho_y}{2} (\nabla_y (\mathbf{F}_k^+)^{n+1} + \nabla_y^2 (\mathbf{F}_k^+)^{\overline{n+1}}) \\ & + \frac{\rho_y}{2} (\Delta_y^2 (\mathbf{F}_k^-)^{\overline{n+1}} - \Delta_y (\mathbf{F}_k^-)^{n+1}) \\ & - \frac{\rho_z}{2} (\nabla_z (\mathbf{G}_l^+)^{n+1} + \nabla_z^2 (\mathbf{G}_l^+)^{\overline{n+1}}) \\ & + \frac{\rho_z}{2} (\Delta_z^2 (\mathbf{G}_l^-)^{\overline{n+1}} - \Delta_z (\mathbf{G}_l^-)^{n+1}), \end{aligned} \quad (13.22)$$

where $\mathbf{E}_j = \mathbf{E}_{jkl}$, $\mathbf{F}_k = \mathbf{F}_{jkl}$, and $\mathbf{G}_l = \mathbf{G}_{jkl}$. This scheme can be written in terms of the numerical fluxes as was done for the one dimensional case. Thus for each of the split flux terms, the forward and backward differences of the negative and positive flowing fluxes in their respective coordinate directions can be written as in equations (12.32) and (12.31).

Part 2

Thus, if the numerical fluxes for each of the flux vectors are denoted by \mathbf{h}_E , \mathbf{h}_F , and \mathbf{h}_G , the forward and backward flux differences become

$$\Delta E_j^- = \delta E_{j+1/2}^- = ((\mathbf{h}_E)_{j+1/2} - E(x_j)), \quad (13.23)$$

$$\nabla E_j^+ = \delta E_{j-1/2}^+ = -((\mathbf{h}_E)_{j-1/2} - E(x_j)), \quad (13.24)$$

$$\Delta F_k^- = \delta F_{k+1/2}^- = ((\mathbf{h}_F)_{k+1/2} - F(y_k)), \quad (13.25)$$

$$\nabla F_k^+ = \delta F_{k-1/2}^+ = -((\mathbf{h}_F)_{k-1/2} - F(y_k)), \quad (13.26)$$

$$\nabla G_l^+ = \delta G_{l-1/2}^+ = -((\mathbf{h}_G)_{l-1/2} - G(z_l)), \quad (13.27)$$

and

$$\nabla G_l^+ = \delta G_{l-1/2}^+ = -((\mathbf{h}_G)_{l-1/2} - G(z_l)). \quad (13.28)$$

With these definitions, the Warming and Beam predictor-corrector scheme given in equations (13.21) and (13.22) can be written in terms of the numerical fluxes \mathbf{h}_E , \mathbf{h}_F , and \mathbf{h}_G . The predictor becomes

$$\begin{aligned} u_{jkl}^{n+1} = & \frac{1}{2} (u_{jkl}^n + \overline{u_{jkl}^{n+1}}) - \frac{\rho_x}{2} ((\mathbf{h}_E)_{j+1/2}^{n+1} - (\mathbf{h}_E)_{j-1/2}^{n+1}) \\ & - \frac{\rho_y}{2} ((\mathbf{h}_F)_{k+1/2}^{n+1} - (\mathbf{h}_F)_{k-1/2}^{n+1}) \\ & - \frac{\rho_z}{2} ((\mathbf{h}_G)_{l+1/2}^{n+1} - (\mathbf{h}_G)_{l-1/2}^{n+1}) \end{aligned} \quad (13.29)$$

and the corrector is written in the form

Part 2

$$\begin{aligned}
\mathbf{u}_{jkl}^{n+1} = & \frac{1}{2} (\mathbf{u}_{jkl}^n + \mathbf{u}_{jkl}^{\overline{n+1}}) - \frac{\rho_x}{2} ((\mathbf{h}_E)_{j+1/2}^{\overline{n+1}} - (\mathbf{h}_E)_{j-1/2}^{\overline{n+1}}) \\
& - \frac{\rho_y}{2} ((\mathbf{h}_F)_{k+1/2}^{\overline{n+1}} - (\mathbf{h}_F)_{k-1/2}^{\overline{n+1}}) \\
& - \frac{\rho_z}{2} ((\mathbf{h}_G)_{l+1/2}^{\overline{n+1}} - (\mathbf{h}_G)_{l-1/2}^{\overline{n+1}}) \\
& - \frac{\rho_x}{2} (\delta_x(\mathbf{E}^+)_{j-1/2}^{\overline{n+1}} - \delta_x(\mathbf{E}^+)_{j-3/2}^{n+1}) \\
& + \frac{\rho_x}{2} (\delta_x(\mathbf{E}^-)_{j+3/2}^{\overline{n+1}} - \delta_x(\mathbf{E}^-)_{j+1/2}^{n+1}) \\
& - \frac{\rho_y}{2} (\delta_y(\mathbf{F}^+)_{k-1/2}^{\overline{n+1}} - \delta_y(\mathbf{F}^+)_{k-3/2}^{n+1}) \\
& + \frac{\rho_y}{2} (\delta_y(\mathbf{F}^-)_{k+3/2}^{\overline{n+1}} - \delta_y(\mathbf{F}^-)_{k+1/2}^{n+1}) \\
& - \frac{\rho_z}{2} (\delta_z(\mathbf{G}^+)_{l-1/2}^{\overline{n+1}} - \delta_z(\mathbf{G}^+)_{l-3/2}^{n+1}) \\
& + \frac{\rho_z}{2} (\delta_z(\mathbf{G}^-)_{l+3/2}^{\overline{n+1}} - \delta_z(\mathbf{G}^-)_{l+1/2}^{n+1}). \tag{13.30}
\end{aligned}$$

The Courant number for this scheme is $2/(\sqrt{3})$ and therefore the time step must be chosen such that

$$\rho \lambda_{\max} \leq \frac{2}{\sqrt{3}} \tag{13.31}$$

where λ_{\max} is the largest eigenvalue of all the Jacobian matrices A_E , A_F , and A_G . Also, it is assumed that $\rho = \rho_x = \rho_y = \rho_z$. Thus, this upwind scheme has a larger Courant number than any of the previous schemes presented, including the Rotated Richtmyer scheme. The two-dimensional scheme can be easily obtained from the above scheme. Note however that the two-dimensional scheme will have a Courant number of $\sqrt{2}$.

13.4 Numerical Fluxes for Maxwell's Equations

Before the upwind scheme of the previous section can be implemented for Maxwell's equations, the specific numerical fluxes in each coordinate direction must be determined (i.e. \mathbf{h}_E , \mathbf{h}_F , and \mathbf{h}_G). These can be determined in a straight forward manner by the same procedure used in section 12.4 on page 144. There, the numerical flux was determined for the x-coordinate direction. If the vector analysis presented therein is reproduced for any general coordinate direction with unit vector $\hat{\xi}$, then the numerical fluxes can be written as in equations (12.54) and (12.55) as

$$\begin{aligned} \hat{\xi} \times e_i \mathbf{D}^* \left(\frac{c_{i+1}}{e_{i+1}} + \frac{c_i}{e_i} \right) &= \hat{\xi} \times \{ [(c\mathbf{D})_{i+1} + \hat{\xi} \times (m\mathbf{B})_{i+1}] \\ &\quad + [(c\mathbf{D})_i - \hat{\xi} \times (m\mathbf{B})_i] \} \end{aligned} \quad (13.32)$$

and

$$\begin{aligned} \hat{\xi} \times m_i \mathbf{B}^* \left(\frac{e_{i+1}}{c_{i+1}} + \frac{e_i}{c_i} \right) &= \hat{\xi} \times \{ [(c\mathbf{B})_{i+1} - \hat{\xi} \times (e\mathbf{D})_{i+1}] \\ &\quad + [(c\mathbf{B})_i + \hat{\xi} \times (e\mathbf{D})_i] \} , \end{aligned} \quad (13.33)$$

where the indices i and i+1 represent any of the coordinate indices j, k or l, depending on whether $\hat{\xi}$ is \hat{x} , \hat{y} or \hat{z} respectively (see [Shankar 90]).

Part 2

Since the flux vectors for Maxwell's equations are defined by equations (11.6) to (11.8) the fluxes for rectangular coordinates can be written using equations (13.32) and (13.33) for the fluxes at the interface between two cells denoted by $i+1/2$ where i is either j , k or l . These are given as

$$-(eD_z)_{j+1/2} = \frac{(-(cD_z) + (mB_y))_{j+1} + (-(cD_z) + (mB_y))_j}{(c_j/e_j + c_{j+1}/e_{j+1})}, \quad (13.34)$$

$$(eD_y)_{j+1/2} = \frac{((cD_y) - (mB_z))_{j+1} + ((cD_y) + (mB_z))_j}{(c_j/e_j + c_{j+1}/e_{j+1})}, \quad (13.35)$$

$$(mB_z)_{j+1/2} = \frac{((cB_z) - (eD_y))_{j+1} + ((cB_z) + (eD_y))_j}{(c_j/m_j + c_{j+1}/m_{j+1})}, \quad (13.36)$$

$$-(mB_y)_{j+1/2} = \frac{(-(cB_y) - (eD_z))_{j+1} + (-(cB_y) + (eD_z))_j}{(c_j/m_j + c_{j+1}/m_{j+1})} \quad (13.37)$$

for the x-coordinate direction,

$$(eD_z)_{k+1/2} = \frac{((cD_z) - (mB_x))_{k+1} + ((cD_z) + (mB_x))_k}{(c_k/e_k + c_{k+1}/e_{k+1})}, \quad (13.38)$$

$$-(eD_x)_{k+1/2} = \frac{(-(cD_x) - (mB_z))_{k+1} + (-(cD_x) + (mB_z))_k}{(c_k/e_k + c_{k+1}/e_{k+1})}, \quad (13.39)$$

$$-(mB_z)_{k+1/2} = \frac{(-(cB_z) - (eD_x))_{k+1} + (-(cB_z) + (eD_x))_k}{(c_k/m_k + c_{k+1}/m_{k+1})}, \quad (13.40)$$

$$(mB_x)_{k+1/2} = \frac{((cB_x) - (eD_z))_{k+1} + ((cB_x) + (eD_z))_k}{(c_k/m_k + c_{k+1}/m_{k+1})} \quad (13.41)$$

for the y-coordinate direction, and

Part 2

$$-(eD_y)_{1+1/2} = \frac{(-(cD_y) - (mB_x))_{1+1} + (-(cD_y) + (mB_x))_1}{(c_1/e_1 + c_{1+1}/e_{1+1})}, \quad (13.42)$$

$$(eD_x)_{1+1/2} = \frac{((cD_x) - (mB_y))_{1+1} + ((cD_x) + (mB_y))_1}{(c_1/e_1 + c_{1+1}/e_{1+1})}, \quad (13.43)$$

$$(mB_y)_{1+1/2} = \frac{((cB_y) - (eD_x))_{1+1} + ((cB_y) + (eD_x))_1}{(c_1/m_1 + c_{1+1}/m_{1+1})}, \quad (13.44)$$

$$-(mB_x)_{1+1/2} = \frac{(-(cB_x) - (eD_y))_{1+1} + (-(cB_x) + (eD_y))_1}{(c_1/m_1 + c_{1+1}/m_{1+1})} \quad (13.45)$$

for the z-coordinate direction. Note the similarity between these numerical fluxes and those of equations (11.59) to (11.62). Thus this method of determining the numerical fluxes at the cell interfaces is equivalent to solving the *characteristic problem* in each of the coordinate directions independently. Recall though that when that method was used the Δx in each cell was set during the application of the method (for a given Δt). Here, no such specification has been made, although it will be seen that this method will loose accuracy when applied well below the Courant limit.

Chapter 14

Finite Difference

Practical Implementation and Results

The finite difference schemes presented in the previous chapter for Maxwell's equations in two-dimensional space are implemented on a Sun Microsystems' SPARCstation 1™. In order to achieve the greatest utility from the program, special attention was given to the practical aspects of the implementation. That is, *computational speed* and *memory requirements*. The main difficulty lies not with the speed of the computations, since all the schemes discussed are explicit schemes, but rather with the storage space required for the schemes.

14.1 Memory Requirements

In three-dimensional space, the memory requirements for a practical sized problem can be formidable. For example, the total memory requirement in bytes, B_T , for a finite difference program can be estimated as

$$B_T = N_x \times N_y \times N_z \times B_{node} = N_T \times B_{node} \quad (14.1)$$

where N_x , N_y , and N_z are the number of mesh points in the x , y , and z directions respectively (assuming a rectangular lattice), and B_{node} is the number of bytes of storage

Part 2

space required at each node in the lattice. If a scheme is used where all six components of \mathbf{D} and \mathbf{B} are stored at every node, then

$$B_{\text{node}} \geq 6 \times B_{\text{component}} \quad (14.2)$$

where $B_{\text{component}}$ is the number of bytes required for each component of the solution vector. If *double precision* is used then $B_{\text{component}} = 8$ (for the SPARCstation 1). As well as these, the conductivity, permittivity, and permeability associated with each nodal cell may have to be stored, especially for heterogeneous structures. Thus, the number of bytes per node become

$$B_{\text{node}} \geq 6 \times B_{\text{component}} + 3 \times B_{\text{material}} \quad (14.3)$$

where B_{material} corresponds to the bytes required to store the material constants. If *single precision* is used for these, then $B_{\text{material}} = 4$ (again for the SPARCstation 1) and B_{node} is at least equal to 60. That is, 60 bytes of storage space for each node in the lattice. For a lattice with $N_x = N_y = N_z = 100$, the total storage requirement for the problem, given by equation (14.1), is 60 MBytes. This does not include *overhead* storage which will be required, such as for the storage of the program itself and other intermediate variables used in the calculation. A lattice of this size is not, by any means, large enough to accurately represent a practical electromagnetic interaction problem such as the coupling of energy to a communication system. On the other hand the 60 MBytes of memory required for this problem is well beyond the capabilities of most engineering workstations (for example the colour SPARCstation 1 has a maximum of 16 MBytes of memory available).

Actually, the above memory requirements assume brute force implementation of the schemes. Using state of the art programming techniques, these requirements can be modestly reduced, but not to the extent required to solve electromagnetic interaction problems in complex systems. Thus, these schemes are currently feasible only for the study of specific interaction mechanisms such as coupling through shields and onto cables, or

Part 2

possibly, with the use of a super-computer, for such problems as the penetration of electromagnetic energy into biological tissues (see Taflove [Taflove 88]).

14.2 Practical Implementation: Dynamic Memory Allocation

In order to take advantage of advanced programming techniques, the C language is used in the implementation of the finite difference schemes. This allows the dynamic allocation of storage space to the lattice nodes only when it is required. During the solution of a typical electromagnetic interaction problem it is often the case that many of the nodes at a certain time step do not contain a disturbance. This is especially true when the excitation is in the form of a sharp time domain pulse. For example, in the propagation of an electromagnetic pulse through a shield, the disturbance is localized in space at early interaction times and only starts to spread spatially as the interaction progresses.

This spatial localization of the disturbance can be taken advantage of when a scheme is implemented by allocating memory to a lattice node only if it contains a disturbance at the current time step or has the possibility of containing a disturbance at the next time step. In the same way, memory is *unallocated* or removed from a lattice node when the node does not contain a disturbance at the current time step and does not have the possibility of containing a disturbance at the next time step. This allocating and unallocating of memory has the effect of *propagating* the memory storage for the nodes through the lattice with the disturbance.

This process is implemented by first only allocating memory to an array of *pointers* to the data structures which hold the information for each lattice node. Thus, if 10000 nodes make up a 100X100 finite difference lattice, then a 100X100 array of pointers to the nodal data structure is allocated, requiring a total of 4 KBytes of memory (a pointer requires 4 bytes of memory). The nodal data structure consists of the data types required to represent the solution vector at each node and to keep the material constants for the node's cell. For the three-dimensional Maxwell's equations each data structure consists of six double

Part 2

precision variables. Since the material inhomogeneities are usually constant with time, it is best to define a separate data structure for the three single precision variables required to hold the material constants for the lattice. These data structures are illustrated in Figure 71.

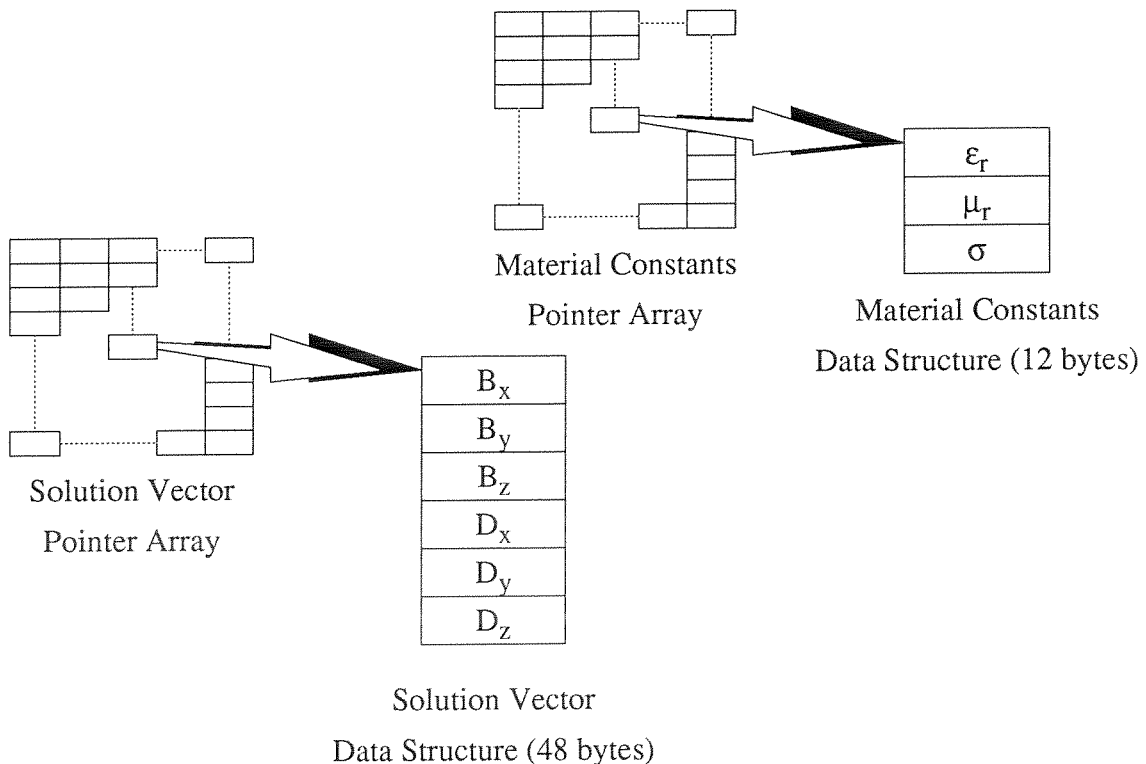


Figure 71 Example of solution vector and material constants data structures

The next step is to input the initial conditions into the lattice as well as the required material constants. This consists of allocating the data structure memory for each node required by the initial conditions to have a non-zero disturbance at time zero. The actual value of the disturbance is then stored in the appropriate data location for a given solution vector component. If a cell contains material constants which are not that of free space, then that cell's material constant data structure memory is allocated and the specific material constants for that cell are stored. In this way, only cells with non-free space material constants have their material constant data structure memory allocated.

Part 2

Once the initial conditions are input, the finite difference algorithm is applied to find the disturbance at the next time step. This consists of performing three steps:

- 1) allocate nodes which are neighbors to a non-zero node,**
- 2) execute the finite difference algorithm, and**
- 3) unallocate nodes which are zero and have all neighbors as zero.**

In this context, the term neighbor is dependent on the domain of dependence (or the spatial bandwidth) of the finite difference scheme. For example, in the leap-frog and Lax-Wendroff schemes, a disturbance at one node can propagate only to the nearest neighbors of that node in each spatial direction. On the other hand, in the upwind scheme, a disturbance at one node can propagate to its *two* nearest neighbors in each spatial direction.

The above procedure helps in the problem of large memory requirements. In order to save on the time required to compute the disturbance at each time step, an obvious technique is to not perform the finite difference algorithm at unallocated nodes. If the solution vector data structure of a node is unallocated then it has already been determined a priori that a disturbance cannot propagate to this node at the next time step, thus it is justified to skip the calculation altogether.

In order that every node in the lattice does not have to be checked as to whether it is *in* (i.e. allocated) or *out* (i.e. unallocated) before a calculation is performed, all the nodes which are *in* are kept in a *linked list* (see Horspool [Horspool 86]). The finite difference algorithm is then only performed on the nodes in the linked list. For example, at time zero only the nodes with given initial conditions along with their neighbors are in the linked list. In this way the calculations at each time step are performed quicker when there are only a few nodes *in* the lattice. This is usually the case at the beginning of a problem when the disturbance is fairly localized. Every time a discontinuity is met in the lattice the disturbance is *spread* spatially and more nodes will be *in*, having the effect of slowing the computation time for each time step.

Part 2

14.3 Results for Two-Dimensional TM Fields

The finite difference schemes given in *Chapter 13* are applied to Maxwell's equations for the case of two-dimensional TM fields. Specifically, the leap-frog scheme (Yee algorithm) given by equations (13.6) and (13.7), the Lax-Wendroff scheme (Rotated Richtmyer) given by equation (13.17), and the split flux-vector/upwind scheme (Shankar-Osher) given by equations (13.29) and (13.30) are used to determine the electromagnetic fields for two test cases. These are:

- 1) the fields propagated from a line source with imposed D_z field, and
- 2) these same fields as they propagate through a perfectly conducting shield with a thick gap in the middle.

In both these cases the line source is excited with a Gaussian pulse given by

$$D_z(t) \Big|_{\substack{x, y \\ \text{on line}}} = 1.0e^{(\log(a)(t-t_0)^2)/b}, \quad (14.4)$$

where the parameters are given as: $a = 0.1$, $t_0 = 10^{-8}$, and $b = 10^{-17}$. The time domain waveform corresponding to this function is given in Figure 72.

The purpose of the first test case is to compare the propagation of the fields through the two-dimensional lattice with no obstructions. This first case is also used to test the *absorbing boundary conditions* which were used to truncate the numerical lattice. That is, since all the schemes have computational molecule which is centered spatially, a special technique is required at the boundary of the numerical lattice to ensure that the fields are not reflected back into the lattice.

Much work has been done on these absorbing boundary conditions in recent years (see for example Fang [Fang 88], and Taflove [Taflove 90]). These higher order methods

Part 2

are not used here since the main purpose is to compare the finite difference schemes themselves.

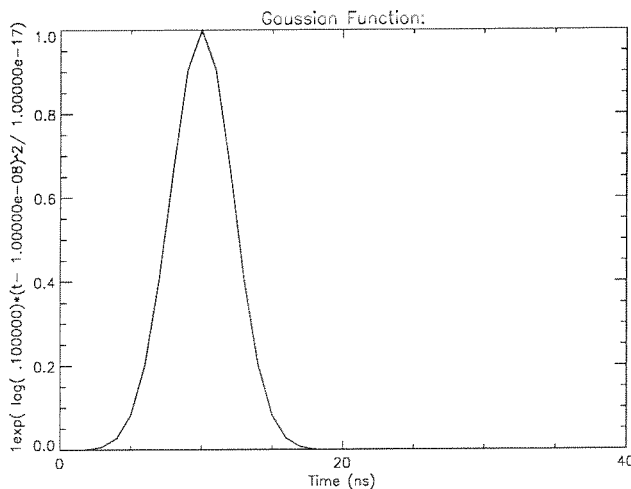


Figure 72 Time domain Gaussian pulse

For the leap-frog method it is assumed that at the outer boundary of the lattice the field components are propagated unattenuated to an artificial grid point outside the lattice boundary. For example, the D_z field component at the artificial point (x_{Nx+1}, y_k) outside the lattice boundary point (x_{Nx}, y_k) is assumed to take on the components of D_z at (x_{Nx}, y_k) for the previous time step. Thus, for a boundary point (x_{Nx}, y_k) , at the right side of the lattice equations (13.6) and (13.7) become

$$\mathbf{D}_{N_x k}^{n+1} = \mathbf{D}_{N_x k}^n + \frac{\Delta t}{2} (\mathbf{s}_{N_x k}^{n+1} + \mathbf{s}_{N_x k}^n) - \rho_y (\mathbf{F}_k^n - \mathbf{F}_{k-1}^n), \quad (14.5)$$

and

$$\mathbf{B}_{N_x k}^{n+1} = \mathbf{B}_{N_x k}^n + \frac{\Delta t}{2} (\mathbf{s}_{N_x k}^{n+1} + \mathbf{s}_{N_x k}^n) - \rho_y (\mathbf{F}_{k+1}^n - \mathbf{F}_k^n). \quad (14.6)$$

Results for the first test case using the leap-frog method and the above boundary conditions are given in Figure 73. Notice that small reflections from the numerical boundary still occur, but are tolerable for the current application.

Part 2

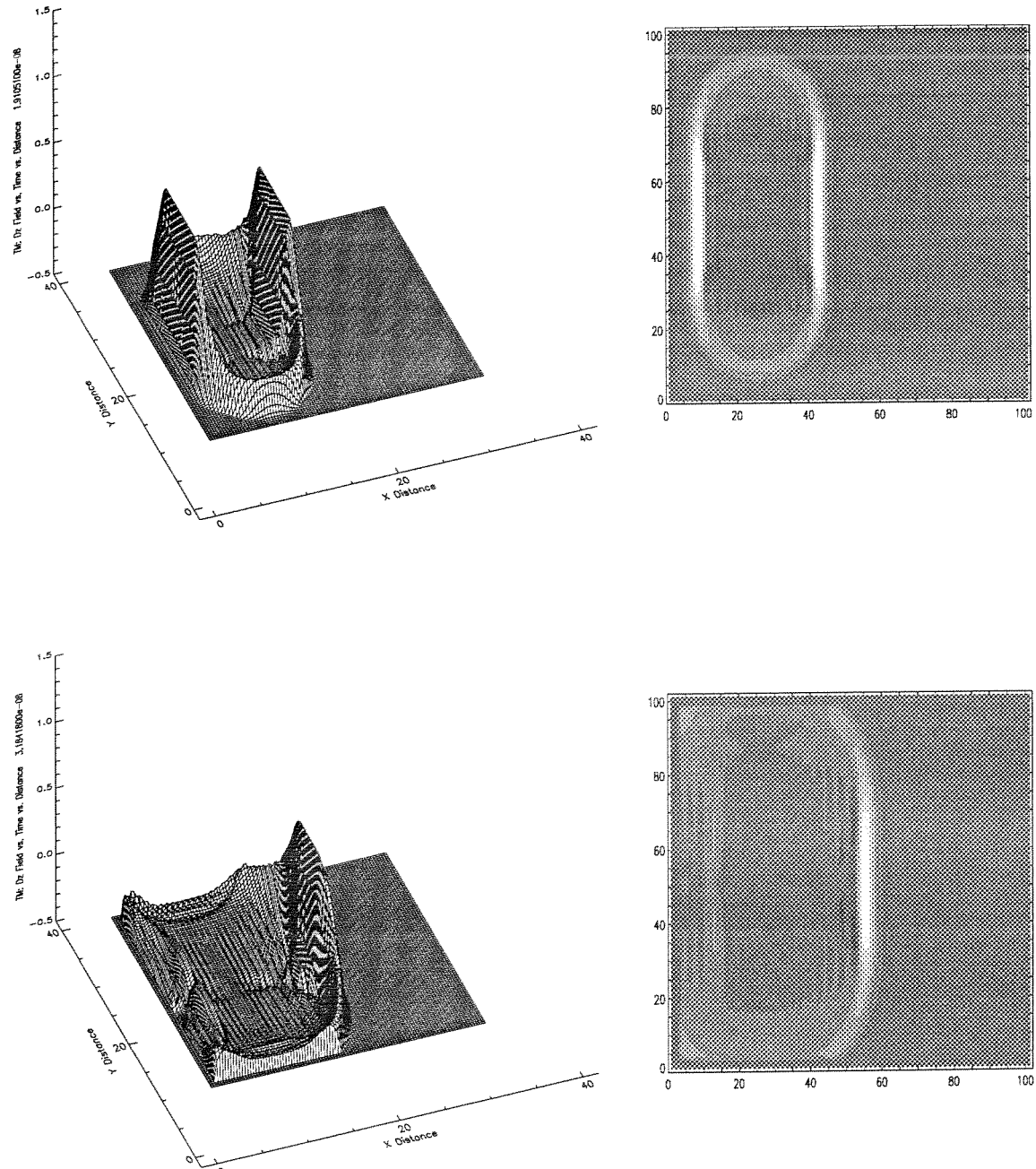


Figure 73 Leap-frog solution (D_z) for a Gaussian **D** line source

Part 2

The absorbing boundary conditions for the other two schemes, that is the Lax-Wendroff and the split flux-vector upwind schemes are handled quite differently. Recall that these schemes are predictor corrector type schemes based on the flux at the interface between two neighboring cells.

In the Lax-Wendroff two-step scheme (using the Rotated Richtmyer method) the flux is approximated by the predictor step given in equation (13.17). It is natural in this scheme to assume that at a boundary point the contribution to this flux from outside the boundary is zero. Thus at the node (x_{N_x}, y_k) , on the right side of the lattice boundary the predictor for this scheme becomes

$$u_{N_x k}^{n*} = (\mu_x \mu_y) u_{N_x k}^n - \frac{[\rho_x \mu_y \delta_x E_{N_x k}^n + \rho_y \mu_x \delta_y F_{N_x k}^n]}{2}, \quad (14.7)$$

where $E_{N_x+1/2, k} = 0$.

A similar procedure is performed for the split flux-vector upwind scheme of equations (13.29) and (13.30). In this case, the numerical flux is calculated with any components outside the lattice set equal to zero. Thus, the flux at the outside cell boundary $(x_{N_x+1/2}, y_k)$ may be calculated for example from equation (13.34) as

$$-(e D_z)_{N_x + 1/2} = \frac{(- (c D_z) + (m B_y))_{N_x}}{(c/e)_{N_x} + (c/e)_{N_x}}. \quad (14.8)$$

This procedure can be justified by the method of characteristics and implies that no disturbance propagates on the inward characteristic line from outside the lattice.

Results for the Lax-Wendroff and split flux-vector upwind (Shankar-Osher) schemes are given in Figure 74 and Figure 75 respectively. As can be seen from these results, the absorbing boundary conditions given above perform very well (with the exception of small reflections from the corners of the lattice).

Part 2

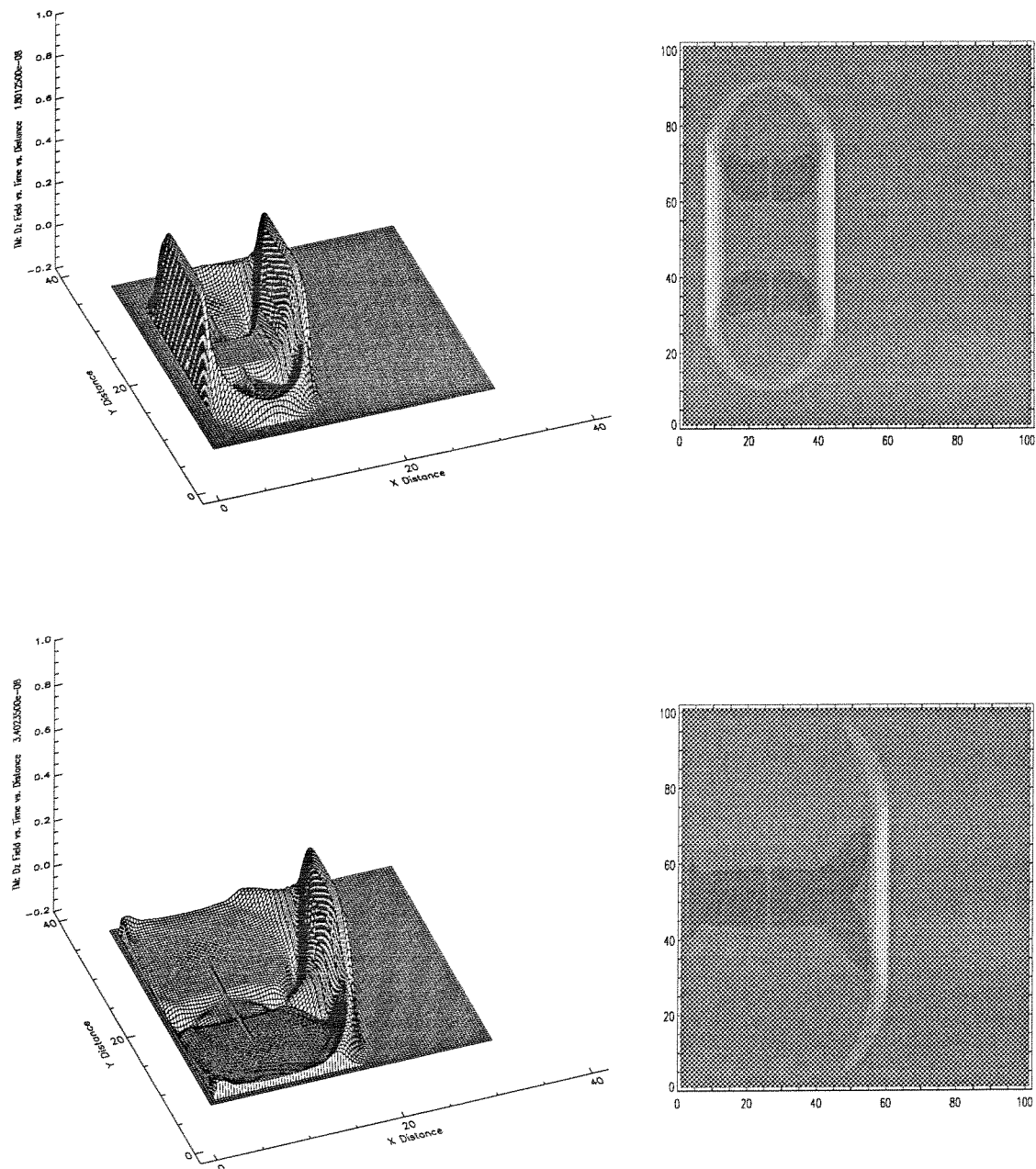


Figure 74 Lax-Wendroff solution (D_z) for a Gaussian \mathbf{D} line source

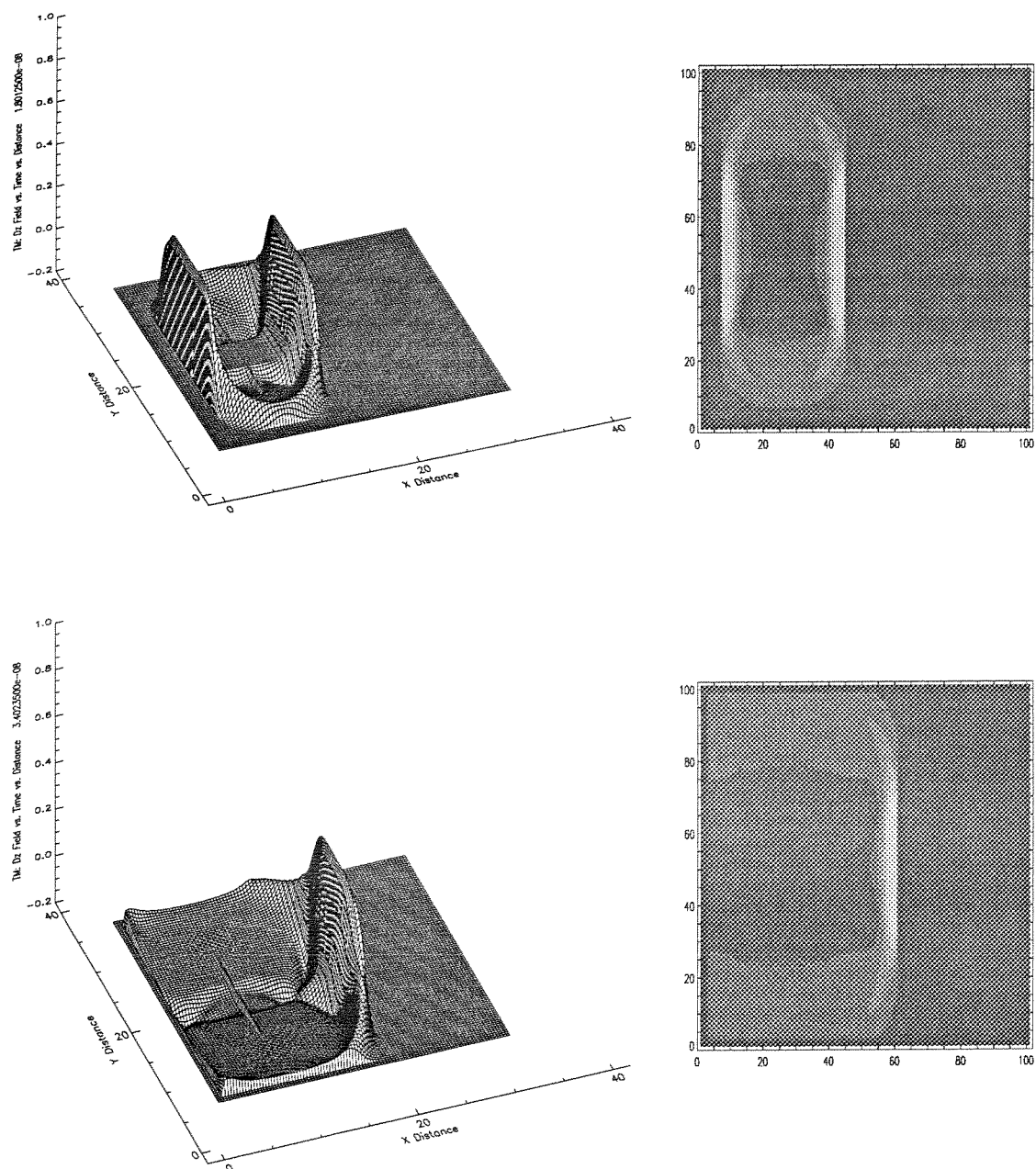
Part 2

Figure 75 Shankar-Osher solution (D_z) for a Gaussian \mathbf{D} line source

Part 2

The next test case is that of the same Gaussian line source but now a thick shield with a gap is located in the lattice. This requires that the algorithms for each finite difference scheme be capable of handling perfectly conducting boundaries. The specific geometry of the shield along with the location of the line source is shown in Figure 76. The line source and shield are placed closer to the center of the lattice for the leap-frog scheme in order to sustain a longer *clear time* before reflections arrive from the outer boundary.

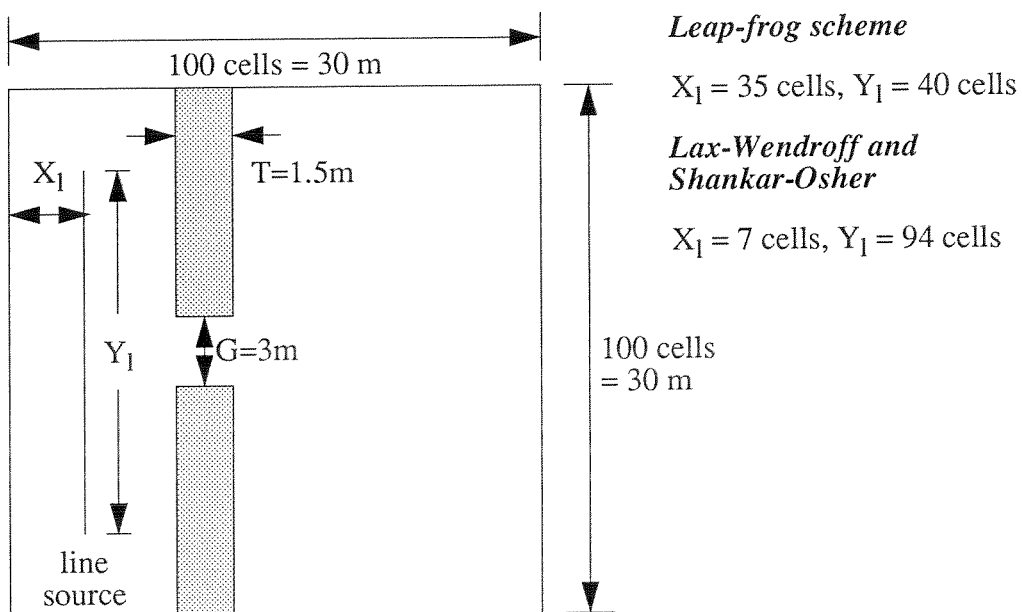


Figure 76 Test case 2: perfectly conducting thick shield with gap

This is achieved very simply for the leap-frog scheme (see Yee [Yee 66]) since only one component of the solution vector is located at a specific point in space. For the TM case, the appropriate boundary condition is that the tangential electric field, D_z , be zero at the surface of a perfect conductor. This is implemented easily by skipping the calculation of D_z at node points which have been defined to have infinite conductivity. Note that, due to the staggered and interlaced lattice used in the Yee algorithm, some ambiguity in the exact location of the conducting boundary results. Results are shown in Figure 77.

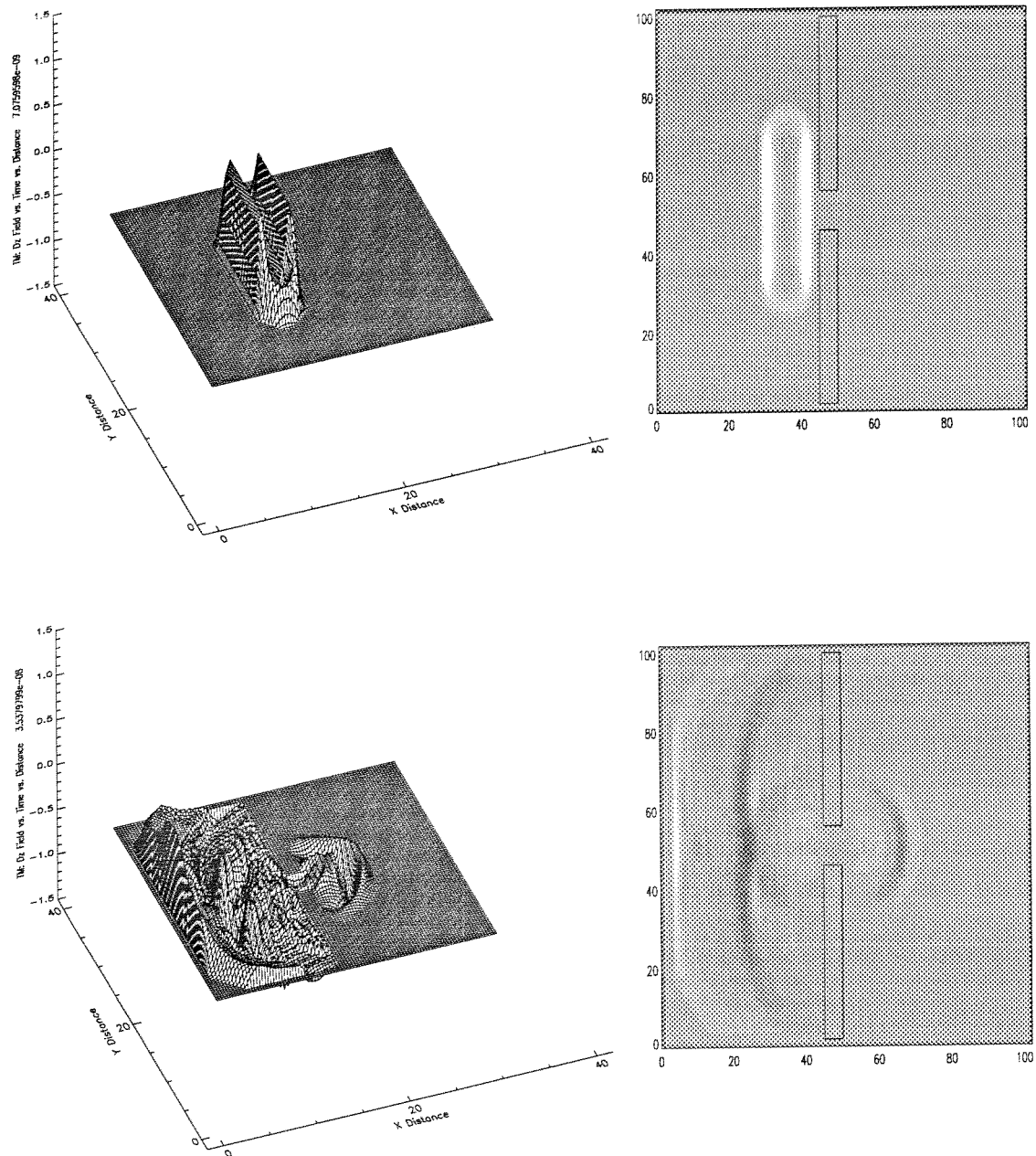
Part 2

Figure 77 Leap-frog solution (D_z) for TM shielding of Gaussian pulse

Part 2

The imposition of the appropriate boundary conditions at a perfectly conducting boundary is not as straight forward for the Lax-Wendroff and the split flux-vector upwind schemes as it is for the Yee algorithm. This is because all the solution vector components exist at each node point in the lattice.

For the Lax-Wendroff scheme, both solutions calculated by the predictor and the corrector use flux functions which return zero for the D_z field in a conducting medium. As well as this, the corrector makes sure that the D_z field is set to zero in a conducting medium. Thus, referring to Figure 78, if the perfectly conducting medium exists to the right of the point x_{j+1} then $(D_z)_{j+1} = 0$, but B_{j+1} is calculated normally, from the intermediate values at $t^{n+1/2}$ calculated by the predictor.

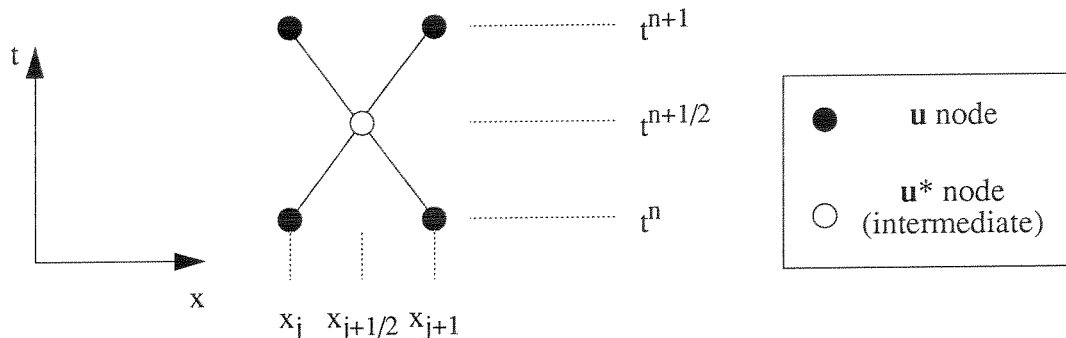


Figure 78 Perfect conducting boundary condition for Lax-Wendroff

For the Shankar-Osher scheme, the numerical fluxes must be determined in such a way that the total tangential electric field at a conducting boundary is equal to zero. Thus, equations (13.34) and (13.38) are set to zero, and the tangential \mathbf{H} field (H_y) is calculated by setting the fluxes as well as the speed of propagation in the conductor to zero in equation (13.37), that is

$$-(mB_y)_{j+1/2} = (- (mB_y) + (cD_z))_j \quad (14.9)$$

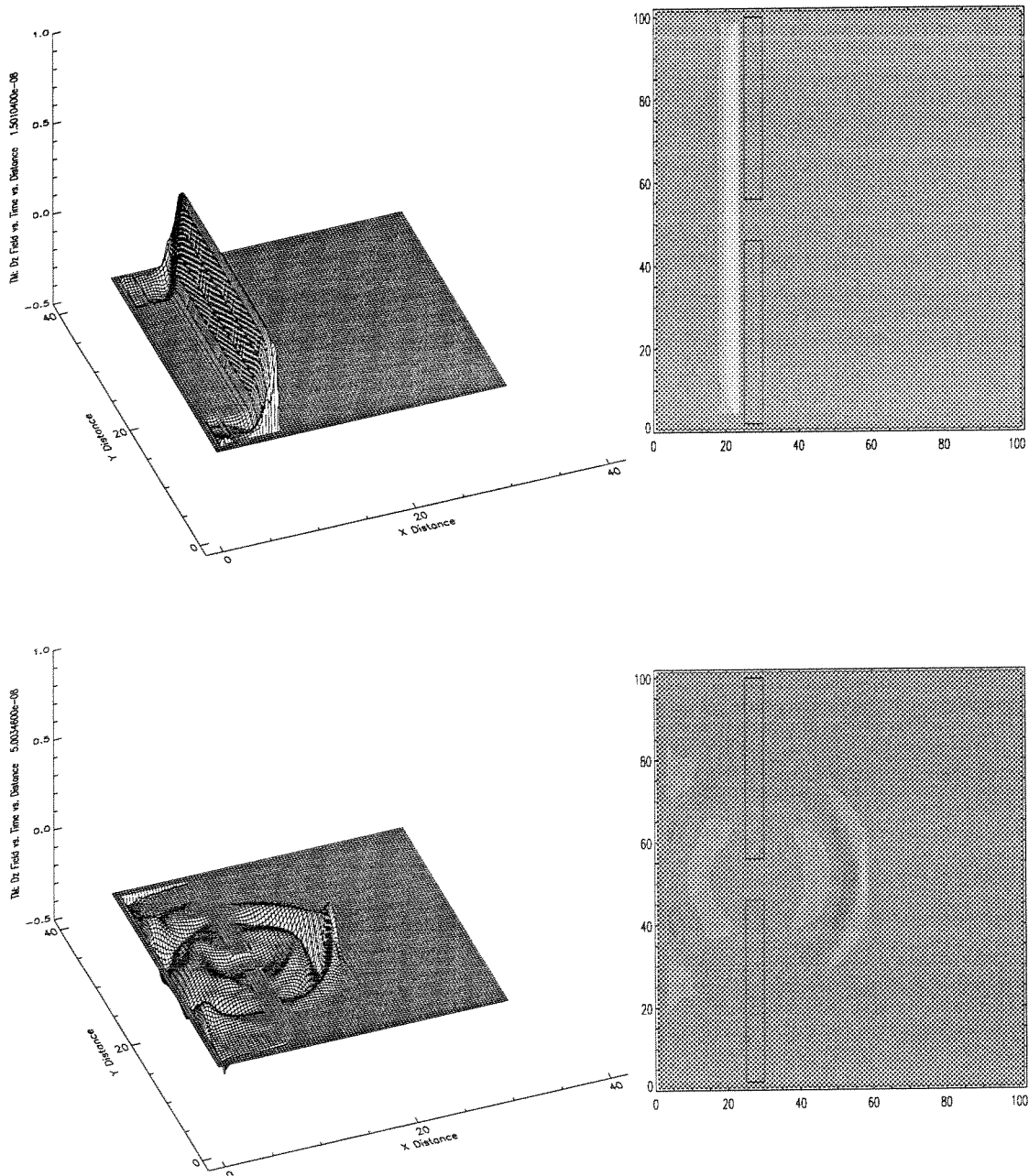
Part 2

Figure 79 Lax-Wendroff solution (D_z) for TM shielding of Gaussian pulse

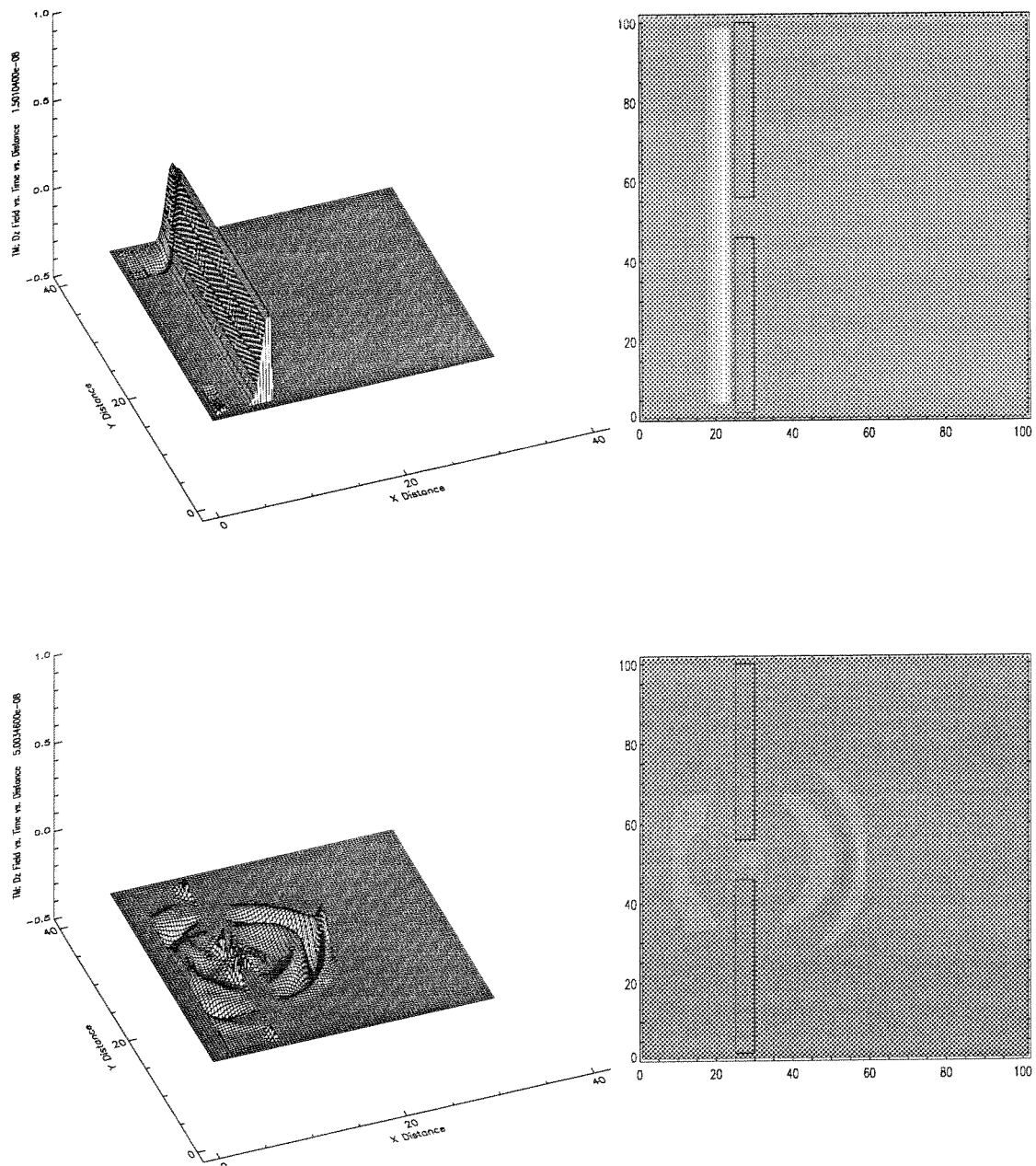
Part 2

Figure 80 Shankar-Osher solution (D_z) for TM shielding of Gaussian pulse

Part 2

A similar procedure is used for a perfectly conducting boundary in the y-coordinate direction. Note that for this scheme, the conducting boundary is assumed to be located at a half grid point (i.e. $x_{j+1/2}$). Results of test case two, for the Lax-Wendroff and the Shankar-Osher are given in Figure 79 and Figure 80 respectively. As can be seen from these figures, a *wake* forms behind the pulse which penetrates the shield.

In general, the leap-frog scheme is the simplest to understand and implement. It also requires the least amount of storage space since it is based on an interlaced mesh. The Lax-Wendroff scheme requires twice the storage space as the leap-frog scheme since an intermediate solution must be stored for the whole solution vector at time $t^{n+1/2}$. It should be noted, though, that a solution for the total solution vector is achieved and there exists no ambiguity to the location of material boundaries.

Finally, the split flux-vector upwind scheme (Shankar-Osher) is the most difficult to understand and implement. It also requires three times the storage space of the leap-frog scheme and is slightly slower. The main advantage of this scheme is in the *proper* handling of the fluxes at cell boundaries. For the linear problems considered herein, this scheme may not be the most practical to use. For, problems with a high degree of inhomogeneities or for non-linear problems, this scheme has definite advantages.

14.4 Three Dimensional Schemes

A program for the three dimensional Maxwell's equations has been written. The advantage of the finite difference schemes presented herein is that, except for practical implementation issues, generalization to higher dimensions is simple. Due to the relatively small amount of memory available on the SPARCstation 1, only problems with a maximum mesh size of 40X40X40 are feasible. Thus, no problems of practical interest could be solved.

Chapter 15

Finite Elements for 2-D Shield Problems

The finite element method is a general mathematical procedure which enables one to obtain approximate solutions to differential equations. The method can be derived via the *Method of Weighted Residuals* (see Lapidus [Lapidus 82]). Details of this procedure and its implementation will not be given here since the software package PDE/PROTRAN (see [IMSL 86], [Sewell 85]) is used.

15.1 Formulation of 2-D Shielding Problems

Two dimensional time-domain shielding problems are formulated for specific problems of the type shown in Figure 81. An incident plane wave enters from the right hand side of the figure and the shield is assumed to be perfectly conducting (i.e. $\sigma = \infty$) (see LoVetri [LoVetri 90]).

If the *magnetic vector potential* \mathbf{A} is defined by (see Jackson [Jackson 75], and Eyges [Eyges 80])

$$\mathbf{B} = \mu \mathbf{H} = \nabla \times \mathbf{A}, \quad (15.1)$$

then the electric field is given as

$$\mathbf{E} = -\left(\frac{\partial \mathbf{A}}{\partial t} + \nabla \phi\right). \quad (15.2)$$

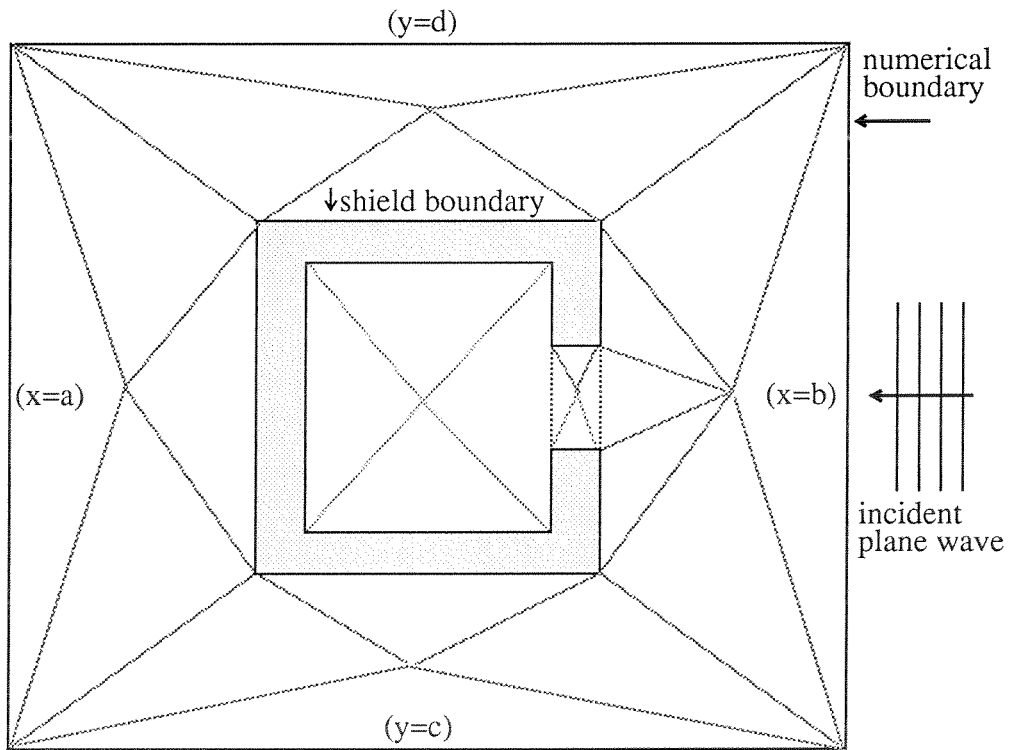
Part 2

Figure 81 Initial Triangulation of 2-D Shielding Problem

The potential \mathbf{A} will be a solution of the inhomogeneous wave equation. In a sourceless region, \mathbf{A} will be a solution of the homogeneous wave equation. If it is further assumed that $\mathbf{A} = A_z \hat{z}$ then the scalar wave equation arises

$$\nabla^2 A_z - \mu \epsilon \frac{\partial^2 A_z}{\partial t^2} = 0. \quad (15.3)$$

With this assumption, the only existing fields are E_z , B_x , and B_y (i.e. TM fields) which can be obtained in terms of the potential A_z as

$$E_z = -\frac{\partial A_z}{\partial t}, B_x = \frac{\partial A_z}{\partial y}, \text{ and } B_y = -\frac{\partial A_z}{\partial x}. \quad (15.4)$$

Part 2

Initial and boundary conditions can be derived for the problem. If it is assumed that no fields exist at time $t = 0$ then this implies

$$A_z(x, y, t=0) = 0. \quad (15.5)$$

If the incident plane wave consists of the two components E_z , and B_y then the boundary condition on the right side of the numerical mesh ($x=b$) can be written as a inhomogeneous Neumann boundary condition

$$B_y(b, y, t) = -\frac{\partial A_z}{\partial x}, c \leq y \leq d, t \geq 0 \quad (15.6)$$

The boundary conditions around the rest of the numerical mesh are approximated by homogeneous Neumann boundary conditions. This is valid as long as the time of the calculation does not proceed long enough for reflections from the shield to appear at these boundaries. At the shield boundaries the electric field E_z must be equal to zero. Thus this implies a Dirichlet boundary condition for A_z on the shield boundaries.

15.2 Program Validation and Numerical Results

The IMSL software package PDE/PROTRAN for solving general two space dimensional time domain partial differential equations is used. This software is implemented on an IBM3090 main frame computer. It is capable of solving systems of up to nine partial differential equations in three independent variables. The systems are cast in the general form

$$C\mathbf{u}_t^j = A_x^j + B_y^j + F^j, j = 1 \dots 9., \quad (15.7)$$

where

$$C = C(x, y, t, \mathbf{u}), \quad (15.8)$$

Part 2

$$A = A(x, y, t, u, u_x, u_y), \quad (15.9)$$

$$B = B(x, y, t, u, u_x, u_y), \quad (15.10)$$

and

$$F = F(x, y, t, u, u_x, u_y). \quad (15.11)$$

Thus, for the case where the vector functions A , B , and F are not dependent on u_x and u_y , the above system is in the form of the general conservation law equations.

The above system is solved over a domain R with boundary δR . On the boundary, specific boundary conditions of the form

$$u = f_b(x, y, t), \text{ on } \delta R_1, \quad (15.12)$$

and

$$A \cdot n_x + B \cdot n_y = g_b(x, y, t, u), \text{ on } \delta R_2, \quad (15.13)$$

where n_x and n_y are the unit outward normals to the boundary δR_2 and $\delta R = \delta R_1 + \delta R_2$.

In order, to provide some sort of validation for the program, it is first run for the one-dimensional Maxwell's equations in the form of equation (11.24). That is

$$\frac{\partial}{\partial t}(\epsilon E_y) - \frac{\partial}{\partial z}(H_x) = 0, \quad (15.14)$$

$$\frac{\partial}{\partial t}(\mu H_x) - \frac{\partial}{\partial z}(E_y) = 0, \quad (15.15)$$

with boundary conditions given by

$$E_y(-2, t) = E_y(2, t) = 0, \quad (15.16)$$

and initial condition

Part 2

$$E_y(z, 0) = e^{(\log(0.0001) \times z^2)}, \quad (15.17)$$

that is, a Gaussian distribution in space is assumed for the initial electric field.

The program allows two methods of time integration which are the Backward Euler Implicit scheme ($O(\Delta t)$), and the Cranknicolson Implicit scheme ($O(\Delta t^2)$). Although the Cranknicolson Implicit scheme is more accurate than the Backward Euler Implicit scheme it is found that, for hyperbolic type equations, the Euler method is more stable.

Although this test problem is a one-dimensional problem, it is solved by PDE/PROTRAN by setting B of equation (15.10) to zero and using only two layers of triangles in the y-coordinate direction. Results of the computation are compared with that produced by the exact difference solution given by equations (11.46) and (11.47) and are given in Figure 82 and Figure 83 for the E field and the H field respectively. As can be seen from this figure, the PDE/PROTRAN solution is very accurate but many triangles are required to obtain this accuracy. For these results, 320 second order triangles were used, and a time step of $\Delta t = 0.2 \times 10^{-10}$ was required.

For the two dimensional shield a double exponential excitation is used as the time domain waveform for the incident plane wave, that is

$$\left. -\frac{\partial A}{\partial x} \right|_{x=b} = e^{-\frac{t}{t_f}} - e^{-\frac{t}{t_r}}. \quad (15.18)$$

A rise time of $t_r = 0.5$ ns, and a fall time of $t_f = 1.0$ ns, is used to represent the field of an NEMP wave (nuclear electromagnetic pulse). Vector plots of the **B** field are shown in Figure 84. The dimensions of the shield can be seen in the contour plots of the figure where the units are meters. The aperture length is 0.5 meters, the shield thickness is 0.15 meters, and the outside cross-section of the shield is 0.8 meters square.

Part 2

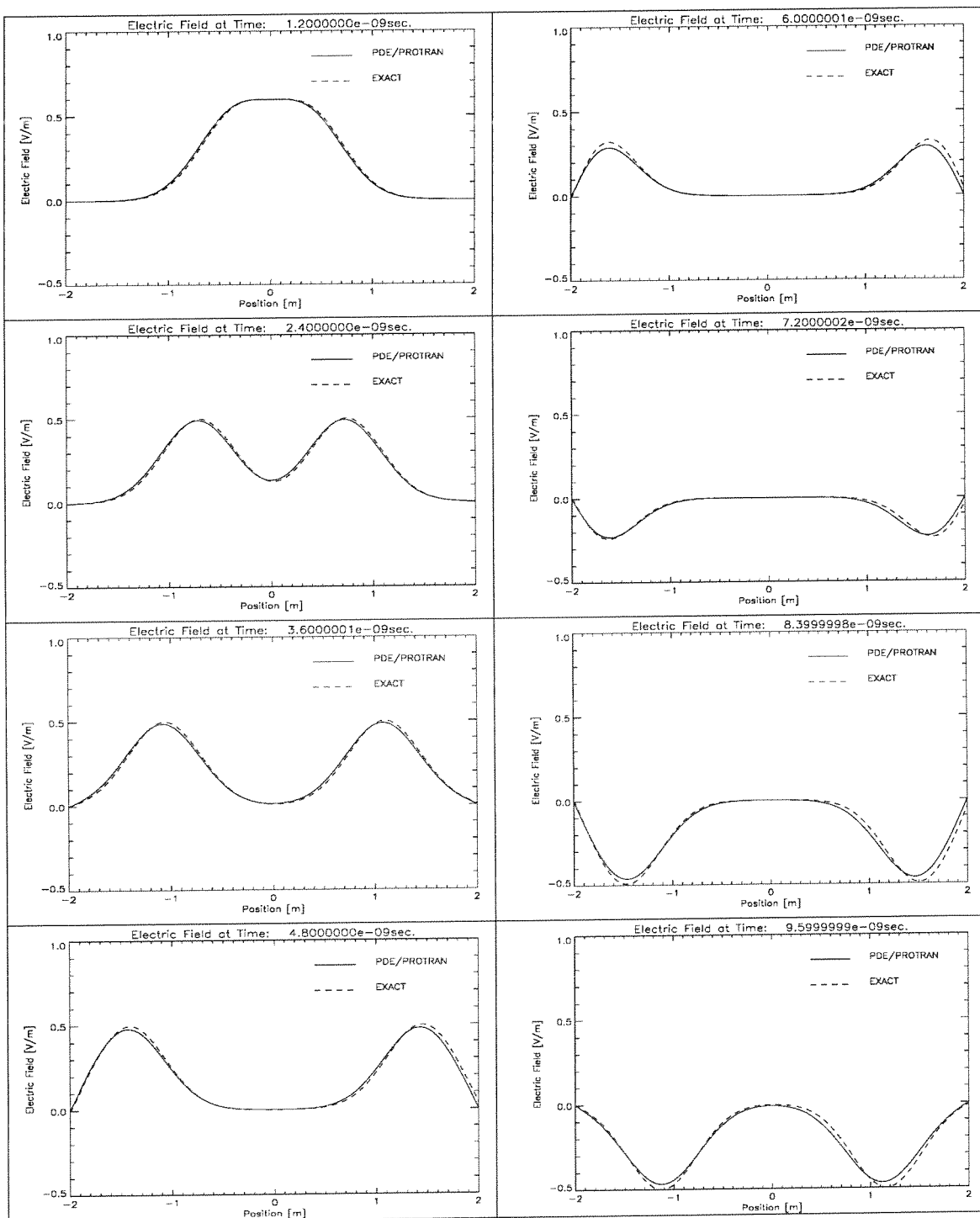


Figure 82 One-dimensional test problem for PDE/PROTRAN (E field)

Part 2

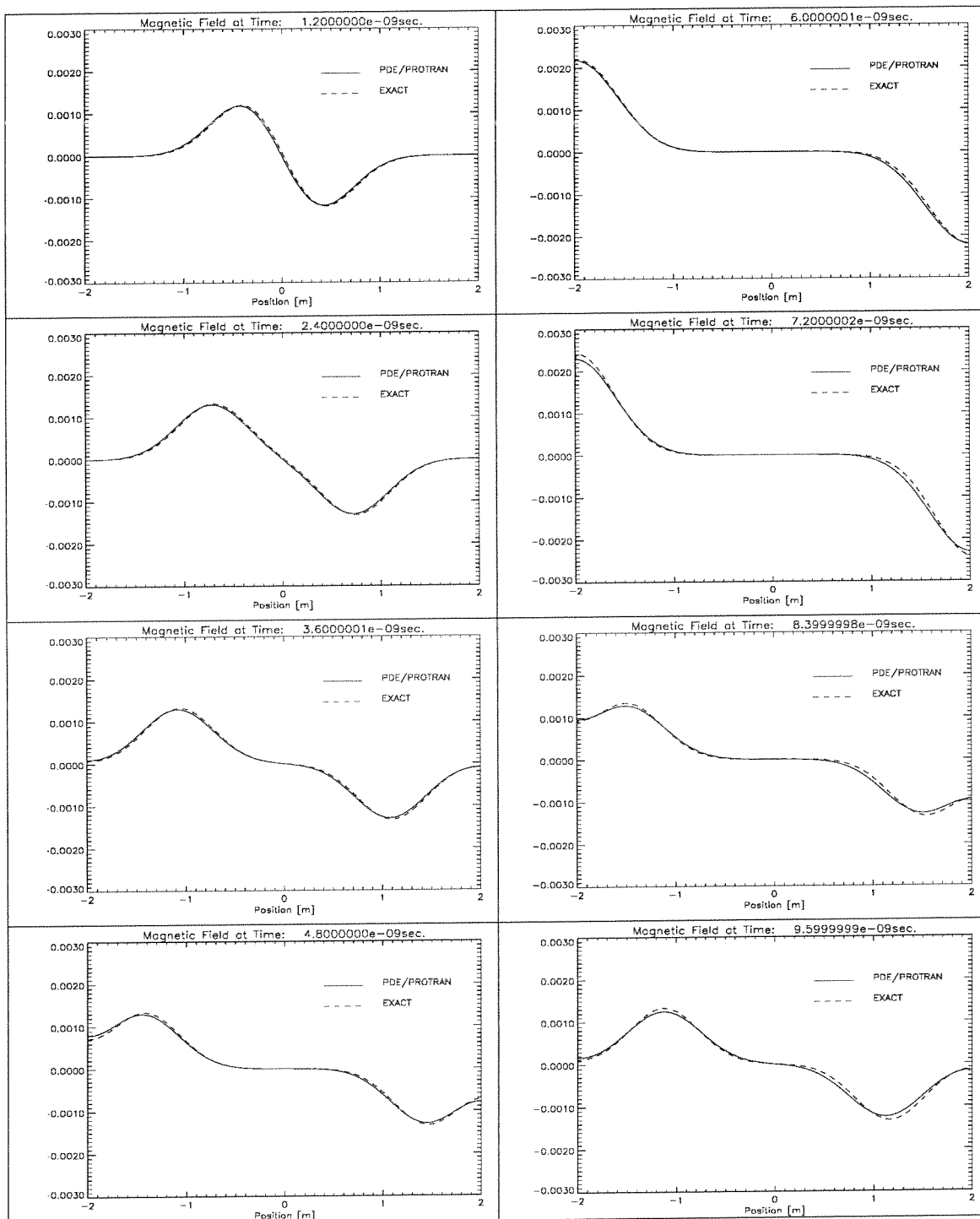


Figure 83 One-dimensional test problem for PDE/PROTRAN (H field)

Part 2

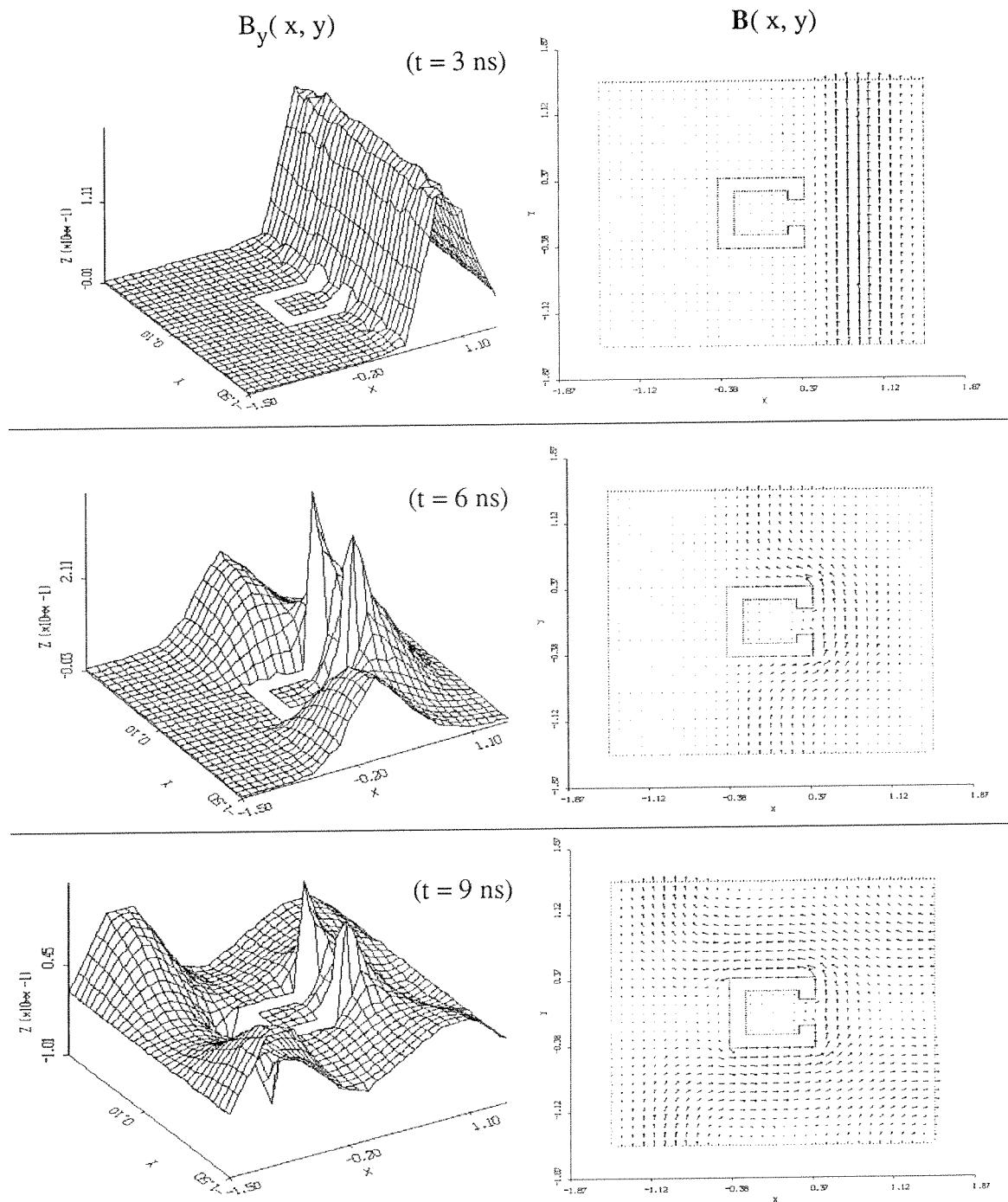


Figure 84 Two-dimensional shield problem (\mathbf{B} field)

Chapter 16

Conclusions and Future Work for Numerical Techniques

Some numerical techniques for solving Maxwell's equations have been discussed and implemented. It has been shown how there exist many ways to difference these equations (one of the simplest being the Yee algorithm). New techniques, based on the formulation of Maxwell's equations as a system of hyperbolic conservation laws have been studied, compared, and implemented. For simple problems, the simplest technique should be used since these usually use less computer resources. For the modelling of more advanced interaction phenomena, the more complex numerical techniques such as the split flux-vector upwind schemes are required.

It has been shown how advanced programming techniques can be used to efficiently implement finite difference schemes. These techniques take advantage of dynamic memory allocation to optimize the use of memory during calculations.

The numerical techniques presented in the previous seven chapters are only a small sample of the available methods for the solution of electromagnetic interaction problems. The finite difference method, however, is one of the most powerful methods for the solution of hyperbolic systems of equations. On the other hand, the finite element method, which was briefly discussed in the last chapter, is more adapted to elliptic and parabolic type

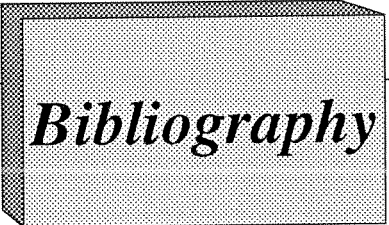
Part 2

partial differential equations (see Lapidus [Lapidus 82]). The finite element method's advantage, of a variable mesh size, is eliminated when solving hyperbolic systems since discontinuous solutions may propagate throughout the mesh, and these discontinuities require a high resolution grid in order to be resolved.

When a non-linear medium is present, initially smooth solutions may become discontinuous and *high resolution* finite difference schemes are required to resolve these sharp discontinuities. A similar situation occurs when the initial conditions contain a discontinuity, since this is propagated throughout the physical domain. Thus, advancements in the field of numerical techniques for the solution of these equations are required. Some *high resolution* finite difference schemes, called ENO schemes (for essentially non-oscillatory) due to Shu and Osher [Shu 88, 89], have been formulated. These schemes are good candidates for application to Maxwell's equations in non-linear media.

The severe practical limitations in the implementation of three-dimensional finite difference schemes, for use in solving complex interaction problems, has been discussed. These limitations cannot be solved solely by the use of larger and larger computers. Advanced programming methods must be used to implement these algorithms. Also, the study and formulation of more efficient algorithms is an area of research which will have rewarding effects in the field of electromagnetic interaction modelling.

The future work, for the numerical modelling of electromagnetic interaction problems, can be summarized as being in two specific areas. The first, is the study and formulation of better, more robust algorithms for the solution of Maxwell's equations in general non-linear media, and the second, is the study of advanced implementation techniques to take advantage of available computer power.



Bibliography

- [Adobe 85] Adobe Systems Inc., **PostScript Language Reference Maunual**, Addison-Wesley publishing Company Inc., Reading, Mass., 1985.
- [Adobe 87] Adobe Systems Inc., **PostScript Language Tutorial and Cookbook**, Addison-Wesley publishing Company Inc., Reading, Mass., August, 1987.
- [Ahuja 90] Ahuja, R. K., Mehlhorn, K., Orlin, J. B., and Tarjan, R. E., *Faster Algorithms for the Shortest Path Problem*, J. of the Ass. for Comp. Mach., Vol. 37, No. 2, pp 213-223, April 1990.
- [Arden 89] Arden, M.J., Gosling J. and Rosenthal, D. S. H., **The NeWS Book**, Springer-Verlag,1989.
- [Barrett 90a] Barrett, T. W., *Comments on "Solution of Maxwell's Equations for General Nonperiodic Waves in Lossy Media"*, IEEE Trans. Electromagn. Compat., Vol. EMC-31, No. 2, pp 197 - 199, May, 1989.
- [Barrett 90b] Barrett, T. W., *Comments on "Some Comments on Harmuth and His Critics"*, IEEE Trans. Electromagn. Compat., Vol. EMC-31, No. 2, pp 201 - 202, May, 1989.
- [Baum 80] Baum, C. E., *Electromagnetic Topology, A Formal Approach to the Analysis and Design of Systems*, Interaction Notes, Note 400, Air Force Weapons Lab, September, 1980.

Bibliography

- [Baum 85] Baum, C. E., *On the Use of Electromagnetic Topology for the Decomposition of Scattering Matrices for Complex Physical Structures*, Interaction Notes, Note 454, Air Force Weapons Lab, July, 1985.
- [Bondy 76] Bondy, J. A., and Murty, U. S. R., **Graph Theory with Applications**, American Elsevier Pub. Co., Inc., 1976.
- [Brigham 74] Brigham, E. O., **The Fast Fourier Transform**, Prentice-Hall Inc., Englewood Cliffs, N.J., 1974.
- [Clocksin 84] Clocksin, W. F. and Mellish, C. S., **Programming in Prolog**, Springer-Verlag, New York, 1984.
- [Courant 52] Courant, R., Isaacson, E., and Rees, M., *On the solution of Nonlinear Hyperbolic Differential Equations by Finite Differences*, Comm. on Pure and Appl. Math.. Vol. 5, p 243, 1952.
- [Courant 62] Courant, R. and Hilbert, D., **Methods of Mathematical Physics**, Interscience Publishers (John Wiley & Sons), New York, 1962.
- [Dahlquist 74] Dahlquist, G., Björck, Å., and Anderson, N. (translator), **Numerical Methods**, Prentice-Hall, Inc., New Jersey, 1974.
- [Dechter 90] Dechter, R., *Enhancement Schemes for Constraint Processing: Backjumping, Learning, and Cutset Decomposition*, Artificial Intelligence, Vol. 41, No. 3, pp 273 - 312, January, 1990.
- [Dijkstra 59] Dijkstra, E. W., *A Note on Two Problems in Connexion with Graphs*, Numerische Mathematik, Vol. 1, pp 269 - 271, 1959.
- [Duff 88] Duff, W. G., **Fundamentals of Electromagnetic Compatibility**, A Handbook Series on Electromagnetic Interference and Compatibility, Vol. 1, Interference Control Technologies, Inc, Gainesville, Virginia, 1988.

Bibliography

- [Eyges 80] Eyges, L., **The Classical Electromagnetic Field**, Dover Publications, Inc., New York, 1980.
- [Fang 88] Fang, J., and Mei, K. K., *A Super-Absorbing Boundary Algorithm for Solving Electromagnetic Problems by Time-Domain Finite-Difference Method*, IEEE AP-S Inter. Symp., Vol. 2, pp 472 - 475, Syracuse, N.Y., June 6-10, 1988.
- [Garabedian 64] Garabedian, P. R., **Partial Differential Equations**, John Wiley & Sons, Inc., New York, 1964.
- [Guo 86] Guo, J., and Showers, R. M., *Response of Coaxial Cable over a Finite Ground Plane to an External Electromagnetic Field*, 1986 IEEE Int. Symp. on EMC, pp 220 - 224, San Diego, CA, Sept. 16 - 18, 1986.
- [Gray 88] Gray, J. E., and Bowen, S. P., *Some Comments on Harmuth and His Critics*, IEEE Trans. Electromagn. Compat., Vol. EMC-30, No. 4, pp 586 - 589, Nov., 1988.
- [Harmuth 86a] Harmuth, H. F., *Correction of Maxwell's equations for Signals I*, IEEE Trans. Electromagn. Compat., Vol. EMC-28, No. 4, pp 250 - 258, Nov., 1986.
- [Harmuth 86b] Harmuth, H. F., *Correction of Maxwell's equations for Signals II*, IEEE Trans. Electromagn. Compat., Vol. EMC-28, No. 4, pp 259 - 266, Nov., 1986.
- [Harrington 61] Harrington, R. F., **Time-Harmonic Electromagnetic Fields**, McGraw-Hill Book Co., New York, 1961.
- [Harten 83] Harten, A., Lax, P. D., and Van Leer, B., *On Upstream Differencing and Godunov-Type Schemes for Hyperbolic Conservation Laws*, SIAM Review, Vol. 25, No. 1, pp 35 - 61, 1983.

Bibliography

- [Horspool 86] Horspool, R. N., **C: Programming in the Berkeley UNIX Environment**, Prentice-Hall Canada Inc., Scarborough, Ont., 1986.
- [Ince 56] Ince, E. L., **Ordinary Differential Equations**, Dover Publications, Inc., New York, 1956.
- [Jackson 75] Jackson, J. D., **Classical Electrodynamics**, John Wiley & Sons, New York, 1975.
- [Jones 64] Jones, D. S., **The Theory of Electromagnetism**, Pergamon Press, Oxford, 1964.
- [Keiser 87] Keiser, B., **Principles of Electromagnetic Compatibility**, Artech House, Norwood, Massachusetts, 1987.
- [Körner 88] Körner, T. W., **Fourier Analysis**, Cambridge University Press, Cambridge, 1988.
- [Lapidus 82] Lapidus, L., and Pinder, G. F., **Numerical Solution of Partial Differential Equations in Science and Engineering**, John Wiley & Sons, New York, 1982.
- [Lax 73] Lax, P. D. *Hyperbolic Systems of Conservation Laws and the Mathematical Theory of Shock Waves*, CBMS Regional Conference Series in Applied Mathematics 11, Soc. for Ind. and Appl. Math. (SIAM), Philadelphia. 1973.
- [Lee 86] Lee, K. S. H., (editor), **EMP Interaction: Principles, Techniques, and Reference Data**, Hemisphere Pub. Corp., Harper & Row Inc., Washington, 1986.
- [LoVetri 89] LoVetri, J., Abu-Hakima, S., Podgorski, A. S., Costache, G. I., *HardSys: Applying Expert System Techniques to Electromagnetic Hardening*, IEEE 1989 National Symposium on Electromagnetic Compatibility, pp 383 - 385, Denver, Co., May 23-25, 1989.

Bibliography

- [LoVetri 90a] LoVetri, J., and Costache, G. I., *Time Domain Finite Element Analysis of 2-D Shields*, 1990 IEEE AP-S Int. Symp. and URSI Radio Sci. Meeting, pp , Dallas, TX, 15-17 August, 1990.
- [LoVetri 90b] LoVetri, J., and Graham, D. P. W., *Constraint Propagation Through Electromagnetic Interaction Topologies*, ANTEM'90, Symp. on Antenna Tech. and Appl. Electromagnetics, 15-17 August, 1990.
- [LoVetri 90c] LoVetri, J., and Podgorski, A. S., *Evaluation of HardSys: A Simple EMI Expert System*, 1990 IEEE Int. Symp. on EMC, Washington, D.C., 21-23 August, 1990.
- [McDonnel 78] McDonnel Douglas Astronautics Co. **Integrated Circuit Electromagnetic Susceptibility Handbook**, Report MDG-E1929, Box 516, St. Louis, Missouri, (314) 232-0232, August 1978.
- [Messier 85] Messier, M. A., *EMP Hardening Topology Expert System (Hard Top)*, Interaction Notes, Note 449, Air Force Weapons Lab, June, 1985.
- [Messier 86] Messier, M. A., *EMP Hardening Topology Expert System (Hard Top)*, Electromagnetics, Vol. 6, no. 1, pp 79 - 97, 1986.
- [Mil-Std-461C] **Electromagnetic Emission and Susceptibility Requirements for the Control of Electromagnetic Interference**, Military Standard 461C, Department of Defense, U.S.A., 4 August 1986.
- [Mil-Std-462] **Measurement of Electromagnetic Interference Characteristics**, Military Standard 462, Department of Defense, U.S.A., 31 July 1967.
- [Mitchell 80] Mitchell, A. R., and Griffiths, D. F., **The Finite Difference Method in Partial Differential Equations**, John Wiley & Sons, New York, 1980.

Bibliography

- [Montanari 74] Montanari, U., *Networks of Constraints: Fundamental Properties and Application to Picture Processing*, Information Science, Vol. 7, pp 95 - 132, 1974.
- [Noss 86] Noss, R. S., *Alternative Labeling Schemes in Electromagnetic Topology*, Electromagnetics, Vol. 6, no. 1, pp 21 - 31, 1986.
- [Osher 82] Osher, S., and Solomon, F., *Upwind Difference Schemes for Hyperbolic Systems of Conservation Laws*, Mathematics of Computation, Vol. 38, No. 158, pp 339 - 374, April, 1982.
- [Osher 82] Osher, S., *Riemann Solvers, The Entropy Condition, and Difference Approximations*, SIAM J. of Numer. Anal., Vol. 21, No. 2, pp 217 - 235, April, 1984.
- [Ott 88] Ott, H. W., **Noise Reduction Techniques in Electronic Systems**, John Wiley & Sons, New York, 1988.
- [PDE 86] IMSL, **PDE/PROTRAN: A System for the Solution of Partial Differential Equations**, User's Manual, IMSL, Houston, Texas, 1986.
- [Podgorski 90a] Podgorski, A. S., *Composite Electromagnetic Pulse Threat*, 1990 IEEE Int. Symp. on EMC, Washington, D.C., 21-23 August, 1990.
- [Podgorski 90b] Podgorski, A. S., *Lightning Standards for Aircraft Protection*, 1990 IEEE Int. Symp. on EMC, Washington, D.C., 21-23 August, 1990.
- [Raut 86] Raut, R., *On the Computation of Electromagnetic Field Components from a Practical Printed Circuit Board*, 1986 IEEE Int. Symp. on EMC, pp 161 - 166, San Diego, CA, Sept. 16 - 18, 1986.
- [Richtmyer 67] Richtmyer, R. D., and Morton, K. W., **Difference Methods for Initial-Value Problems**, Interscience Publishers, New York, 1967.

Bibliography

- [Richtmyer 78] Richtmyer, R. D., **Principles of Advanced Mathematical Physics, Volume I**, Springer-Verlag, New York, 1978.
- [Roden 79] Roden, M. S., **Analog and Digital Communication Systems**, Prentice-Hall Inc., Englewood Cliffs, N.J., 1979.
- [Roe 81] Roe, P. L., *Approximate Riemann Solvers, Parameter Vectors, and Difference Schemes*, J. of Comp. Phys., Vol. 43, pp 357 - 372, 1981.
- [Schulz 88] Schulz, R. B., Plantz, V. C. and Brush, D. R., *Shielding Theory and Practice*, IEEE Trans. Electromagn. Compat., vol. 30, no. 3, pp 187 - 201, August, 1988.
- [Sewell 85] Sewell, G., **Analysis of a Finite Element Method: PDE/PROTRAN**, Springer-Verlag, New York, 1985.
- [Shankar 89] Shankar, V., Hall, W. F., Mohammadian, A. H., *A Time-Domain Differential Solver for Electromagnetic Scattering Problems*, Proceedings of the IEEE, Vol. 77, No. 5, pp 709 - 721, May, 1989.
- [Shankar 90] Shankar, V., Mohammadian, A. H., Hall, W. F., *A Time-Domain Finite-Volume Treatment for the Maxwell Equations*, Electromagnetics, Vol. 10, No. 1-2, pp 127 - 145, 1990.
- [Shu 88] Shu, C-W, and Osher, S., *Efficient Implementation of Essentially Non-oscillatory Shock-Capturing Schemes*, J. of Comp. Phys., Vol. 77, pp 439 - 471, 1988.
- [Shu 89] Shu, C-W, and Osher, S., *Efficient Implementation of Essentially Non-oscillatory Shock-Capturing Schemes, II*, J. of Comp. Phys., Vol. 83, pp 32 - 78, 1989.
- [Smith 77] Smith, A. A. Jr., **Coupling of External Electromagnetic Fields to Transmission Lines**, John Wiley and Sons, New York, 1977.

Bibliography

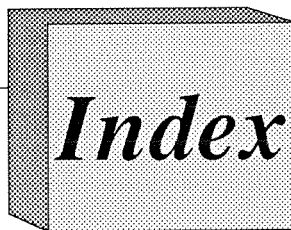
- [Sod 85] Sod, G. A., **Numerical Methods in Fluid Dynamics: Initial and Initial Boundary-Value Problems**, Cambridge University Press, Cambridge, 1985.
- [Stabler 86] Stabler Jr., E. P., *Object-Oriented Programming in Prolog*, AI Expert, pp 46-57, October 1986.
- [Steger 81] Steger, J. L., and Warming, R. F., *Flux Vector Splitting of the Inviscid Gasdynamic Equations with Applications to Finite-Difference Methods*, J. of Comp. Phys., Vol. 40, pp 263 - 293, 1981.
- [Sterling 86] Sterling L. and Shapiro E., **The Art of Prolog**, MIT Press, Cambridge, Massachusetts, 1986.
- [Stratton 41] Stratton, J. A., **Electromagnetic Theory**, McGraw-Hill Book Co., New York, 1941.
- [Strikwerda 89] Strikwerda, J. C., **Finite Difference Schemes and Partial Differential Equations**, Wadsworth & Brooks/Cole Advanced Books & Software, Pacific Grove, Ca., 1989.
- [Sussman 80] Sussman, G. J. and Steele, G. L., *Constraints - A Language for Expressing Almost-Hierarchical Descriptions*, Artificial Intelligence Journal, Vol. 14, pp 1 - 39, 1980.
- [Sweby 84] Sweby, P. K., *High Resolution Schemes using Flux Limiters for Hyperbolic Conservation Laws*, SIAM J. of Numer. Anal., Vol. 21, No. 5, pp 995 - 1011, October, 1984.
- [Tai 71] Tai, C., **Dyadic Green's Functions in Electromagnetic Theory**, Intext Educational Publishers, Scanton, 1971.

Bibliography

- [Taflove 88] Taflove, A., and Umashankar, K. R., *Finite-Difference Time-Domain (FD-TD) Modeling of Electromagnetic Wave Scattering and Interaction Problems*, IEEE Ant. and Prop. Soc. Newsletter, pp 5 - 20, April, 1988.
- [Taflove 90] Taflove, A., and Umashankar, K. R., *The finite-Difference Time-Domain Method for Modeling of Electromagnetic Wave Interactions with Arbitrary Structures*, in **Pier 2: Progress in Electromagnetic Research/Finite Element and Finite Difference Methods in Electromagnetic Scattering**, (Ed. M. A. Morgan), Elsevier, New York, 1990.
- [Taylor 90] Taylor, T., **HardDraw: A Drawing Tool Interface to the HardSys Electromagnetic Hardening Advisor**, National Research Council of Canada, Ottawa, April, 1990.
- [Tesche 78] Tesche, F. M., *Topological Concepts for Internal EMP Interaction*, IEEE Trans. on Ant. and Prop., Vol. AP-26, No. 1, pp 60 - 64, Jan., 1978.
- [Warming 76] Warming, R. F., and Beam, R. M., *Upwind Second-Order Difference Schemes and Applications in Aerodynamic Flows*, AIAA Journal, Vol. 14, No. 9, pp 1241 - 1249, September, 1976.
- [White 73] White, D. R. J., **Electromagnetic Interference and Compatibility (EMI Control Methods and Techniques)**, Vol. 1-6, Don White Consultants, Gainesville, Virginia, 1973.
- [Wilson 72] Wilson, J. C., *Stability of Richtmyer Type Difference Schemes in any Finite Number of Space Variables and Their Comparison with Multistep Strang Schemes*, J. Inst. Maths. and Applics., Vol. 10, pp 238 - 257, 1972.

Bibliography

- [Vance 78] Vance, E. F., **Coupling to Shielded Cables**, John Wiley and Sons, Inc., New York, 1978.
- [van Hoff 89a] **GoodNeWS1.3 User Guide**, The Turing Institute, Glasgow, Scotland, September, 1989.
- [van Hoff 89b] **HyperNeWS1.3 User Manual**, The Turing Institute, Glasgow, Scotland, September, 1989.
- [Vitek 89] Vitek, C., *Predicting the Shielding Effectiveness of Rectangular Apertures*, IEEE 1989 National Symposium on EMC, Denver, Colorado, pp 27 - 32, May 23 - 25, 1989.
- [Quintus 88] **Quintus Prolog Development System Manual (Release 2.4)**, Quintus Computer Systems Inc., Mountain View, California.
- [X11/NeWS 89] Sun Microsystems, **X11/NeWS Release 1.0 Manual**, Sun Microsystems Inc., Mountain View, CA, August, 1989.
- [Yee 66] Yee, S. K., *Numerical Solution of Initial Boundary Value Problems Involving Maxwell's Equations in Isotropic Media*, IEEE Trans. on Ant. and Prop., Vol. AP-14, No. 3, pp 302 -307, May, 1966.
- [Ziolkowski 83] Ziolkowski, R. W., Madsen, N. K., Carpenter, R. C., *Three-Dimensional Computer Modeling of Electromagnetic Fields: A Global Lookback Lattice Truncation Scheme*, J. of Comp. Phys., Vol. 50, pp 360 - 408, 1983.



Index

A

absorbing boundary conditions 175
algorithmic techniques 109

B

$B(x,t)$ 112
bipartite graph
graph 32
boundary operator 22
broadband emission
coherent 50
incoherent 50

C 91

C

characteristic line 124
characteristic lines 119
conductivity 114
conservation form 136
conservation laws 115
constitutive equations 113
constraints 73
continuity equation 113
contour operator 22
Courant number 138

D

$D(x,t)$ 112

Dijkstra's algorithm 27
directed attributes 33
directed graph
digraph 33
displacement current 113
divergence theorem 116
domain of dependence 140
double precision 171
dynamic allocation 172

E

$E(x,t)$ 112
edges
graph 32
electric charge density 112
electric current density 112
electric field intensity 112
electric flux density 112
electrical topology 21
electromagnetic components 21
electromagnetic hardening 17
electromagnetic interaction modelling 17
electromagnetic pulse 17
electromagnetic topology 21
electromagnetically hard 17
EMP 17

Index

F

far field 45
 Faraday's law 113
 FCC 18
 finite difference scheme
 consistency 135
 finite difference scheme
 convergence 135
 stability 135
 finite difference techniques 133
 operator notation 133
 fluid dynamics 115
 flux vector splitting technique 142

G

Gauss law 114
 genuinely nonlinear 118
 GoodNeWS 90, 91
 graph 32
 acyclic 26
 bipartite 25
 components 26
 connected 26
 connected vertices 26
 cut edge 30
 cut vertex 30
 cycle 26
 directed 33
 disconnected 26
 grouped vertex 31
 grouping 30
 intersection 25
 k-cycle 26

maximum degree 25
 minimum degree 25
 path 26
 distance 27
 length 27
 simple 24
 trail 26
 tree 26
 minimum spanning 27
 union 25
 vertex degree 25
 walk 26
 closed 26
 internal vertices 26
 length 26
 origin 26
 section 26
 terminus 26
 weighted 27

H

$H(x,t)$ 112
 high-impedance fields 46
 hyperbolic systems of conservation laws 115
 HyperNeWS 90
I
 incidence function
 graph 24
 induction field 46
 initial-boundary value problems 133
 interaction path
 cc-paths 63
 cf-paths 63
 fc-paths 63

Index

- ff-path 63
 interaction paths 21
 interaction sequence diagram 21
- J**
 $J(x,t)$ 112
 jump condition 127
- K**
 k-waves 120
- L**
 Lax-Richtmyer equivalence theorem 136
 Lax-Wendroff method 138
 Lax-Wendroff theorem 137
 linearly degenerate 119
 linked list 174
 low-impedance fields 46
- M**
 MacCormack scheme 142
 magnetic field intensity 112
 magnetic flux density 112
 magnetic vector potential 187
 Maxwell's equations 112
 Method of Weighted Residuals 187
 Mil-Std-461C 18
- N**
 narrowband emission 50
 near field 45
- NeWS 20, 91
 NeWS™ 90
 nodes 32
- O**
 Ohm's law 113
- P**
 permeability 114
 permitivity 114
 PostScript 91
- Q**
 quantization
 of field strength 48
 of frequency range 41
 Quintus Prolog 20, 90
- R**
 radiation field 46
 Rankine-Hugoniot jump relation 119, 120
 $\rho(x,t)$ 112
 Richtmyer scheme
 modified Richtmyer scheme 161, 162
 rotated Richtmyer scheme 161, 162
 Riemann Problem 120
 Riemann problem 145
- S**
 shield imperfections 78
 shielding effectiveness 60
 shielding topology 21

Index

single precision 171
subgraph 25
 disjoint 25
 edge-disjoint 25
 spanning 25
Sun 20
Sun Microsystems 90
supergraph 25
system susceptibility
 permanent damage 57
 upset 57

T

tensors 114
test function 136
two-step method 139

U

upwind method 141

V

vertices
 graph 32
volume decomposition 22

W

wave equation
 one-way scalar 141
wave impedance 45
weak solution 136
wideband emission 50